NASA Contractor Report 4333

Injection Efficiency of Bound Modes

Claudio Oliveira Egalon

CONTRACT NAS1-18347
NOVEMBER 1990

NASA

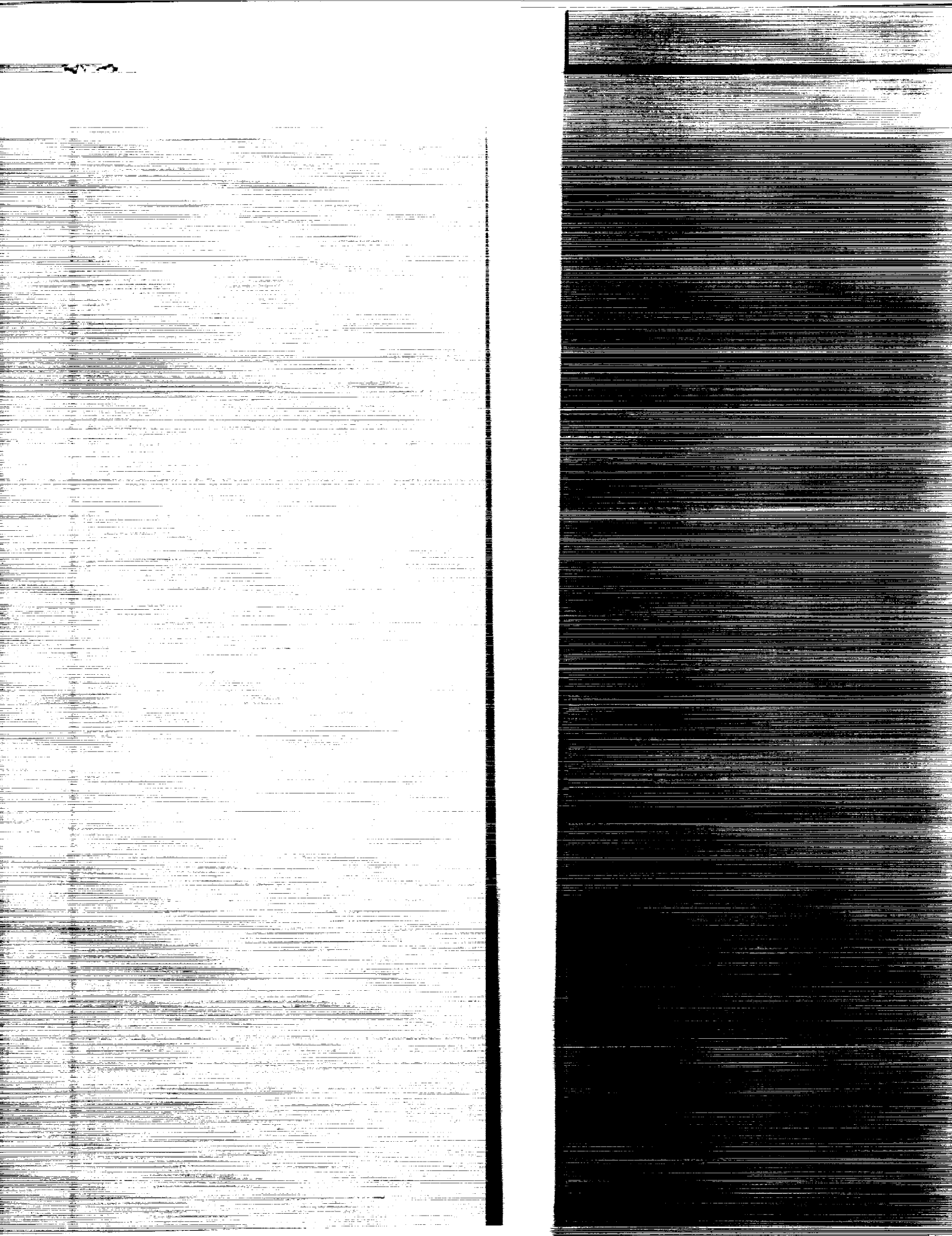

NASA Contractor Report 4333

Injection Efficiency of Bound Modes

Claudio Oliveira Egalon
The College of William and Mary
Williamsburg, Virginia

Prepared for
Langley Research Center
under Contract NAS1-18347

National Aeronautics and
Space Administration
Office of Management
Scientific and Technical
Information Division

1990

TABLE OF CONTENTS

ACKNOWLEDGMENTS

The author would like to thank Dietrich Marcuse from Bell Labs for reviewing part of this work. He has provided many suggestions and discovered a last minute discrepancy which was promptly corrected. His previous work helped shape this thesis and his experience in the field proved to be invaluable. The author is in debt to Bob Lieberman, also with Bell Labs. He has reviewed part of this work and made suggestions. He also provided the author with a sample of a fluorescent fiber for future experimental verification of the results presented here. Doug Christensen, from University of Utah, made suggestions and provided fruitful discussions. His work, which is related to this dissertation, has stimulated the author to conduct further research in the field. John Cantrell, with NASA Langley, helped clarify a critical point before the manuscript took its final form. Steve Lackie and Thomas Glass, with ORD, helped the author gain insight of this problem at the very beginning. Rick Weenings, The College of William and Mary, proposed many thought provoking questions during and after the defense. The gang of NMSB, NASA, for being tolerant with me during these two intense years and also for helping me out with questions and suggestions. Don Phillips, NASA, for providing me with his own computer time at a moment when computer resources were very scarce. George Vahala and Carl Carlson, William and Mary, for serving in the dissertation committee. They have reviewed this work and provided comments. Chris Welch, William and Mary, reviewed the dissertation, provided comments and ideas, picked up inconsistencies and helped refine the final manuscript. Joe Heyman, NASA, for lending moral, material and technical support. He has reviewed the dissertation, discussed the topic with the author, helped in the preparation of the defense and made interesting suggestions for additional work. And (last but not least) Bob Rogowski, NASA, friend, advisor and colleague. He has proposed the problem, offered his own time and guidance and provided moral and technical support during this critical phase of my career. His patience and experience in the field were instrumental during the whole phase of this project. Without his support this work would not be possible at all.

LIST OF TABLES

Table Page

LIST OF FIGURES

Figure Page

ABSTRACT

Previous work on efficiency of light injection into the core of a fiber from a thin film and a bulk distribution of sources in the cladding, have made use of the fields of a weakly guiding fiber. This approximation simplifies the analysis of the power efficiency by introducing universal values for the eigenvalues of different fibers with same V-number, but can not predict accurately the behavior of the injected light into a fiber with arbitrary differences in indices of refraction. We have used the exact field solution in the expressions of the power efficiency, P_{eff}, and analyzed its behavior as a function of the remaining parameters. Although more complicated and harder to interpret, our formulas allow us to analyze the power injection efficiency of fibers with arbitrary differences in the indices of refraction. The results obtained are relevant for the design of more efficient optical fiber distributed sensors. The conclusions follow.

We have confirmed weakly guiding results obtained previously. However, we have found that the P_{eff} does not always increase with the V-number but with the difference in the indices of refraction, n_{core}-n_{clad}.

For fixed a/λ, indices of refraction, n_{core} and n_{clad} and normalized inner and outer radius, R_{in} and R_{out}, the P_{eff} is independent of the core radius, a, and the wavelength, λ, for any uniform cylindrical distribution of cladding sources. This suggests that a/λ, R_{in} and R_{out} are independent variables.

For the bulk distribution we have found that P_{eff} increases with the wavelength, λ, and decreases with the fiber core radius, a, i.e., it *decreases* with the V-number. However, for the thin film, the P_{eff} remains almost constant with the wavelength, λ, and fiber core radius, a.

INJECTION EFFICIENCY OF BOUND MODES

I. INTRODUCTION

I-1 Justification

In this work we have obtained expressions for the power injection efficiency, P_{eff}, from cladding sources of a step index profile cylindrical optical fiber using the Maxwell's Equations. We have also determined the general behavior of P_{eff} against the parameters of this problem extending previous work done by Marcuse [1988] on the efficiency of core light injection from sources in the cladding. Our results are unique in the sense that we have made use of the exact field solution of the cylindrical optical fiber to calculate the power efficiency due to the emission of evanescent waves and analyzed its behavior as a function of parameters and their combinations not previously treated. Previous results that are related to our work, have either made use of the geometric optics theory to calculate and optimize the output signal of a fluorescent coated fiber [Glass et. al., 1987; Love et. al., 1988] or used the weakly guiding approximation of the fields to calculate the power efficiency [Marcuse, 1988]. The first approach, geometric optics, is accurate only for multimode fibers and the second approach, weakly guiding approximation, can not predict the behavior of a fiber that has a large difference between the core and cladding indices of refraction. In this work, we have used the exact field solution in the expression of the power efficiency in order to take into account the shortcomings of both approaches. In this

way, we have been able to determine accurately the behavior of a few mode optical fibers and the behavior of fibers that have an arbitrary difference of indices of refraction. Our results can be used to model optical fiber chemical sensors that have a fluorescent or chemiluminescent cladding.

I-2 Overview

In this Chapter we present an overview of previous theoretical and experimental results that are related to this work. In Chapter II, we derive the fields of both arbitrary and weakly guiding fibers with an infinite cladding. A more detailed presentation of the results in that Chapter can be found in many good optical fiber textbooks [Snyder et. al., 1983; Marcuse, 1974; Midwinter, 1979] and earlier papers on this subject [Snitzer, 1961; Gloge, 1971 and references therein]. In Chapter III, we derive the power injection efficiency from sources in the cladding using the exact field solution of an optical fiber. For the first time, this derivation allows us to predict the behavior of fluorescent cladding fibers with arbitrary differences in indices of refraction. The weakly guiding approximation referred to earlier, can be used only with fibers that have similar core/cladding indices of refraction.

Chapter IV is central to this work. It presents the numerical results obtained from our FORTRAN program which has made use of the formulas derived in Chapters II and III. In that Chapter, we have plotted the behavior of the power efficiency of a fiber as a function of its parameters namely, the core radius, a, the indices of refraction n_{core} and n_{clad}, and the wavelength, λ.

We have also plotted the power efficiency against a combination of these parameters as n_{core}-n_{clad} and the V-number under certain conditions. There, the results for a new independent variable, a/λ, is discussed. Our work has confirmed previous weakly guiding results, given a new insight into the behavior of an optical fiber with an arbitrary difference in the indices of refraction and helped determine the configuration of a highly efficient fiber. These results are relevant in that they point toward the design of improved optical chemical distributed sensors.

Finally, in Chapter V, we have concluded and summarized the results obtained here and recommended further additional work that could both verify and improve our theory.

I-3 Theoretical and Experimental Background

Optical fiber sensors have been used to measure current, pressure, temperature, and other physical observables [Culshaw, 1984 and references therein]. They can also be used to monitor vibrations in flexible structures and detect chemical species [Rogowski et. al., 1988; Hardy et. al., 1975; Lieberman et. al., 1988; Lieberman et. al., 1990; Blyler et. al., 1988; Wolfbeis et. al., 1988]. Many optical techniques have been employed in conjunction with optical fibers. They exploit both the wave and corpuscular nature of light. Geometrical optics theory is used whenever the wave aspect of light can be disregarded and for this reason it is an incomplete theory.

Here, we will be mostly concerned with the wave aspect of light. By using Maxwell's Equations, phenomena like evanescent waves can be studied and predicted more accurately. It is the concept of evanescent wave that is central to this work. It comes into play whenever radiation is totally internally reflected between two dielectric media of different indices of refraction. Although most of the incident power is reflected, part of the radiation penetrates a very thin layer of the dielectric of lower index of refraction. This penetrating radiation is termed the *evanescent* component of the field and is characterized by

1) an amplitude that has an exponential-like decay from the dielectric boundary and

2) a direction of propagation that is parallel to the dielectrics interface [Jackson, 1975; Ghatak et. al., 1978].

As consequence of 2, all the power in the dielectric medium of lower index propagates parallel to the interface (Figure I-1).

Evanescent waves are responsible for the Goos-Hänchen Effect. It occurs whenever a totally internally reflected light beam in a plane dielectric interface undergoes a lateral shift due to the penetration of the field into the lower refractive index medium or evanescent region [Ghatak et. al., 1978; Midwinter, 1979]. The larger the wavelength of the radiation the larger the lateral shift.

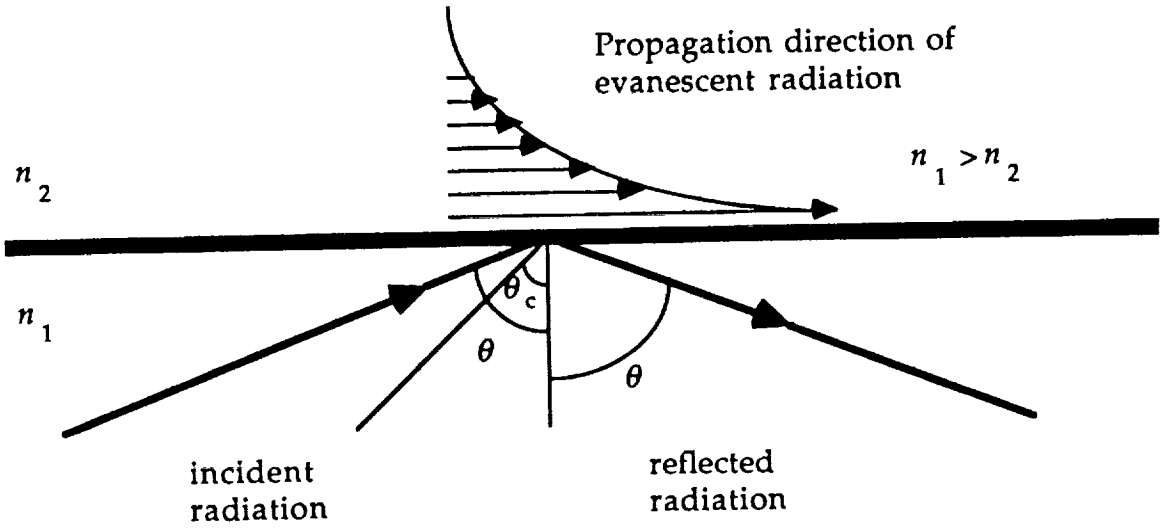

Figure I-1. The field amplitude of the evanescent wave decays exponentially further from the media interface. Its direction of propagation is parallel to the interface. θ_c is the critical angle.

Evanescent waves can also give rise to other unusual phenomena. They can be absorbed and used to excite fluorescent sources in the evanescent region [Tai et. al., 1987; Glass et. al., 1987; Carniglia et. al., 1972; Lee et. al., 1979; Love et. al., 1988]. The principle of reciprocity, in conjunction with the above results, would lead us to expect that the inverse process should also take place [Carniglia et. al., 1972]. In other words, if an excited molecule placed near the interface of two dielectrics in the lower index of refraction region can emit evanescent waves, we should be able to detect radiation propagating at an angle higher than the critical angle (Figure I-2). Such high angle propagation was observed by Selenyi [1913] and Fröhlich [1921] and quantitatively explained by Carniglia et. al. [1972].

In conclusion, evanescent waves can be used to excite sources in the evanescent region. The inverse process, emission of evanescent waves by excited molecules can also take place and is a well-established phenomenon.

I-4 Previous Work on Evanescent Wave Sensor

The evanescent wave concept has been theoretically and experimentally investigated and widely used for sensing purposes [Tai et. al., 1987; Glass et. al., 1987; Carniglia et. al., 1972; Lee et. al., 1979; Love et. al., 1988; Selenyi, 1913; Fröhlich, 1921; Lieberman et. al., 1990; Cox et. al., 1985; Lieberman et. al., 1988; Christensen et. al., 1989; Marcuse, 1988].

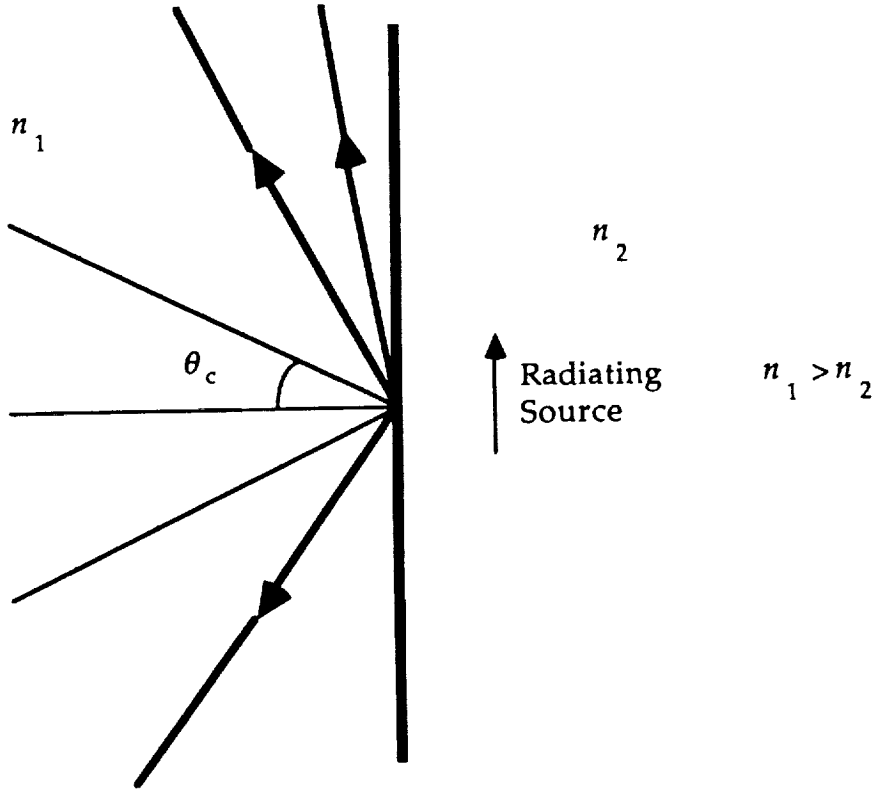

Figure I-2. Source placed near the interface of two media in the region of lower refractive index. Light rays observed at $\theta > \theta_c$ (arrows in medium 1), are due to the evanescent waves emitted by the source in medium 2.

Tai et. al. have used solely the absorption of the evanescent wave to determine the concentration of methane-gas with a tapered optical fiber [Tai et. al., 1987]. In their approach, a He-Ne laser excites bound modes in the fiber. The chemical species surrounding the tapered region of the fiber, absorbs the evanescent wave associated with these modes at a specific wavelength. This absorption can be detected at the end of the fiber as a decrease in the output signal level and is related to the concentration.

The effect of the numerical aperture (*N.A.*) on signal level of multimode fibers with fluorescent substances in the evanescent zone was treated (2). Using a *N.A.* smaller than the maximum *N.A.* of the sensor, the authors have excited fluorescent sources in the evanescent zone. Due to the emission of evanescent wave, some of the light is trapped in the core as bound modes and can be detected at both ends of the fiber. Due to the background noise, the signal was chosen to be collected at the proximal end of the fiber. The theory developed was shown to be in good agreement with the experimental results.

The effect of the numerical aperture (*N.A.*) of injected light on signal level of multimode fibers coated with a fluorescent substance in the evanescent zone was treated [Glass et. al., 1987]. Using a *N.A.* smaller than the maximum *N.A.* of the sensor, the authors injected light into a multimode fiber. The evanescent field of the radiation excited the fluorescent sources. Due to the emission of evanescent wave, some of the light is trapped in the core as bound modes and can be detected at both ends of the fiber. Due to the background noise, the signal was chosen to be collected at the proximal end of

the fiber [Hirschfeld et. al., 1984; 1984a; Block et. al., 1984; Block et. al., 1986]. The theory developed used geometric optics and was shown to be in good agreement with the experimental results.

Using the emission of evanescent photons, Lieberman et. al. have developed an optical fiber sensor with a fluorescent cladding to detect molecular oxygen [Lieberman et. al., 1990]. In this case, an optical fiber is clad during manufacture with a polymer which has a fluorescent dye dissolved in it (the dye itself is sensitive to the presence of molecular oxygen [Cox et. al., 1985]). The dye dissolved in the polymer, Poly-dimethyl Siloxane, PDMS, acts like a fluorescent cladding when excited by side-illumination at a wavelength within the excitation range of the dye. In a way similar to the one described before, evanescent photons from the cladding are injected as bound modes in the core and the homogeneous photons are leaked out. In a similar sensor, an oxygen sensitive fluorescent coating was applied to a fiber having a fluorescent core. The homogeneous photons from the coating sources excited the fluorescent sources in the core [Lieberman et. al., 1988]. The result was a 100-fold increase in the efficiency of the sensor when compared with the previous one. In both cases, the fluorescence intensity is quenched by oxygen and its partial pressure could be determined [Cox et. al., 1985].

Christensen et. al. have used a FDTD (Finite Difference Time Domain) analysis to determine the percentage of power that is guided in a single direction in a planar waveguide with fluorescent sources outside the core [Christensen et. al., 1989]. His approach differed from Marcuse's who derived

an expression for the power efficiency of a step profile fiber using the weakly guiding approximation [Marcuse, 1988]. Marcuse has applied his results to the sensor described by Lieberman et. al. [1990]. Agreement between theory and experiment was within an order of magnitude for a single experimental data point. Further experimental work is required to verify the theory.

In this thesis we extend previous work done by Marcuse [1988] on the efficiency of core light injection from sources in the cladding.

Assuming that the cladding sources are already excited, Marcuse computed the fraction of the power that is trapped in one direction as bound modes in the core of a weakly-guiding step-profile fiber. This fraction is the ratio of the power that is injected into the core of the fiber as bound modes, P_{core} to the total power radiated by the sources, P_{rad}. He also assumed a fiber with infinite cladding and treated it for both positively and negatively guiding fibers, $n_{core} > n_{clad}$ and $n_{clad} > n_{core}$ respectively. Assuming each source as being an infinitesimal electric current j with random phase and orientation, he analysed two different distributions:

1) sources that are uniformly distributed in the cladding and

2) sources that are concentrated in the core-cladding boundary (thin film) (Figure I-3).

In this extension, we treat only positively guiding fibers for the above source distributions. We derive our formulas by using the exact solution of the fields of the cylindrical optical fiber with an infinite cladding. Such an approach

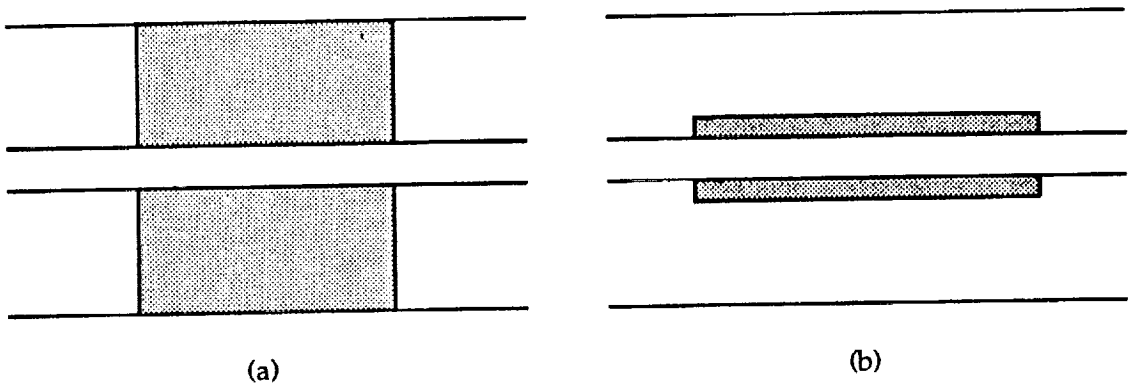

Figure I-3. Sources uniformly distributed in the cladding (bulk distribution) (a) and sources distributed at the core/cladding interface (thin film distribution) (b).

allows us to account for arbitrary differences between n_{core} and n_{clad}. Although the cladding sources also excite low loss leaky modes that may be detected in short fibers [Marcuse, 1988], we have treated only the injection due to the evanescent field. We are applying these results to design an atomic oxygen optical fiber sensor which uses evanescent-wavecoupling. Such a sensor would be part of a smart structure and could detect and monitor the action of atomic oxygen on space structures. It could easily be deployed on NASA's missions.

I-5 Conclusion

Since optical fibers were initially developed for communications purposes, there had been a need to design fibers with low pulse dispersion. Weakly guiding fibers seem to fulfill this need. This has led to the formulation and widespread usage of the weakly guiding approximation which is simpler than the exact case. In contrast, it was only recently that the potential of optical fibers for sensing purposes was realized. In consequence, it was also realized that weakly guiding fibers are not necessarily best suited for sensing purposes. Although the exact field solution can explain sensor fibers a simpler and different approach that can treat these fibers has to be formulated. The possibility of formulation of a new, innovative and simpler approach can not be discarded. It should allow a fair description of the properties of fiber sensors in the same way that weakly guiding approximation is a good approximation for communication fibers.

II. BOUND MODES OF A STEP PROFILE FIBER

II-1 Introduction

The system to be studied, the cylindrical optical fiber, consists basically of a glass-rod of index of refraction n_{core} surrounded by a dielectric material of index of refraction n_{clad} ,where

$$n_{core} > n_{clad}. \tag{II-1}$$

The region with index of refraction n_{core} is referred as the *core* of the fiber. The outside region with index of refraction n_{clad} is referred as *cladding* (Figure II-1).

A cylindrical optical waveguide can support two kinds of modes: radiation and bound modes. The total electromagnetic fields of the waveguide can be expressed as a sum of these two modes. In ray theory, light beams that have an incident angle smaller than the critical angle correspond to the radiation field. Those are the refracted rays. On the other hand, electromagnetic fields that propagate indefinitely inside the waveguide structure are expressed as bound modes. In general, most of the bound mode energy propagates inside the core of the fiber. The portion that penetrates into the cladding, the region of lower index of refraction, is termed the evanescent field. As discussed

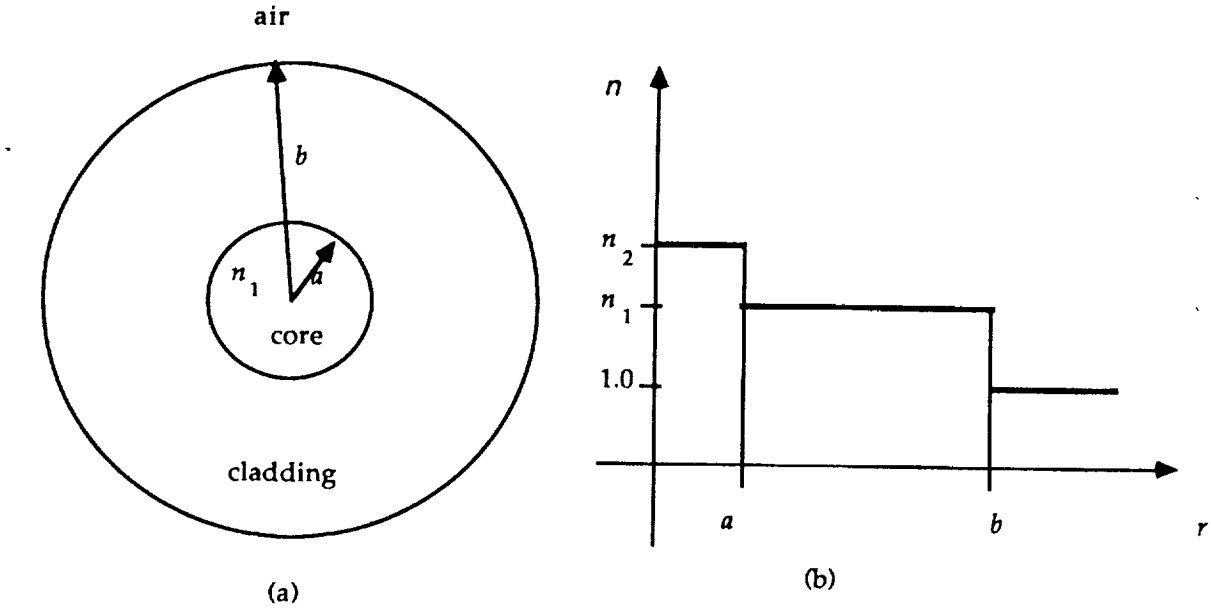

Figure II-1. Three layers cylindrical optical fiber with core radius a and cladding radius b (a). Variation of the index of refraction n with the radius r (b). For practical purposes the cladding radius b is assumed to be infinite.

previously, there is no ray counterpart for the evanescent field. However, for those fields that are not evanescent their geometrical counterpart are represented by rays that are totally internally reflected, having an angle of incidence greater than the critical angle (Figure II-2).

Bound and radiation modes are excited by injecting electromagnetic energy from sources into the fiber. Lasers, diodes and fluorescent molecules can be used for this purpose. As discussed in the previous chapter, we will be concerned only with the excitation of an optical fiber due to fluorescent sources distributed in the cladding.

Excited fluorescent sources distributed in the cladding of an optical fiber generate radiation fields and can inject bound modes (Figure II-3). For sensing purposes, bound modes are more important. They propagate indefinitely in the core of the fiber and can be easily collected for analysis. In addition to that, any perturbation to the trapped field can be used to get information on the surroundings of the fiber. The bound modes excited by the sources in the fiber cladding are closely related to the evanescent field. *Without evanescent fields, bound modes can not be excited from sources in the cladding.*

It is the aim of this chapter to present a mathematical expression describing the bound modes of a cylindrical optical fiber. We start by presenting a well-known relationship between the transverse and longitudinal fields. We proceed with the derivation of the vector wave equation and find the

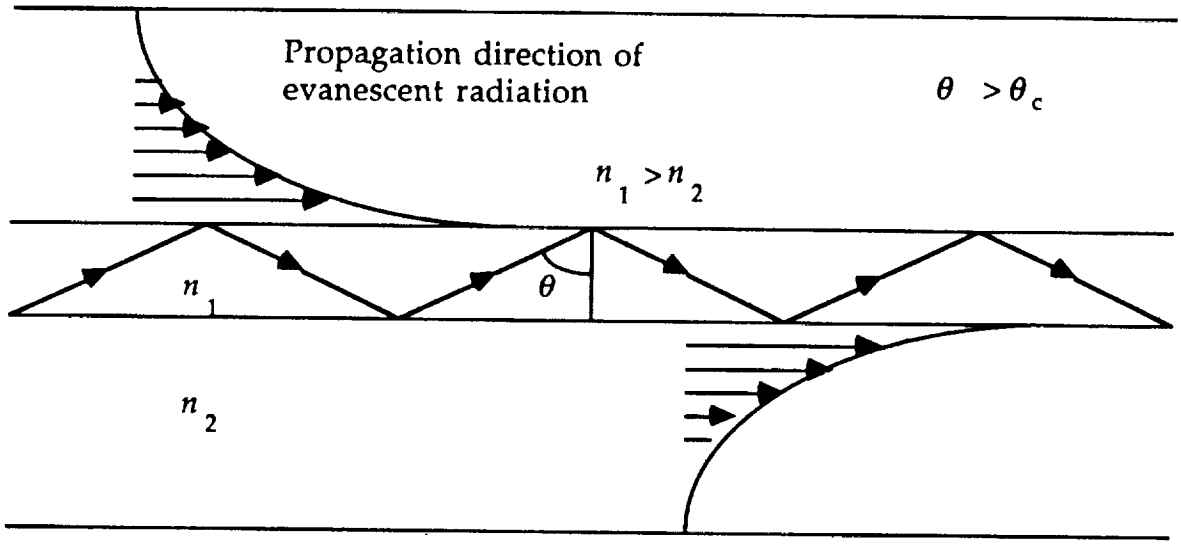

Figure II-2. Bound modes (rays) and their evanescent counterpart in an optical fiber.

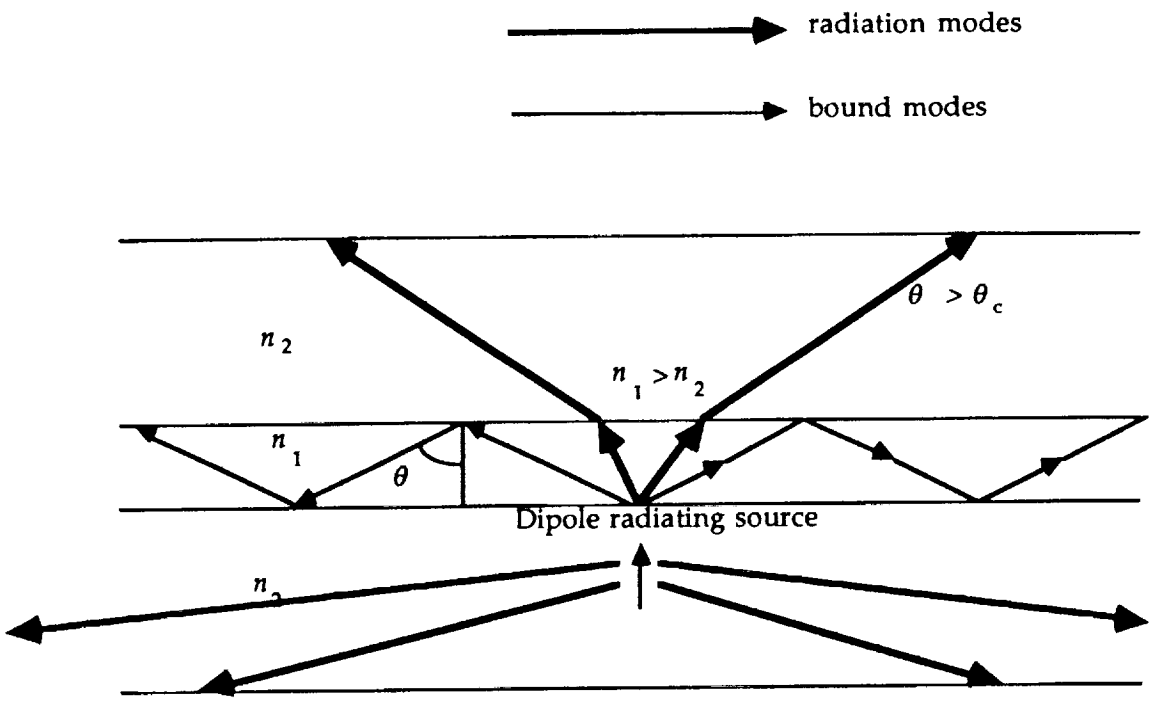

Figure II-3. Sources in the cladding of an optical fiber can emit evanescent wave. Some of the evanescent energy is trapped as forward and backward propagating modes. However, in general, most of the it goes toward radiation modes.

solution of the longitudinal components of the fields. From the previous results we derive the transverse components of the fields. Using the boundary conditions and an appropriate normalization, we find the amplitude coefficients and the eigenvalue equations. We conclude the chapter by displaying the fields and the eigenvalue equation of a weakly guiding fiber.

II-2 Relation Between Transverse and Longitudinal Fields

Propagation of light along non-absorbing optical waveguides in regions sufficiently far from any source of excitation is most conveniently described by a sum over the bound modes of the waveguide. Bound modes are solutions of the source-free Maxwell equations. We assume an implicit time dependence $\exp(-i\omega t)$ in the field vectors. The dielectric constant $\varepsilon(x,y,z)$ can be written as a function of the index of refraction $n(x,y,z)$,

$$\varepsilon = \varepsilon_0 n^2. \tag{II-2}$$

For nonmagnetic materials the magnetic permeability μ is very nearly equal to the free-space value μ_0. Under these conditions and using the rationalized MKS units, the source-free Maxwell's equations are expressible in the form

$$\nabla \times \boldsymbol{E} = i\sqrt{\frac{\mu_0}{\varepsilon_0}}k\,\boldsymbol{H} \tag{II-3a}$$

$$\nabla \times H = -i\sqrt{\frac{\varepsilon_0}{\mu_0}}\, kn^2 E \qquad \text{(II-3b)}$$

$$\nabla.(n^2 E) = 0 \qquad \text{(II-3c)}$$

$$\nabla.H = 0 \qquad \text{(II-3d)}$$

where $k = 2\pi / \lambda$ is the free-space circular wave number and λ is the wavelength of the light in free space.

The refractive index profile of the step index fiber doesn't vary with the distance along the waveguide, i.e., it is independent of z. Such fibers are said to be *translationally invariant* [Snyder et. al., 1983]. Its electric and magnetic fields can be expressed as superposition of fields with the separable form

$$E\,(x,y,z,) = e\,(x,y\,)\exp(i\,\beta z) \qquad \text{(II-4a)}$$

$$H\,(x,y,z) = h\,(x,y\,)\exp(i\,\beta z) \qquad \text{(II-4b)}$$

where β is found from the boundary conditions.

It is useful to separate the fields in components parallel and transverse to the fiber axis

$$E\,(x,y,z) = \left(e_t\,(x,y\,) + \hat{z}e_z\,(x,y\,)\right)\exp(i\,\beta z) \qquad \text{(II-5a)}$$

$$H(x,y,z) = \left(h_t(x,y) + \hat{z}h_z(x,y)\right)\exp(i\beta z). \qquad \text{(II-5b)}$$

Substituting equations II-5 in II-3 and separating the resulting equations into transverse and longitudinal components, we get

$$e_t = -\sqrt{\frac{\mu_0}{\varepsilon_0}}\frac{1}{k n^2}\hat{z}\times\left(\beta h_t + i\,\nabla_t h_z\right), \qquad \text{(II-6a)}$$

$$h_t = \sqrt{\frac{\varepsilon_0}{\mu_0}}\frac{1}{k}\hat{z}\times\left(\beta e_t + i\,\nabla_t e_z\right), \qquad \text{(II-6b)}$$

$$e_z = \frac{i}{\beta}\left(\nabla_t . e_t + i\left(e_t . \nabla_t\right)\ln n^2\right) \quad \text{and} \qquad \text{(II-6c)}$$

$$h_z = \frac{i}{\beta}\,\nabla_t . h_t . \qquad \text{(II-6d)}$$

Substituting (II-6a) in (II-6b) we get

$$h_t = \frac{i}{k^2 n^2 - \beta^2}\left(\beta\nabla_t h_z + k n^2\sqrt{\frac{\varepsilon_0}{\mu_0}}\hat{z}\times\nabla_t e_z\right). \qquad \text{(II-7)}$$

Substituting (II-7) in (II-6a) we have

$$e_t = \frac{i}{k^2 n^2 - \beta^2}\left(\beta\,\nabla_t e_z - k\sqrt{\frac{\mu_0}{\varepsilon_0}}\,\hat{z}\times\nabla_t h_z\right). \qquad \text{(II-8)}$$

It can be seen from (II-7) and (II-8) that the transverse fields are a function of the longitudinal fields only. Consequently if we can find the z-component of the fields, we automatically have the whole solution.

II-3 The Homogeneous Vector Wave Equations

In order to find the longitudinal components of the fields, we transform the Maxwell equations, Equations (II-3), into a more convenient form. We will carry out this derivation just for the H- field. The derivation for the E- field is similar.

Using Equation (II-3b) we can write E in terms of H. Substituting this result in Equation (II-3a) we get

$$\nabla \times \left(\frac{\nabla \times H}{n^2} \right) = k^2 H \tag{II-9}$$

For a step profile fiber with infinite cladding n is given by

$$n = \begin{cases} n_{\text{core}} & 0 < r < a \\ \\ n_{\text{clad}} & a < r < \infty \end{cases} \tag{II-10}$$

where a is the core radius and r is the radial cylindrical coordinate. As it can be seen from (II-10), the index of refraction is constant throughout the fiber except at the core-cladding interface. Consequently, within the core and the

cladding, Equation (II-9) and its *E*- field counterpart will satisfy the equations

$$\nabla \times (\nabla \times H) = k^2 n^2 H \qquad \text{(II-11a)}$$

$$\nabla \times (\nabla \times E) = k^2 n^2 E \qquad \text{(II-11b)}$$

respectively. Expanding the left hand side of Equations (II-11) and substituting Equations (II-3c) and (II-3d) in the expansion, we get

$$\vec{\nabla}^2 H = -k^2 n^2 H \qquad \text{(II-11c)}$$

$$\vec{\nabla}^2 E = -k^2 n^2 E \qquad \text{(II-11d)}$$

We must emphasize that the operator in the left hand-side of the above equations, $\vec{\nabla}^2$, is a *vector* operator, not to be confused with the *scalar* Laplacian operator, ∇^2. In a curvilinear system of coordinates, the vector operator couples the components of the fields this makes

$$\vec{\nabla}^2 \neq \nabla^2.$$

However, in the Cartesian system of coordinates,

$$\vec{\nabla}^2 = \nabla^2$$

[Snyder et. al., 1983]. We should warn that Jackson [1975] does not make this distinction in his Vector Formulas displayed inside the front cover. This gives a false impression that the relationship $\vec{\nabla}^2 = \nabla^2$ always holds.

It must be stated that Equations (II-11) do not hold at the interface but only within the core and the cladding. If we want to know the field *everywhere* in the fiber, including the interface, we have to impose the boundary conditions of Maxwell's equations in Equations (II-11) [Snyder et. al., 1983].

Equations (II-11) are known as the Homogeneous Vector Wave Equations (source-free).

II-4 Solution of the Longitudinal Fields

Since the fiber is cylindrically symmetric it is convenient to use a cylindrical coordinate system to solve Equations (II-11). The two vector differential equations obtained above can be broken down in six scalar differential equations. Four of them involve the transverse components of the fields which are coupled to each other in the equation. The other two involve the z-components of the fields only. As discussed before we can specify all fields in the fiber just by solving the longitudinal components. The equations that are of interest to us are expressed below

$$\frac{\partial^2 e_z}{\partial r^2} + \frac{1}{r}\frac{\partial e_z}{\partial r} + \frac{1}{r^2}\frac{\partial^2 e_z}{\partial \phi^2} + \left(k^2 n^2 - \beta^2\right) e_z = 0 \qquad \text{(II-12a)}$$

$$\frac{\partial^2 h_z}{\partial r^2} + \frac{1}{r}\frac{\partial h_z}{\partial r} + \frac{1}{r^2}\frac{\partial^2 h_z}{\partial \phi^2} + \left(k^2 n^2 - \beta^2\right) h_z = 0 \qquad \text{(II-12b)}$$

As it can be seen from above, the equation for h_z has the same functional form of e_z. For this reason we can solve our problem by treating only one of the equations. Defining new variables we can rewrite Equations (II-12) as

$$\frac{\partial^2 e_z}{\partial R^2} + \frac{1}{R}\frac{\partial e_z}{\partial R} + \frac{1}{R^2}\frac{\partial^2 e_z}{\partial \phi^2} + U^2 e_z = 0; \quad 0 \le R < 1 \qquad \text{(II-13a)}$$

$$\frac{\partial^2 e_z}{\partial R^2} + \frac{1}{R}\frac{\partial e_z}{\partial R} + \frac{1}{R^2}\frac{\partial^2 e_z}{\partial \phi^2} - W^2 e_z = 0; \quad 1 < R < \infty \qquad \text{(II-13b)}$$

where R is the normalized radius $R = r/a$,

$$U = a\sqrt{k^2 n_{\text{core}}^2 - \beta^2} \quad \text{and} \qquad \text{(II-13c)}$$

$$W = a\sqrt{\beta^2 - k^2 n_{\text{clad}}^2} \qquad \text{(II-13d)}$$

It is also useful to define

$$V = ak\sqrt{n_{core}^2 - n_{clad}^2} = \sqrt{U^2 + W^2}. \qquad \text{(II-13e)}$$

The V-number defined above is a measure of the number of modes that propagate in the fiber. The lower it is, the lesser the number of propagating modes. On the other hand, the parameters U and W are a measure of how close to cut-off a particular mode is (we will see later on that each mode has a particular U and W values). Notice that their maximum value is V. A mode that is close to cut-off, has a U (W) value close to V (zero). In the same way, a mode that is further from cut-off, has a U (W) value close to zero (V).

Equations (II-13) can be separated into the equations

$$\frac{R^2}{F}\frac{d^2F}{dR^2} + \frac{R}{F}\frac{dF}{dR} + U^2R^2 = -\frac{1}{\Phi}\frac{d^2\Phi}{d\phi^2} = \nu^2; \quad 0 \le R < 1 \qquad \text{(II-14a)}$$

$$\frac{R^2}{F}\frac{d^2F}{dR^2} + \frac{R}{F}\frac{dF}{dR} - W^2R^2 = -\frac{1}{\Phi}\frac{d^2\Phi}{d\phi^2} = \nu^2; \quad 1 < R < \infty \qquad \text{(II-14b)}$$

where we have made $e_z = F(R)\Phi(\phi)$. By solving Equations (II-14) and imposing the condition of continuity of the longitudinal components across the interface, i.e., at $R = 1$ we finally find

$$e_z = A_{\nu,\mu}\frac{J_\nu(U_{\nu,\mu}R)}{J_\nu(U_{\nu,\mu})}f_\nu(\phi), \quad h_z = B_{\nu,\mu}\frac{J_\nu(U_{\nu,\mu}R)}{J_\nu(U_{\nu,\mu})}g_\nu(\phi); \quad 0 \le R < 1 \qquad \text{(II-15a)}$$

$$e_z = A_{\nu,\mu}\frac{K_\nu(W_{\nu,\mu}R)}{K_\nu(W_{\nu,\mu})}f_\nu(\phi),\quad h_z = B_{\nu,\mu}\frac{K_\nu(W_{\nu,\mu}R)}{K_\nu(W_{\nu,\mu})}g_\nu(\phi);\ 1 < R < \infty. \qquad \text{(II-15b)}$$

where

$$f_\nu(\phi) = \begin{cases}\cos(\nu\phi)\\ \\ \sin(\nu\phi)\end{cases};\qquad g_\nu(\phi) = \begin{cases}-\sin(\nu\phi) & \text{even modes}\\ \\ \cos(\nu\phi) & \text{odd modes}\end{cases}$$

$J_\nu(U_{\nu,\mu})$ and $K_\nu(W_{\nu,\mu})$ are the Bessel function and the modified Bessel function respectively.

The second subscripted index in A, U and W is consequence of further boundary conditions. We will see later that by imposing continuity of the tangential field components at the fiber interface we get an eigenvalue equation for each mode ν. The μ index arises because of the possibility of multiple roots in the eigenvalue equation. The double index notation is also carried along to the propagation constant β.

II-5 Solution of the Transverse Fields

Now we can determine the transverse components of the fields. They are found by substituting Equations (II-15) in (II-7) and (II-8). The final result is written below

$$e_r = \begin{cases} \dfrac{C_1 J_{\nu-1}(U_{\nu,\mu} R) - C_2 J_{\nu+1}(U_{\nu,\mu} R)}{J_\nu (U_{\nu,\mu})} f_\nu(\varphi) & 0 \le R \le 1 \\ \dfrac{U_{\nu,\mu}}{W_{\nu,\mu}} \dfrac{C_1 K_{\nu-1}(W_{\nu,\mu} R) + C_2 K_{\nu+1}(W_{\nu,\mu} R)}{K_\nu (W_{\nu,\mu})} f_\nu(\varphi) & 1 \le R < \infty \end{cases} \tag{II-16a}$$

$$e_\varphi = \begin{cases} \dfrac{C_1 J_{\nu-1}(U_{\nu,\mu} R) + C_2 J_{\nu+1}(U_{\nu,\mu} R)}{J_\nu (U_{\nu,\mu})} g_\nu(\varphi) & 0 \le R \le 1 \\ \dfrac{U_{\nu,\mu}}{W_{\nu,\mu}} \dfrac{C_1 K_{\nu-1}(W_{\nu,\mu} R) - C_2 K_{\nu+1}(W_{\nu,\mu} R)}{K_\nu (W_{\nu,\mu})} g_\nu(\varphi) & 1 \le R < \infty \end{cases} \tag{II-16b}$$

$$h_r = \begin{cases} \dfrac{C_3 J_{\nu-1}(U_{\nu,\mu} R) - C_4 J_{\nu+1}(U_{\nu,\mu} R)}{J_\nu (U_{\nu,\mu})} g_\nu(\varphi) & 0 \le R \le 1 \\ \dfrac{U_{\nu,\mu}}{W_{\nu,\mu}} \dfrac{C_5 K_{\nu-1}(W_{\nu,\mu} R) + C_6 K_{\nu+1}(W_{\nu,\mu} R)}{K_\nu (W_{\nu,\mu})} g_\nu(\varphi) & 1 \le R < \infty \end{cases} \tag{II-16c}$$

$$h_\phi = \begin{cases} \dfrac{C_3 J_{\nu-1}(U_{\nu,\mu} R) + C_4 J_{\nu+1}(U_{\nu,\mu} R)}{J_\nu (U_{\nu,\mu})} f_\nu(\varphi) & 0 \le R \le 1 \\ \dfrac{U_{\nu,\mu}}{W_{\nu,\mu}} \dfrac{C_5 K_{\nu-1}(W_{\nu,\mu} R) - C_6 K_{\nu+1}(W_{\nu,\mu} R)}{K_\nu (W_{\nu,\mu})} f_\nu(\varphi) & 1 \le R < \infty \end{cases} \tag{II-16d}$$

where

$$C_1 = \frac{i}{2aU_{\nu,\mu}} \left(\beta_{\nu,\mu} A_{\nu,\mu} - \sqrt{\frac{\mu_0}{\varepsilon_0}} k B_{\nu,\mu} \right);$$

$$C_2 = \frac{i}{2aU_{\nu,\mu}} \left(\beta_{\nu,\mu} A_{\nu,\mu} + \sqrt{\frac{\mu_0}{\varepsilon_0}} k B_{\nu,\mu} \right);$$

$$C_3 = \frac{i}{2aU_{\nu,\mu}} \left(\beta_{\nu,\mu} B_{\nu,\mu} - \sqrt{\frac{\varepsilon_0}{\mu_0}} k n_{core}^2 A_{\nu,\mu} \right);$$

$$C_4 = \frac{i}{2aU_{\nu,\mu}}\left(\beta_{\nu,\mu} B_{\nu,\mu} + \sqrt{\frac{\varepsilon_0}{\mu_0}}\, kn^2_{\text{core}}\, A_{\nu,\mu}\right);$$

$$C_5 = \frac{i}{2aU_{\nu,\mu}}\left(\beta_{\nu,\mu} B_{\nu,\mu} - \sqrt{\frac{\varepsilon_0}{\mu_0}}\, kn^2_{\text{clad}}\, A_{\nu,\mu}\right);$$

$$C_6 = \frac{i}{2aU_{\nu,\mu}}\left(\beta_{\nu,\mu} B_{\nu,\mu} + \sqrt{\frac{\varepsilon_0}{\mu_0}}\, kn^2_{\text{clad}}\, A_{\nu,\mu}\right).$$

As discussed before, the components of the fields in the region $R>1$ is termed the evanescent field.

The final solution reflects the existence of three kind of modes

1) Transverse Electric Modes (TE Modes), $\nu = 0$
2) Transverse Magnetic Modes (TM Modes), $\nu = 0$
3) Hybrid Modes (EH and HE Modes), $\nu \neq 0$.

TE Modes are modes whose e_z components are null. TM Modes has a longitudinal magnetic field h_z equal to zero. Hybrid Modes have both longitudinal electric and magnetic fields. They can be further classified in terms of relative amounts of E_z and H_z components [Snitzer, 1961].

II-6 Coefficients of Amplitude

We can find the ratio of the coefficients of amplitude $A_{\nu,\mu}$ and $B_{\nu,\mu}$ by applying the boundary condition of the transverse fields ϕ at the interface.

Using the continuity of e_ϕ at R= 1 we get

$$\frac{A_{\nu,\mu}}{B_{\nu,\mu}} = \frac{kU_{\nu,\mu}^2\, W_{\nu,\mu}^2}{\nu\, \beta_{\nu,\mu}\, V^2} \sqrt{\frac{\mu_0}{\varepsilon_0}} \left(\frac{1}{U_{\nu,\mu}} \frac{J_\nu'(U_{\nu,\mu})}{J_\nu(U_{\nu,\mu})} + \frac{1}{W_{\nu,\mu}} \frac{K_\nu'(W_{\nu,\mu})}{K_\nu(W_{\nu,\mu})} \right) \tag{II-17a}$$

Doing the same for the h_ϕ components we get

$$\frac{B_{\nu,\mu}}{A_{\nu,\mu}} = \frac{kU_{\nu,\mu}^2\, W_{\nu,\mu}^2}{\nu\, \beta_{\nu,\mu}\, V^2} \sqrt{\frac{\varepsilon_0}{\mu_0}} \left(\frac{n_{core}^2}{U_{\nu,\mu}} \frac{J_\nu'(U_{\nu,\mu})}{J_\nu(U_{\nu,\mu})} + \frac{n_{clad}^2}{W_{\nu,\mu}} \frac{K_\nu'(W_{\nu,\mu})}{K_\nu(W_{\nu,\mu})} \right). \tag{II-17b}$$

The prime in the above equations represent a derivative with respect to the argument. As seen from above, we can either use (II-17a) or (II-17b) in our field solutions. As discussed by Snyder et. al. [1983], the amplitude $A_{\nu,\mu}$ could be set equal to the unity. However, it is chosen for consistency with the weak-guidance approximation ($n_{core} \approx n_{clad}$). Following Snyder's normalization [Snyder et. al., 1983], we finally have

i) for TE Modes

$$e_r = e_z = h_\phi = 0 \tag{II-18a}$$

$$e_\phi = \begin{cases} -\dfrac{J_1(U_{0,\mu} R)}{J_1(U_{0,\mu})} & 0 \le R \le 1 \\ -\dfrac{K_1(W_{0,\mu} R)}{K_1(W_{0,\mu})} & 1 \le R < \infty \end{cases} \tag{II-18b}$$

$$h_r = \begin{cases} \sqrt{\frac{\varepsilon_0}{\mu_0}} \frac{\beta_{0,\mu}}{k} \frac{J_1(U_{0,\mu} R)}{J_1(U_{0,\mu})} & 0 \le R \le 1 \\ \sqrt{\frac{\varepsilon_0}{\mu_0}} \frac{\beta_{0,\mu}}{k} \frac{K_1(W_{0,\mu} R)}{K_1(W_{0,\mu})} & 1 \le R < \infty \end{cases} \qquad \text{(II-18c)}$$

$$h_z = \begin{cases} i \sqrt{\frac{\varepsilon_0}{\mu_0}} \frac{U_{0,\mu}}{ka} \frac{J_0(U_{0,\mu} R)}{J_1(U_{0,\mu})} & 0 \le R \le 1 \\ -i \sqrt{\frac{\varepsilon_0}{\mu_0}} \frac{W_{0,\mu}}{ka} \frac{K_0(W_{0,\mu} R)}{K_1(W_{0,\mu})} & 1 \le R < \infty \end{cases} \qquad \text{(II-18d)}$$

ii) for TM Modes

$$h_r = h_z = e_\phi = 0 \qquad \text{(II-19a)}$$

$$e_r = \begin{cases} \frac{J_1(U_{0,\mu} R)}{J_1(U_{0,\mu})} & 0 \le R \le 1 \\ \frac{n_{\text{core}}^2 K_1(W_{0,\mu} R)}{n_{\text{clad}}^2 K_1(W_{0,\mu})} & 1 \le R < \infty \end{cases} \qquad \text{(II-19b)}$$

$$e_z = \begin{cases} \frac{i U_{0,\mu}}{a \beta_{0,\mu}} \frac{J_0(U_{0,\mu} R)}{J_1(U_{0,\mu})} & 0 \le R \le 1 \\ -\frac{i n_{\text{core}}^2}{n_{\text{clad}}^2} \frac{W_{0,\mu}}{a \beta_{0,\mu}} \frac{K_0(W_{0,\mu} R)}{K_1(W_{0,\mu})} & 1 \le R < \infty \end{cases} \qquad \text{(II-19c)}$$

$$h_\phi = \begin{cases} \sqrt{\frac{\varepsilon_0}{\mu_0}} \frac{k\, n_{core}^2}{\beta_{0,\mu}} \frac{J_1(U_{0,\mu} R)}{J_1(U_{0,\mu})} & 0 \le R \le 1 \\ \sqrt{\frac{\varepsilon_0}{\mu_0}} \frac{k\, n_{core}^2}{\beta_{0,\mu}} \frac{K_1(W_{0,\mu} R)}{K_1(W_{0,\mu})} & 1 \le R < \infty \end{cases} \qquad \text{(II-19d)}$$

iii) for Hybrid Modes

$$e_r = \begin{cases} -\frac{a_1 J_{\nu-1}(U_{\nu,\mu} R) + a_2 J_{\nu+1}(U_{\nu,\mu} R)}{J_\nu(U_{\nu,\mu})} f_\nu(\varphi) & 0 \le R \le 1 \\ -\frac{U_{\nu,\mu}}{W_{\nu,\mu}} \frac{a_1 K_{\nu-1}(W_{\nu,\mu} R) - a_2 K_{\nu+1}(W_{\nu,\mu} R)}{K_\nu(W_{\nu,\mu})} f_\nu(\varphi) & 1 \le R < \infty \end{cases} \qquad \text{(II-20a)}$$

$$e_\varphi = \begin{cases} -\frac{a_1 J_{\nu-1}(U_{\nu,\mu} R) - a_2 J_{\nu+1}(U_{\nu,\mu} R)}{J_\nu(U_{\nu,\mu})} g_\nu(\varphi) & 0 \le R \le 1 \\ -\frac{U_{\nu,\mu}}{W_{\nu,\mu}} \frac{a_1 K_{\nu-1}(W_{\nu,\mu} R) + a_2 K_{\nu+1}(W_{\nu,\mu} R)}{K_\nu(W_{\nu,\mu})} g_\nu(\varphi) & 1 \le R < \infty \end{cases} \qquad \text{(II-20b)}$$

$$e_z = \begin{cases} -\frac{iU_{\nu,\mu}}{a\,\beta_{\nu,\mu}} \frac{J_\nu(U_{\nu,\mu} R)}{J_\nu(U_{\nu,\mu})} f_\nu(\varphi) & 0 \le R \le 1 \\ -\frac{iU_{\nu,\mu}}{a\,\beta_{\nu,\mu}} \frac{K_\nu(W_{\nu,\mu} R)}{K_\nu(W_{\nu,\mu})} f_\nu(\varphi) & 1 \le R < \infty \end{cases} \qquad \text{(II-20c)}$$

$$h_r = \begin{cases} \sqrt{\frac{\varepsilon_0}{\mu_0}} \frac{k n_{core}^2}{\beta_{\nu,\mu}} \frac{a_3 J_{\nu-1}(U_{\nu,\mu} R) - a_4 J_{\nu+1}(U_{\nu,\mu} R)}{J_\nu(U_{\nu,\mu})} g_\nu(\varphi) & 0 \le R \le 1 \\ \sqrt{\frac{\varepsilon_0}{\mu_0}} \frac{k n_{core}^2}{\beta_{\nu,\mu}} \frac{U_{\nu,\mu}}{W_{\nu,\mu}} \frac{a_5 K_{\nu-1}(W_{\nu,\mu} R) + a_6 K_{\nu+1}(W_{\nu,\mu} R)}{K_\nu(W_{\nu,\mu})} g_\nu(\varphi) & 1 \le R < \infty \end{cases} \qquad \text{(II-20d)}$$

$$h_\phi = \begin{cases} -\sqrt{\frac{\varepsilon_0}{\mu_0}}\,\frac{kn_{core}^2}{\beta_{\nu,\mu}}\,\frac{a_3 J_{\nu-1}(U_{\nu,\mu}R) + a_4 J_{\nu+1}(U_{\nu,\mu}R)}{J_\nu(U_{\nu,\mu})} f_\nu(\varphi) & 0 \le R \le 1 \\ -\sqrt{\frac{\varepsilon_0}{\mu_0}}\,\frac{kn_{core}^2}{\beta_{\nu,\mu}}\,\frac{U_{\nu,\mu}}{W_{\nu,\mu}}\,\frac{a_5 K_{\nu-1}(W_{\nu,\mu}R) - a_6 K_{\nu+1}(W_{\nu,\mu}R)}{K_\nu(W_{\nu,\mu})} f_\nu(\varphi) & 1 \le R < \infty \end{cases} \tag{II-20e}$$

$$h_z = \begin{cases} -i\sqrt{\frac{\varepsilon_0}{\mu_0}}\,\frac{U_{\nu,\mu}F_2}{ka}\,\frac{J_\nu(U_{\nu,\mu}R)}{J_\nu(U_{\nu,\mu})} g_\nu(\varphi) & 0 \le R \le 1 \\ -i\sqrt{\frac{\varepsilon_0}{\mu_0}}\,\frac{U_{\nu,\mu}F_2}{ka}\,\frac{K_\nu(W_{\nu,\mu}R)}{K_\nu(W_{\nu,\mu})} g_\nu(\varphi) & 1 \le R < \infty \end{cases} \tag{II-20f}$$

where

$$a_1 = \frac{(F_2 - 1)}{2};\ a_2 = \frac{(F_2 + 1)}{2};$$

$$a_3 = \frac{(F_1 - 1)}{2};\ a_4 = \frac{(F_1 + 1)}{2};$$

$$a_5 = \frac{F_1}{2} - \frac{1}{2}\left(\frac{n_{clad}}{n_{core}}\right)^2;\quad a_6 = \frac{F_1}{2} + \frac{1}{2}\left(\frac{n_{clad}}{n_{core}}\right)^2;$$

$$F_1 = \left(\frac{U_{\nu,\mu}W_{\nu,\mu}}{V}\right)^2 \frac{b_1 + (n_{clad}/n_{core})^2 b_2}{\nu};\qquad F_2 = \left(\frac{V}{U_{\nu,\mu}W_{\nu,\mu}}\right)^2 \frac{\nu}{b_1 + b_2};$$

$$b_1 = \frac{1}{2U_{\nu,\mu}}\left\{\frac{J_{\nu-1}(U_{\nu,\mu})}{J_\nu(U_{\nu,\mu})} - \frac{J_{\nu+1}(U_{\nu,\mu})}{J_\nu(U_{\nu,\mu})}\right\}$$

and

$$b_2 = -\frac{1}{2W_{\nu,\mu}}\left\{\frac{K_{\nu-1}(W_{\nu,\mu})}{K_\nu(W_{\nu,\mu})} + \frac{K_{\nu+1}(W_{\nu,\mu})}{K_\nu(W_{\nu,\mu})}\right\}.$$

Our problem will have solution only if the inverse of (II-17b) is equal to

(II-17a). This equality leads us to the eigenvalue equation and is discussed in the next section.

II-7 The Eigenvalue Equations

Right now we still do not know how to find the eigenvalues $\beta_{\nu,\mu}$, $U_{\nu,\mu}$ and $W_{\nu,\mu}$. For the TM and TE modes they can be found in a straightforward way just by imposing continuity of the z-components of the fields at the interface ($R=1$). For the hybrid modes the eigenvalue equation is found from Equations (II-17). The resulting equations are transcendental in their arguments and are solved through numerical or graphical techniques. These equations, referred as the *eigenvalue equations* are displayed below for each mode [Snyder et. al., 1983; Snitzer, 1961].

i) TE Modes (continuity of h_z)

$$U_{0,\mu}\frac{J_0(U_{0,\mu})}{J_1(U_{0,\mu})} + W_{0,\mu}\frac{K_0(W_{0,\mu}R)}{K_1(W_{0,\mu})} = 0 \qquad \text{(II-21a)}$$

ii) TM Modes (continuity of e_z)

$$U_{0,\mu}\frac{J_0(U_{0,\mu})}{J_1(U_{0,\mu})} + W_{0,\mu}\frac{n_{\text{core}}^2}{n_{\text{clad}}^2}\frac{K_0(W_{0,\mu})}{K_1(W_{0,\mu})} = 0 \qquad \text{(II-21b)}$$

iii) Hybrid Modes (Equations (II-17))

$$\left(\frac{J_\nu'(U_{\nu,\mu})}{U_{\nu,\mu} J_\nu(U_{\nu,\mu})} + \frac{n_{clad}^2}{n_{core}^2} \frac{K_\nu'(W_{\nu,\mu})}{W_{\nu,\mu} K_\nu(W_{\nu,\mu})}\right) \times$$

$$\left(\frac{J_\nu'(U_{\nu,\mu})}{U_{\nu,\mu} J_\nu(U_{\nu,\mu})} + \frac{K_\nu'(W_{\nu,\mu})}{W_{\nu,\mu} K_\nu(W_{\nu,\mu})}\right) = \left(\frac{\nu\beta_{\nu,\mu}}{kn_{core}}\right)^2 \left(\frac{V}{U_{\nu,\mu} W_{\nu,\mu}}\right)^4 \quad . \text{(II-21c)}$$

Equations (II-21) can be solved numerically with the help of Equations (II-13c), (II-13d) and (II-13e).

It was pointed out by Snítzer [1961] that Equation (II-21c) is quadratic in

$$\frac{J_\nu'(U_{\nu,\mu})}{U_{\nu,\mu} J_\nu(U_{\nu,\mu})}. \qquad \text{(II-22)}$$

Treating (II-22) as an independent variable, Equation (II-21c) can be broken down in two sets of solutions; one of them corresponds to the HE modes and the other to the EH modes. Their form is rather complicated and will not be displayed here.

II-8 Weakly Guiding Fibers

By definition, a weakly guiding fiber is a fiber which has an index of refraction of the core approximately equal to the index of refraction of the cladding [Snyder, 1983; Marcuse, 1974]

$$kn_{core} \approx kn_{clad} \approx \beta. \qquad \text{(II-22)}$$

Such fiber is almost similar to an unbound uniform medium. Being such it is a good approximation to assume that its fields are quasi Transverse Electromagnetic, quasi TEM, field. For this reason we use the quasi TEM approximation or

$$e_z \approx h_z \approx 0 \tag{II-23}$$

to solve the wave equation for the transverse fields. Using Equations (II-22) and (II-23) in the vector wave equation and solving it for the Cartesian components of the fields, we find that the transverse fields become solutions of the so called *scalar wave equation*. We want the results of the weakly guiding fiber only for posterior comparison with the exact solution. For this reason, we will limit ourselves to display them here [Snyder et. al., 1983]

i) $HE_{\lambda+1,\mu}$ Modes ($\nu=\lambda+1$, $\lambda \geq 0$)

$$e_{tan} = \begin{cases} (\hat{x}\cos\lambda\phi - \hat{y}\sin\lambda\phi)F_\lambda(R)\,; & \text{even} \\ (\hat{x}\sin\lambda\phi + \hat{y}\cos\lambda\phi)F_\lambda(R)\,; & \text{odd} \end{cases} \tag{II-24a}$$

ii) Transverse Modes ($\nu=0$, $\lambda=1$)

$$e_{tan} = \begin{cases} (\hat{x}\cos\phi + \hat{y}\sin\phi)F_1(R)\,; & \text{TM} \\ (\hat{x}\sin\phi - \hat{y}\cos\phi)F_1(R)\,; & \text{TE} \end{cases} \tag{II-24b}$$

iii) $EH_{\lambda+1,\mu}$ Modes ($\nu=\lambda-1$, $\lambda>1$)

$$e_{\tan} = \begin{cases} (\hat{x}\cos\lambda\phi + \hat{y}\sin\lambda\phi)F_\lambda(R)\ ; & \text{even} \\ (\hat{x}\sin\lambda\phi - \hat{y}\cos\lambda\phi)F_\lambda(R)\ ; & \text{odd} \end{cases} \tag{II-24c}$$

where

$$F_\lambda(R) = \begin{cases} \dfrac{J_\lambda\left(\widetilde{U}_{\lambda,\mu}\,R\right)}{J_\lambda\left(\widetilde{U}_{\lambda,\mu}\right)}\ ; & 0 \le R \le 1 \\ \dfrac{K_\lambda\left(\widetilde{W}_{\lambda,\mu}\,R\right)}{K_\lambda\left(\widetilde{W}_{\lambda,\mu}\right)}\ ; & 1 \le R < \infty \end{cases}$$

The longitudinal z-components are almost zero and will not be displayed here. The eigenvalue equation for the weakly guiding fiber is

$$\widetilde{U}_{\lambda,\mu}\frac{J_{\lambda+1}\left(\widetilde{U}_{\lambda,\mu}\right)}{J_\lambda\left(\widetilde{U}_{\lambda,\mu}\right)} = \widetilde{W}_{\lambda,\mu}\frac{K_{\lambda+1}\left(\widetilde{W}_{\lambda,\mu}\right)}{K_\lambda\left(\widetilde{W}_{\lambda,\mu}\right)} \tag{II-25}$$

where

$$V = \sqrt{\widetilde{U}_{\lambda,\mu}^2 + \widetilde{W}_{\lambda,\mu}^2}\ .$$

The tilde in the eigenvalues was introduced in order to distinguish between the eigenvalues of the exact solution and the eigenvalues of the weakly guiding. The transverse magnetic fields can be found from

$$h_{\tan} \equiv n_{\text{core}}\sqrt{\frac{\varepsilon_o}{\mu_o}}\,\hat{z}\times e_{\tan}. \tag{II-26}$$

III. POWER INJECTION DUE TO SOURCES DISTRIBUTION

III-1 Introduction

Fluorescent sources distributed in the cladding radiate incoherent light and can be modeled as radiating current dipoles with random phase and orientation [Christensen et. al., 1989; Snitzer, 1961; Marcuse, 1988; 1975]. As stated before, the total field injected into the core by these sources can be expressed as a sum over the bound modes. Each mode having an amplitude coefficient, $c_{\nu,\mu}$ or

$$E = \sum_{\nu,\mu} c_{\nu,\mu}\, e_{\nu,\mu} \ . \tag{III-1}$$

Since the total field is excited by the current distribution j in the cladding, it is natural to expect that the amplitude coefficients, $c_{\nu,\mu}$ are related to j. Before deriving such a relationship, we will introduce a very important theorem: the reciprocity theorem. With the help of Maxwell's Equations and the previous theorem, the amplitude coefficient follows [Snyder et. al., 1983]. Next we present a general equation for the power efficiency of a cylindrical fiber with sources distributed in its cladding [Marcuse, 1988; 1975]. Finally, we derive the power efficiency of a cylindrical optical fiber whose fields obey

Equations (II-18) thru (II-20) and compare our results to the weakly guiding results of Marcuse [1988]. Our expressions are derived for the positively guiding fiber for two different distributions:

1) sources uniformly distributed in the cladding and
2) thin film sources distribution.

For further applications of the reciprocity theorem, the reader should refer to Snyder et. al. [1983].

III-2 The Reciprocity Theorem (Conjugated Form)

The conjugated form of the Reciprocity Theorem can be derived by defining a vector function F_c

$$F_c = E \times \overline{H}^* + \overline{E}^* \times H \tag{III-2}$$

where * denotes complex conjugated. The unbarred fields satisfy Maxwell Equations with density current j or [Snyder et. al.,1983]

$$\nabla \times E = i\sqrt{\frac{\mu_o}{\varepsilon_o}}k\, H \tag{III-3a}$$

$$\nabla \times H = j - i\sqrt{\frac{\varepsilon_o}{\mu_o}}k\, n^2 E \tag{III-3b}$$

The barred fields satisfy the conjugated form of those equations or

$$\nabla \times \overline{E}^{*} = -i\sqrt{\frac{\mu_o}{\varepsilon_o}}\, k\, \overline{H}^{*} \qquad \text{(III-4a)}$$

$$\nabla \times \overline{H}^{*} = \bar{j}^{*} + i\sqrt{\frac{\varepsilon_o}{\mu_o}}\, k\, (\overline{n}^{*})^2\, \overline{E}^{*} \,. \qquad \text{(III-4b)}$$

Using the identity for the divergence of two vectors we find

$$\nabla . F_c = \overline{H}^{*} . (\nabla \times . E) - E . (\nabla \times \overline{H}^{*}) - \overline{E}^{*} . (\nabla \times \overline{H}^{*}) + H . (\nabla \times \overline{E}^{*}) \,. \qquad \text{(III-5)}$$

Substituting (III-4) in (III-5) we get

$$\nabla . F_c = -(\overline{E}^{*} . j + E \;\; . \bar{j}^{*}) - i\sqrt{\frac{\varepsilon_o}{\mu_o}}\, k\, ((\overline{n}^{*})_2 - n^2) E . \overline{E}^{*} \qquad \text{(III-6)}$$

Applying the two-dimensional form of the divergence theorem to Equation (III-6) we have

$$\int_S \nabla . F_c \, dS = \frac{\partial}{\partial z} \int_S F_c . \hat{z} dS + \oint_l F_c . \hat{n} dl \,. \qquad \text{(III-7)}$$

If we take S as the infinity cross-section of the cylindrical fibre, S_∞, the line integral then has to be taken along the circle $r \to \infty$, where r is the cylindrical radius. Far from the core/cladding boundary, the amplitude of the fields of the bound modes fall-off exponentially consequently, at $r \to \infty$, the line integral is null. Equation (III-7) reduces to [Snyder et. al., 1983]

$$\int_{S_\infty} \nabla . F_c \, dS = \frac{\partial}{\partial z} \int_{S_\infty} F_c \, . \hat{z} dS \quad . \tag{III-8}$$

Equation (III-8) is the conjugated form of the reciprocity theorem. It relates the fields of two different fibers with indices of refraction n and $\bar{n}$ and current distribution j and $\bar{j}$ respectively.

III-3 Excitation by Current Sources

As it was stated before, the reciprocity theorem relates the fields of two different fibers. By knowing the fields of one fiber we may determine the fields in another. In our case, we would like to determine the forward propagating fields, E and H of a step profile fiber with sources distributed in it (Figure III-1). This fiber has a determined current distribution j and an index profile n. We choose a reference fiber with barred fields $\bar{E}$ and $\bar{H}$, a current distribution $\bar{j} = 0$ and an index profile $\bar{n} = n$. Such reference fiber has a field solution given by Equations (II-18), (II-19) and (II-20) [Snyder et. al. 1983]. Written in another way, we have

$$\bar{E} = e_{\nu,\mu} \exp\left(i\beta_{\nu,\mu} z\right); \quad \bar{H} = h_{\nu,\mu} \exp\left(i\beta_{\nu,\mu} z\right). \tag{III-9}$$

With the results above we can rewrite (III-6) and substitute it in (III-8). Doing that we obtain

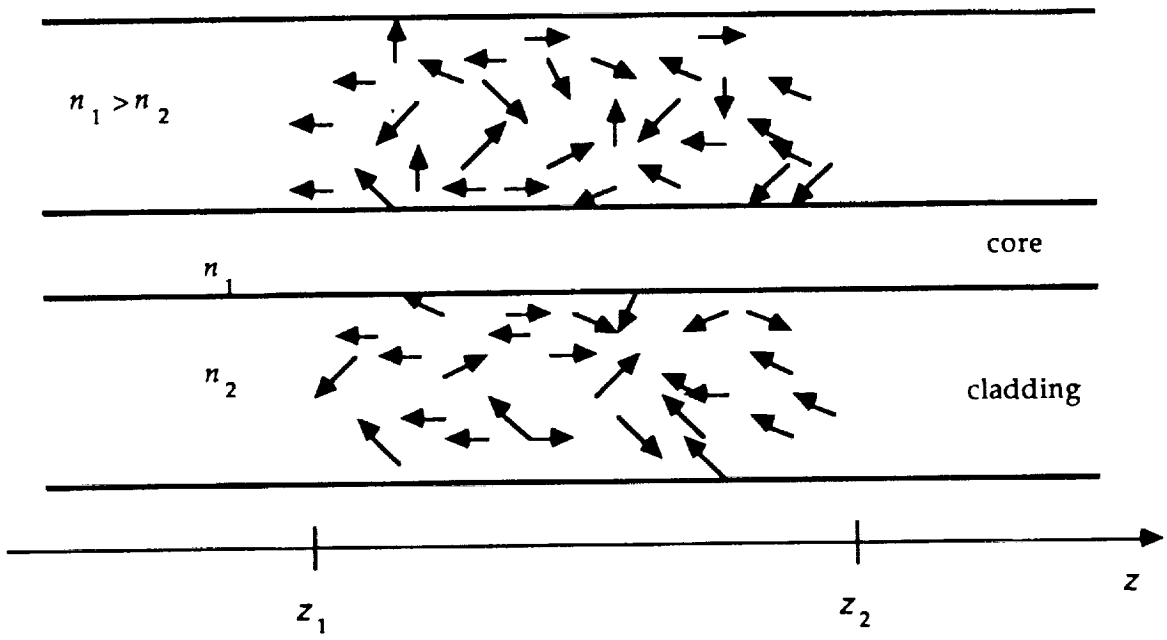

Figure III-1. Sources in the cladding can be treated as current dipole vectors (arrows). Fluorescent molecules can be modeled as dipoles with random phase and orientation.

$$\frac{\partial}{\partial z}\int_{S_\infty} F_c \cdot \hat{z}\, dS = -\int_{S_\infty} e^*_{\nu,\mu} \cdot j\, \dot{e}\exp\left(-i\beta_{\nu,\mu} z\right) dS . \qquad \text{(III-10)}$$

The expansion coefficient in Equation (III-1) is a function of z in the region $z_1 < z < z_2$ and constant outside it. Substituting Equations (III-1) and (III-2) into Equation (III-10) and using the orthogonality condition

$$\int_{S_\infty} \left(e_{\nu,\mu} \times h^*_{\alpha,\beta}\right) \cdot \hat{z}\, dS = \int_{S_\infty} \left(e^*_{\nu,\mu} \times h_{\alpha,\beta}\right) \cdot \hat{z}\, dS = 0 ; \quad \begin{matrix} \nu \neq \alpha \\ \text{or} \\ \mu \neq \beta \end{matrix} \qquad \text{(III-11)}$$

we find

$$\frac{dc_{\nu,\mu}(z)}{dz} = -\frac{1}{4P_{\nu,\mu}} \int_{S_\infty} e^*_{\nu,\mu} \cdot j\, \exp\left(-i\beta_{\nu,\mu} z\right) dS \qquad \text{(III-12)}$$

where $P_{\nu,\mu}$ is the normalization constant given by

$$P_{\nu,\mu} = \frac{1}{2}\left|\int_{S_\infty} \left(e_{\nu,\mu} \times h^*_{\nu,\mu}\right) \cdot \hat{z}\, dS\right| . \qquad \text{(III-13)}$$

Finally integrating Equation (III-12) we get

$$c_{\nu,\mu}(z) = \begin{cases} 0\,; & z \le z_1 \\ -\dfrac{1}{4P_{\nu,\mu}} \displaystyle\int_{z_1}^{z} \int_{S} \underline{e}^{*}_{\nu,\mu} \cdot \underline{j}\, \exp\left(-i\beta_{\nu,\mu} z\right) dS\, dz & z_1 \le z \le z_2 \\ -\dfrac{1}{4P_{\nu,\mu}} \displaystyle\int_{V_{source}} \underline{e}^{*}_{\nu,\mu} \cdot \underline{j}\, \exp\left(-i\beta_{\nu,\mu} z\right) dV & z \ge z_2 \end{cases} \qquad \text{(III-14)}$$

which is a result obtained by Snyder et. al. [1983].

In any experiment, we should expect to collect the light in a region far away from the sources. Consequently, in the above result, we are specifically interested in the region $z \ge z_2$. A slightly different expression can be obtained for backward propagating modes.

III-4 Power Injected into Bound Modes

The power carried by each mode can be expressed in terms of the amplitude and the normalization coefficients and written as

$$|c_{\nu,\mu}|^2 P_{\nu,\mu} \qquad \text{(III-15)}$$

Taking the sum over all modes of the previous expression, we get the total power due to the bound modes, P_{core}[Snyder et. al., 1983; Marcuse, 1988]

$$P_{core} = \sum_{\nu,\mu} |c_{\nu,\mu}|^2 P_{\nu,\mu} \qquad \text{(III-16)}$$

Since there are many sources distributed in the cladding and they have random phase and orientation, we can rewrite Equation (III-16) as

$$\langle P_{core} \rangle = \sum_{\nu,\mu} \langle |c_{\nu,\mu}|^2 \rangle P_{\nu,\mu} \qquad \text{(III-17)}$$

which is the ensemble average of the total power of the field [Marcuse, 1988].

Equations (III-14) and (III-17) provide some clues on the characteristics of the amplitude of the injected modes. For instance, if j has only a z-component, the TE modes will not propagate. In the same way, if the z-component of the electric field of a particular mode is small, so will be the contribution of this mode to P_{core} (the TM_0 mode of the anti-symmetric slab is a good example [Christensen et. al., 1989]). On the other hand, we could also choose the direction of j with respect to $e_{\nu,\mu}$ in such a way to maximize P_{core} However, a more realistic model for fluorescent sources is a random distribution where there is no preferred direction of orientation[Marcuse, 1988; Christensen et.

al., 1989]. In this case, we should expect every mode to be excited.

As discussed before we should consider only that portion of the amplitude coefficient which is at the region $z \geq z_2$. Rewriting it we have

$$c_{\nu,\mu} = -\frac{1}{4P_{\nu,\mu}} \int_{V_{source}} e^{*}_{\nu,\mu} \cdot j \, \exp\left(-i\beta_{\nu,\mu} z\right) dV. \qquad \text{(III-18)}$$

The ensemble average of the square of the modulus of the amplitude coefficient follows

$$\left\langle |c_{\nu,\mu}|^2 \right\rangle = \frac{1}{16P^2_{\nu,\mu}} \left\langle \int_{V_{source}} e^{*}_{\nu,\mu}(r) \cdot j\,(r)\, dV \int_{V'_{source}} e_{\nu,\mu}(r') \cdot j^{*}(r')\, dV' \right\rangle . \qquad \text{(III-19)}$$

Rearranging Equation (III-19), we get

$$\left\langle |c_{\nu,\mu}|^2 \right\rangle = \frac{1}{16P^2_{\nu,\mu}} \left\langle \iint_{V_{source}} e^{*}_{\nu,\mu}(r) \cdot \left(j\,(r)\, j^{*}(r')\right) \cdot e_{\nu,\mu}(r')\, dV\, dV' \right\rangle . \qquad \text{(III-20)}$$

The quantity between parenthesis is a tensor of second rank. It can be represented by the matrix

$$\left\langle |c_{\nu,\mu}|^2 \right\rangle = \frac{1}{16P^2_{\nu,\mu}} \left\langle \iint_{V_{source}} e^{*}_{\nu,\mu}(r) \cdot \left(j\,(r)\, j^{*}(r')\right) \cdot e_{\nu,\mu}(r')\, dV\, dV' \right\rangle . \qquad \text{(III-21)}$$

Equation (III-20) can be further expressed as

$$\left\langle |c_{\nu,\mu}|^2 \right\rangle = \frac{1}{16 P_{\nu,\mu}^2} \iint_{V_{\text{source}}} e_{\nu,\mu}^*(r) \cdot \left\langle j(r)\, j^*(r') \right\rangle \cdot e_{\nu,\mu}(r')\, dV\, dV' \qquad \text{(III-22)}$$

Equation (III-22) was previously obtained by Marcuse [1975]. The term

$$\left\langle j(r)\, j^*(r') \right\rangle$$

is the ensemble average of the current density tensor over many similar systems [Marcuse, 1988]. The current source is composed of many randomly phased and oriented dipoles. Being randomly phased and oriented, the components of j are uncorrelated. This makes the off-diagonal terms of the matrix null or

$$\left\langle j(r)\, j^*(r') \right\rangle = \begin{pmatrix} \left\langle j_x(r)\, j_x^*(r') \right\rangle & 0 & 0 \\ 0 & \left\langle j_y(r)\, j_y^*(r') \right\rangle & 0 \\ 0 & 0 & \left\langle j_z(r)\, j_z^*(r') \right\rangle \end{pmatrix}. \qquad \text{(III-23a)}$$

In the same way, similar components of j are also uncorrelated at different positions or, $j_i(r)$ and $j_i(r')$ ($i = x, y$ and z), are uncorrelated at $r \neq r'$. This makes the diagonal terms proportional to the Dirac delta function or

$$\left\langle j_i(r)\, j_i^*(r') \right\rangle \propto |j_i(r)|^2\, \delta(r - r');\ i = x, y, z\ . \qquad \text{(III-23b)}$$

Since there is no preferred direction of orientation, each component of j contribute the same amount to our result or

$$|j_x| = |j_y| = |j_z| \,. \tag{III-23c}$$

This makes all diagonal terms in the matrix equal to each other. So we can *assume* Equation (III-23a) to be proportional to the unitary tensor $\mathbf{I}$. Thus we can write it as [Marcuse, 1975; 1988]

$$\langle j\,(r)\; j^{*}\,(r')\rangle = S\;\mathbf{I}\,\delta(r - r') \,. \tag{III-23d}$$

Where S is the source strength. Substituting Equation (III-23d) into Equation (III-22) we get [Marcuse, 1975; 1988]

$$\langle |c_{\nu,\mu}|^2 \rangle = \frac{1}{16 P_{\nu,\mu}^2} \int_{V_{\text{source}}} S\;|e_{\nu,\mu}(r)|^2 dV \tag{III-24}$$

which, in conjunction with Equation (III-17), can be used to find the power injected into bound modes

$$P_{\text{core}} = \sum_{\nu,\,\mu} \frac{1}{16 P_{\nu,\mu}} \int_{V_{\text{source}}} S\;|e_{\nu,\mu}(r)|^2\, dV \,. \tag{III-25}$$

Equation (III-24) can also be used to find the ensemble average of the amplitude coefficient of a continuum set of modes.

III-5 Total Power Radiated

In this section we will derive an expression for the total power radiated by the sources in the cladding. The sources are assumed to be already excited. They are distributed uniformly in the cladding between the inner radius r_{in} and the outer radius r_{out} (Figure III-2) in such a way that $a \le r_{in} < r_{out} \le b$. The excited radiation is incoherent and its associated fields can be represented by an integral over a continuum of plane-wave modes. They can be expressed as [Marcuse, 1975; 1974]

$$E_{\kappa,\sigma} = \frac{1}{2\pi}\sqrt{\frac{2\omega\mu_o P_{\kappa,\sigma}}{\beta_{\kappa,\sigma}}}\exp\left(-i\mathbf{k}_{\kappa,\sigma}\cdot\mathbf{r}\right)\hat{\mathbf{e}}_{\kappa,\sigma} \qquad \text{(III-26a)}$$

$$H_{\kappa,\sigma} = \frac{1}{2\pi}\sqrt{\frac{2\omega\mu_o P_{\kappa,\sigma}}{\beta_{\kappa,\sigma}}}\exp\left(-i\mathbf{k}_{\kappa,\sigma}\cdot\mathbf{r}\right)\frac{\mathbf{k}_{\kappa,\sigma}\times\hat{\mathbf{e}}_{\kappa,\sigma}}{\omega\mu_o} \qquad \text{(III-26b)}$$

where ω is the angular frequency, $P_{\kappa,\sigma}$ is the mode normalization, $\hat{\mathbf{e}}_{\kappa,\sigma}$ is the unit vector that determine the direction of $E_{\kappa,\sigma}$, $\mathbf{k}_{\kappa,\sigma}$ is the propagation vector and κ, σ and β are the x, y and z-components of the propagation vector respectively.

The total power radiated is written as an integral over the continuum of modes [Marcuse, 1975; 1974]. Its form is similar to its discrete counterpart, Equation (III-17), and can be expressed as

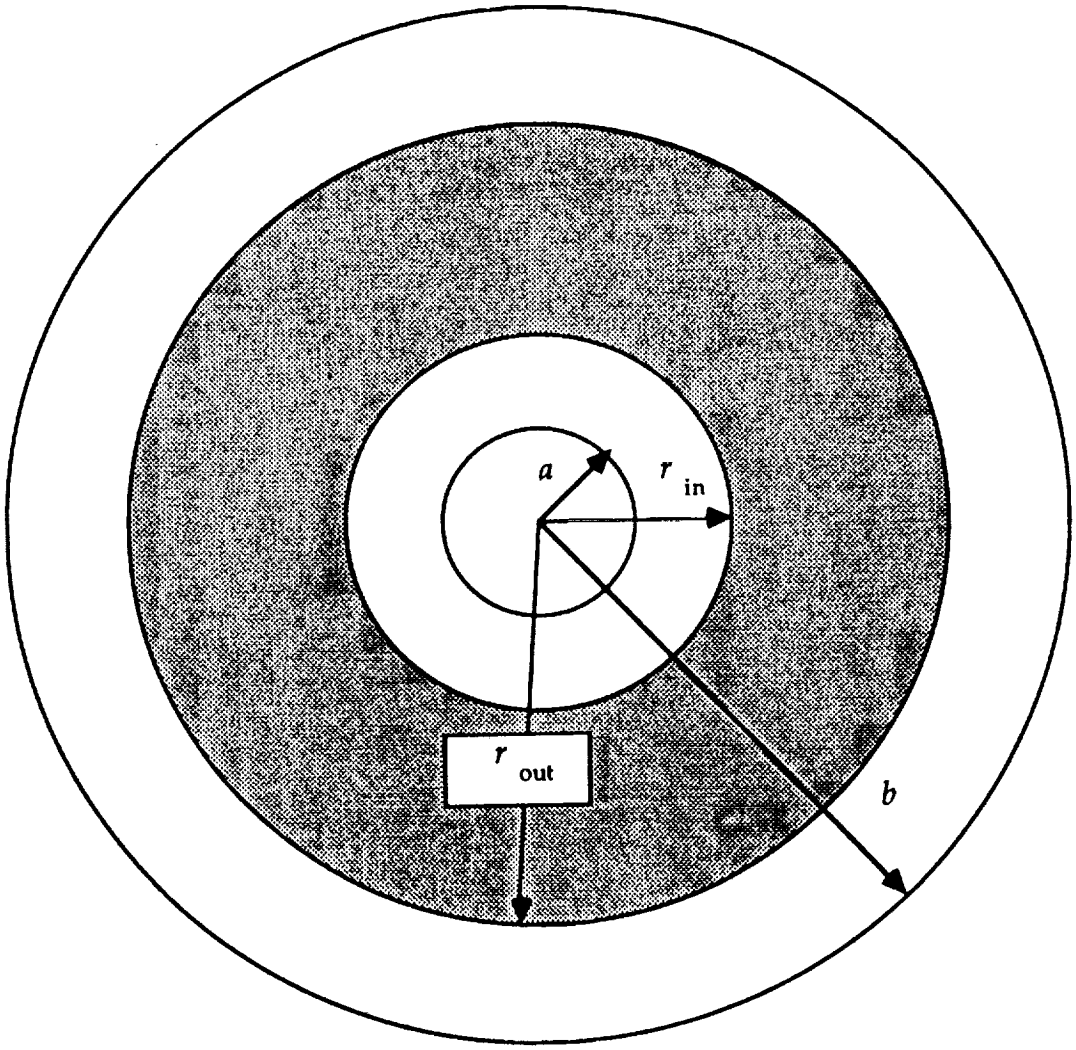

Figure III-2. Sources uniformly distributed between radius r_{in} and r_{out} ($a \leq r_{in} < r_{out} \leq b$).

$$P_{rad} = 2\iint_{-\infty}^{\infty} \langle |c(\kappa,\sigma)|^2 \rangle P_{\kappa,\sigma}\, d\kappa d\sigma \qquad \text{(III-27)}$$

where $\langle |c(\kappa,\sigma)|^2 \rangle$ is the ensemble average of the square of the modulus of the amplitude coefficient of the excited modes. It is given by [Marcuse, 1975]

$$\langle |c(\kappa,\sigma)|^2 \rangle = \frac{1}{16 P_{\kappa,\sigma}^2} \int_{V_{source}} S\ |E_{\kappa,\sigma}(r)|^2 dV\,. \qquad \text{(III-28)}$$

The factor of 2 in Equation (III-27) accounts for two possible polarizations of the transverse electromagnetic wave (TEM) [Jackson, 1975; Marcuse, 1975]. The z-component of the propagation constant is a function of the other components or [Marcuse, 1975]

$$\beta = \sqrt{k^2 n^2 - \kappa^2 - \sigma^2} \qquad \text{(III-29)}$$

where k is the circular wave-number of the free-space excited radiation and n is the index of refraction of the cladding material.

Substituting (III-26a) in (III-28) and assuming a cylindrical distribution of sources with inner radius r_{in} and outer radius r_{out}, we get

$$P_{\kappa,\sigma} \langle |c(\kappa,\sigma)|^2 \rangle = \frac{\omega \mu_o}{32\pi^2} \frac{S}{\beta_{\kappa,\sigma}} L\, \pi \left(r_{out}^2 - r_{in}^2\right). \qquad \text{(III-30)}$$

In the above formula, L, is the length of the fiber along which the fluorescent sources are distributed.

We can find the total power radiated by substituting Equation (III-30) in (III-27) or

$$P_{rad} = 2\frac{\omega\mu_o}{32\pi^2} SL\,\pi\left(r_{out}^2 - r_{in}^2\right)\int\int_{-\infty}^{\infty}\frac{1}{\beta_{\kappa,\sigma}}\,d\kappa\,d\sigma\,. \qquad \text{(III-31)}$$

Equation (III-31) can be easily solved if we express the components of the propagation vector in a spherical coordinate system. In this system the components are expressed as

$$\kappa = n\,k\sin\theta\cos\phi, \qquad \sigma = n\,k\sin\theta\sin\phi, \qquad \beta_{\kappa,\sigma} = n\,k\cos\theta \qquad \text{(III-32a)}$$

$$d\kappa\,d\sigma = (n\,k)^2\cos\theta\sin\theta\,d\theta\,d\phi\,. \qquad \text{(III-32b)}$$

Substituting Equations (III-32) into (III-31) we finally get [Marcuse, 1975; 1988]

$$P_{rad} = \frac{\omega\mu_o}{4} nkSL\left(r_{out}^2 - r_{in}^2\right)\,. \qquad \text{(III-33)}$$

Using Equations (III-33) and (III-25) and writing the angular frequency in terms of the propagation constant, we find the power efficiency

$$\frac{P_{core}}{P_{rad}} = \frac{\sqrt{\varepsilon_o/\mu_o}}{4\left(r_{out}^2 - r_{in}^2\right) n_{clad} k^2 L} \sum_{\nu,\mu} \frac{1}{P_{\nu,\mu}} \int_{V_{source}} \left| e_{\nu,\mu}(r) \right|^2 dV \qquad \text{(III-34)}$$

where the terms inside the sum are due to the bound modes.

Notice that the above result is independent of the cladding radius b. This occurs because of the infinite cladding assumption used in the derivation of the fields in Chapter II. However, later on for the bulk distribution, we will make $r_{out}=b$. Notice that this *does not* mean that the power efficiency is a function of the cladding radius b but a function of the outer radius of the source distribution.

III-6 Power Efficiency

For the exact case, the integral in Equation (III-34) is different for each mode. They involve the integration of the product of the normalized radius by the square of the Bessel K_n function or $RK_n^2(W_{\nu,\mu}R)$ which is tabulated. The normalizations follow from Snyder et. al. [1983] whereas Equations (III-35a), (III-36a) and (III-37a) are the results of this work.

i) $TE_{0,\mu}$ modes

$$\int_{V_{sources}} |e_{0,\mu}|^2 dV = \frac{\pi L a^2}{K_1^2(W_{0,\mu})} \left(R_{out}^2 \left| K_1(W_{0,\mu} R_{out}) \right| - R_{in}^2 \left| K_1(W_{0,\mu} R_{in}) \right| \right) \qquad \text{(III-35a)}$$

$$P_{0,\mu} = \frac{\pi a^2}{2}\sqrt{\frac{\varepsilon_o}{\mu_o}}\frac{\beta_{0,\mu}}{k}\left[\frac{\left|J_1(U_{0,\mu})\right|}{J_1^2(U_{0,\mu})} - \frac{\left|K_1(W_{0,\mu})\right|}{K_1^2(W_{0,\mu})}\right] \qquad \text{(III-35b)}$$

$$= \frac{\pi a^2}{2}\sqrt{\frac{\varepsilon_o}{\mu_o}}\frac{\beta_{0,\mu}}{k}\frac{V^2}{U_{0,\mu}^2}\frac{K_0(W_{0,\mu})K_2(W_{0,\mu})}{K_1^2(W_{0,\mu})} \qquad \text{(III-35c)}$$

ii) $TM_{0,\mu}$ modes

$$\int_{V_{sources}} |e_{0,\mu}|^2\, dV = \frac{n_{core}^4}{n_{clad}^4}\frac{\pi L a^2}{K_1^2(W_{0,\mu})}\left(R_{out}^2\left|K_1(W_{0,\mu}R_{out})\right| - R_{in}^2\left|K_1(W_{0,\mu}R_{in})\right| + \right.$$
$$\left. + \frac{W_{0,\mu}^2}{a^2\beta_{0,\mu}^2}\left(R_{out}^2\left|K_0(W_{0,\mu}R_{out})\right| - R_{in}^2\left|K_0(W_{0,\mu}R_{in})\right|\right)\right) \qquad \text{(III-36a)}$$

$$P_{0,\mu} = a^2\pi\sqrt{\frac{\varepsilon_o}{\mu_o}}\frac{k\,n_{core}^2}{2\beta_{0,\mu}}\left(\frac{\left|J_1(U_{0,\mu})\right|}{J_1^2(U_{0,\mu})} - \frac{n_{core}^2}{n_{clad}^2}\frac{\left|K_1(W_{0,\mu})\right|}{K_1^2(W_{0,\mu})}\right) \qquad \text{(III-36b)}$$

$$= \pi\sqrt{\frac{\varepsilon_o}{\mu_o}}\frac{V^2}{2k\beta_{0,\mu}}\frac{n_{core}^2}{n_{clad}^2}\times$$
$$\left(-1 + \frac{n_{core}^2}{n_{clad}^2}\frac{\beta_{0,\mu}^2 a^2}{U_{0,\mu}^2}\frac{K_0(W_{0,\mu})K_2(W_{0,\mu})}{K_1^2(W_{0,\mu})} - 2\frac{n_{core}^2}{n_{clad}^2}\frac{W_{0,\mu}}{U_{0,\mu}^2}\frac{K_0(W_{0,\mu})}{K_1(W_{0,\mu})}\right) \qquad \text{(III-36c)}$$

iii) $EH_{\nu,\mu}$ and $HE_{\nu,\mu}$ modes ($\nu > 0$)

$$\int_{V_{source}} \left(|e_r|^2 + |e_\varphi|^2 + |e_z|^2\right) dV = \frac{\pi U_{\nu,\mu}^2 L}{2K_\nu^2(W_{\nu,\mu})} \times$$

$$\left(\frac{2a^2 a_1^2}{W_{\nu,\mu}^2} \left(R_{out}^2 \left|\mathbf{K}_{\nu-1}(W_{\nu,\mu} R_{out})\right| - R_{in}^2 \left|\mathbf{K}_{\nu-1}(W_{\nu,\mu} R_{in})\right| \right) + \right.$$

$$+ \frac{2a^2 a_2^2}{W_{\nu,\mu}^2} \left(R_{out}^2 \left|\mathbf{K}_{\nu+1}(W_{\nu,\mu} R_{out})\right| - R_{in}^2 \left|\mathbf{K}_{\nu+1}(W_{\nu,\mu} R_{in})\right| \right) +$$

$$\left. + \frac{R_{out}^2}{\beta_{\nu,\mu}^2} \left|\mathbf{K}_\nu(W_{\nu,\mu} R_{out})\right| - \frac{R_{in}^2}{\beta_{\nu,\mu}^2} \left|\mathbf{K}_\nu(W_{\nu,\mu} R_{in})\right| \right) \qquad \text{(III-37a)}$$

$$P_{\nu,\mu} = \pi a^2 \sqrt{\frac{\varepsilon_o}{\mu_o}} \frac{k n_{core}^2}{2\beta_{\nu,\mu}} \left[\frac{a_1 a_3 \left|J_{\nu-1}(U_{\nu,\mu})\right| + a_2 a_4 \left|J_{\nu+1}(U_{\nu,\mu})\right|}{J_\nu^2(U_{\nu,\mu})} - \right.$$

$$\left. - \frac{U_{\nu,\mu}^2}{W_{\nu,\mu}^2} \frac{a_1 a_5 \left|\mathbf{K}_{\nu-1}(W_{\nu,\mu})\right| + a_2 a_6 \left|\mathbf{K}_{\nu+1}(W_{\nu,\mu})\right|}{K_\nu^2(W_{\nu,\mu})} \right] \qquad \text{(III-37b)}$$

$$\left|\mathbf{K}_l(A)\right| = \begin{vmatrix} K_l(A) & K_{l+1}(A) \\ K_{l-1}(A) & K_l(A) \end{vmatrix}$$

$$\left|\mathbf{J}_l(A)\right| = \begin{vmatrix} J_l(A) & J_{l+1}(A) \\ J_{l-1}(A) & J_l(A) \end{vmatrix}$$

where l is an integer and R_{out} and R_{in} are the normalized outer and inner radius of the fluorescent distribution given by r_{out}/a and r_{in}/a respectively. They obey the inequality $1 \le R_{in} < R_{out}$. Using the eigenvalue equation of the

exact solution of the TE and TM modes and the recurrence relationship of the Bessel function, we can express the ratios $J_\nu(U_{\nu,\mu})/J_{\nu+1}(U_{\nu,\mu})$ and $J_\nu(U_{\nu,\mu})/J_{\nu-1}(U_{\nu,\mu})$ in terms of $K_\nu(W_{\nu,\mu})/K_{\nu+1}(W_{\nu,\mu})$ and $K_\nu(W_{\nu,\mu})/K_{\nu-1}(W_{\nu,\mu})$ respectively (see Marcuse [1974], page 68 for a similar derivation for the weakly guiding approximation). Substituting this result in Equations (III-35b) and (III-36b) we get Equations (III-35c) and (III-36c) respectively. The equation of the power efficiency must take into account the degeneracy of the modes. Consequently, the final equation for the hybrid modes must be multiplied by two, odd and even modes.

For the weakly guiding case the normalization and the integral of Equation (III-34) are the same for every mode. As before, the integral below can be determined in a way similar to the one above. Also, Equation (III-38a) is the result of this work. In the equations below we have used the expressions of the weakly guiding fields in Equations (II-24).

$$\int_{V_{source}} |e_{\lambda,\mu}|^2 \, dV = \frac{\pi a^2 L}{K_\lambda^2(\widetilde{W}_{\lambda,\mu})}\left(R_{out}^2 \left|K_\lambda\left(\widetilde{W}_{\lambda,\mu} R_{out}\right)\right| - R_{in}^2 \left|K_\lambda\left(\widetilde{W}_{\lambda,\mu} R_{in}\right)\right|\right) \qquad \text{(III-38a)}$$

$$P_{\lambda,\mu} = \frac{\pi a^2 n_{clad}}{2}\sqrt{\frac{\varepsilon_o}{\mu_o}}\frac{V^2}{\widetilde{U}_{\lambda,\mu}^2}\frac{K_{\lambda-1}\left(\widetilde{W}_{\lambda,\mu}\right)K_{\lambda+1}\left(\widetilde{W}_{\lambda,\mu}\right)}{K_\lambda^2\left(\widetilde{W}_{\lambda,\mu}\right)} \qquad \text{(III-38b)}$$

where

$$\lambda = \begin{cases} 1 \text{ for TM and TE modes} \\ \nu - 1 \text{ for HE modes} \\ \nu + 1 \text{ for EH modes} \end{cases}$$

We should stress the fact that the results of Equations (III-35a), (III-36a), (III-37a) and (III-38a) are valid for the general cylindrical source distribution depicted in Figure (III-2) *assuming* that the indices of refraction of the cladding and fluorescent sources are similar. Such assumption is necessary in order to avoid further complication in the expressions of the fields which arises whenever the fiber has more than two different indices of refraction (finite cladding). The fields solution for this fiber [Kuhn, 1974 and references therein] is helpful but will not be considered here. This assumption, that the fluorescent sources have to have an index of refraction similar to the cladding one, becomes unnecessary whenever the source distribution is either a thin film ($r_{out}=r_{in}+\delta$, δ small) or a bulk distribution ($r_{out}=b$). In the first case, the index of refraction of the thin film can be neglected because of its small thickness. In the second case, the cladding is completely filled with the fluorescent sources which makes its index of refraction equal to the index of the fluorescent sources.

Notice that the power efficiency of a weakly guiding fiber is dependent on only one index of refraction. As stated before, Equations (III-35) thru (III-38) are independent of the cladding radius, b, because of the infinite cladding assumption in the weakly guiding and exact solutions. Due to two distinct polarizations and the existence of odd and even modes, Equation (III-38a)

should be multiplied by two for λ=0 and by four for λ>0.

Substituting λ=1 (TE/TM modes) in Equation (III-38a) and having in mind that $W_{0,\mu} \rightarrow \widetilde{W}_{1,\mu}$ when $n_{core} \approx n_{clad}$, we notice that Equation (III-35a) is already reduced to the weakly guiding case. Equations (III-35c), (III-36a) and (III-36c) can also be reduced by using the weakly guiding approximation

$$\beta \approx k n_{core} \approx k n_{clad}$$

For simplicity we will not write down the expression for the power efficiency.

We will do so in the next sections. There, we will find the power efficiency for two particular distributions of sources: the bulk distribution and the thin film. Table (III-1) summarizes the results obtained in this Section.

III-7 Power Efficiency of a Bulk Distribution of Sources

An optical fiber with a bulk distribution of fluorescent sources is illustrated in Figure (I-3a). It consists of sources uniformly distributed in the cladding, from the core/cladding to the cladding/third medium boundaries. It can be exemplified, but is not restricted to, a bare fiber core coated with a polymer which has fluorescent molecules dissolved in it, the so called optical fiber distributed sensor [Lieberman et. al., 1990; 1988; Blyler et. al., 1989]. If the radius of the cladding is big enough, Equations (III-35) thru (III-37) can be used to model it.

Choosing a fiber that has a cladding radius b, Equations (III-35) thru (III-37) can be rewritten by making, $r_{in}=a$ and $r_{out}=b$. This makes $R_{in}=1.0$ and $R_{out}=b/a$. A nice simplification arises when we make b very large, i.e, by substituting $r_{out}=b\to\infty$ and $R_{out}\to\infty$ in Equations (III-35a), (III-36a), (III-37a) and (III-38a) we get

$$\int_{V_{source}} |e_{0,\mu}|^2 \, dV = -\frac{\pi L a^2}{K_1^2(W_{0,\mu})} |K_1(W_{0,\mu})| \tag{III-39}$$

$$\int_{V_{source}} |e_{0,\mu}|^2 \, dV = -\frac{n_{core}^4}{n_{clad}^4} \frac{\pi L a^2}{K_1^2(W_{0,\mu})} \left(|K_1(W_{0,\mu})| + \frac{W_{0,\mu}^2}{a^2 \beta_{0,\mu}^2} |K_0(W_{0,\mu})| \right) \tag{III-40}$$

$$\int_{V_{source}} |e_{\nu,\mu}|^2 \, dV = -\frac{\pi L a^2 U_{\nu,\mu}^2}{K_\nu^2(W_{\nu,\mu})} \left(\frac{a_1^2 |K_{\nu-1}(W_{\nu,\mu})| + a_2^2 |K_{\nu+1}(W_{\nu,\mu})|}{W_{\nu,\mu}^2} + \frac{|K_\nu(W_{\nu,\mu})|}{2\beta_{\nu,\mu}^2 a^2} \right) \tag{III-41}$$

$$\int_{V_{source}} |e_{\lambda,\mu}|^2 \, dV = -\frac{\pi L a^2}{K_\lambda^2(\widetilde{W}_{\lambda,\mu})} |K_\lambda(\widetilde{W}_{\lambda,\mu})| \tag{III-42}$$

respectively. At infinite, the determinant $|K_l(A)|$ decays faster than R_{out}. For this reason, all terms containing R_{out} vanish in the limit $R_{out}\to\infty$.

Substituting Equations (III-35b), (III-36b), (III-37b), (III-38b) and (III-39) thru (III-42) into Equation (III-34), we get the power efficiency

TABLE III-1

	MODES	$\int_{V_{sources}} \lvert e_{\nu,\mu}\rvert^2 \, dV$	ASSUMPTIONS
Exact Solution	TE TM Hybrid	Equation (III-35a) Equation (III-36a) Equation (III-37a)	A and B
Weakly guiding	TE, TM and Hybrid	Equation (III-38a)	A thru C

Summary equations for the integral of the square of the electric field over the volume of a cylindrical distribution of sources. Inner and outer radial limits of the distribution are given by r_{in} and r_{out} (see Figure III-2). R_{in} and R_{out} are the normalized inner and outer radius and are given by r_{in}/a and r_{out}/a respectively.

Assumptions:

A. Infinite cladding radius in the fields solutions ($b \rightarrow \infty$).

B. Index of refraction of the source material similar to index of refraction of the cladding ($n_{source} \approx n_{clad}$).

C. Weakly guiding approximation ($n_{core} \approx n_{clad}$).

$$\left.\frac{P_{\text{core}}}{P_{\text{rad}}}\right|_{\text{TE}} = \frac{1}{2V^2\left(b^2-a^2\right)n_{\text{clad}}k}\sum_{\mu}\left|\frac{U_{0,\mu}^2\left|\mathbf{K}_1\right|}{\beta_{0,\mu}K_0\left(W_{0,\mu}\right)K_2\left(W_{0,\mu}\right)}\right| \qquad \text{(III-43a)}$$

$$\left.\frac{P_{\text{core}}}{P_{\text{rad}}}\right|_{\text{TM}} = \frac{n_{\text{core}}^2}{2\left(b^2-a^2\right)k^3n_{\text{clad}}^5}\sum_{\mu}\left|\frac{\beta_{0,\mu}\left(\left|\mathbf{K}_1\right|+\dfrac{W_{0,\mu}^2}{a^2\beta_{0,\mu}^2}\left|\mathbf{K}_0\right|\right)}{K_1^2\left(W_{0,\mu}\right)\left(\dfrac{\left|\mathbf{J}_1\right|}{J_1^2\left(U_{0,\mu}\right)}-\dfrac{n_{\text{core}}^2}{n_{\text{clad}}^2}\dfrac{\left|\mathbf{K}_1\right|}{K_1^2\left(W_{0,\mu}\right)}\right)}\right| \qquad \text{(III-43b)}$$

$$\left.\frac{P_{\text{core}}}{P_{\text{rad}}}\right|_{\substack{\text{EH}\\\text{HE}}} = \frac{1}{\left(b^2-a^2\right)n_{\text{core}}^2n_{\text{clad}}k^3}\times \qquad \text{(III-43c)}$$

$$\sum_{\nu,\mu}\left|\frac{\beta_{\nu,\mu}U_{\nu,\mu}^2\left(\dfrac{a_1^2\left|\mathbf{K}_{\nu-1}\right|+a_2^2\left|\mathbf{K}_{\nu+1}\right|}{W_{\nu,\mu}^2}+\dfrac{\left|\mathbf{K}_\nu\right|}{2\beta_{\nu,\mu}^2a^2}\right)}{K_\nu^2\left(W_{\nu,\mu}\right)\left[\dfrac{a_1a_3\left|\mathbf{J}_{\nu-1}\right|+a_2a_4\left|\mathbf{J}_{\nu+1}\right|}{J_\nu^2\left(U_{\nu,\mu}\right)}-\dfrac{U_{\nu,\mu}^2}{W_{\nu,\mu}^2}\dfrac{a_1a_5\left|\mathbf{K}_{\nu-1}\right|+a_2a_6\left|\mathbf{K}_{\nu+1}\right|}{K_\nu^2\left(W_{\nu,\mu}\right)}\right]}\right|$$

$$\left.\frac{P_{\text{core}}}{P_{\text{rad}}}\right|_{\substack{\text{weakly}\\\text{guiding}}} = \frac{1}{2\left(b^2-a^2\right)V^2n_{\text{clad}}^2k^2}\sum_{\lambda,\mu}\left(4-2\delta_{0,\lambda}\right)\left|\frac{\tilde{U}_{\lambda,\mu}^2\left|\mathbf{K}_\lambda\right|}{K_{\lambda-1}\left(\tilde{W}_{\lambda,\mu}\right)K_{\lambda+1}\left(\tilde{W}_{\lambda,\mu}\right)}\right|$$

(III-43d).

For simplicity, we have dropped the arguments of K_l and J_l. Although the power efficiency of the EH and HE modes have the same form, their eigenvalues are different. Equations (III-43a) thru (III-43c) are the result of this work. However, Equation (III-43d) is essentially similar to Formula (8) of Marcuse [1988]. As discussed before, we had to multiply the original result of Equation (III-43c) by two in order to account for both odd and even modes. Finally the total power efficiency is given by the sum

$$P_{\text{eff}} = \left.\frac{P_{\text{core}}}{P_{\text{rad}}}\right|_{\text{TE}} + \left.\frac{P_{\text{core}}}{P_{\text{rad}}}\right|_{\text{TM}} + \left.\frac{P_{\text{core}}}{P_{\text{rad}}}\right|_{\text{HE}} + \left.\frac{P_{\text{core}}}{P_{\text{rad}}}\right|_{\text{EH}}. \qquad \text{(III-44)}$$

We should stress that Equations (III-43) base on at least two approximations:

1) the infinite cladding approximation, which was introduced in the derivation of the fields in Chapter II and

2) the infinite sources outer radius approximation introduced in Equations (III-39) thru (III-42).

As discussed before, the first approximation results in expressions for the fields which are independent of the cladding radius b. It also results in a cut-off frequency equal to zero for the fundamental mode. Although the infinite cladding assumption is widely used, it is the finiteness of the cladding that imposes a non-zero cut-off frequency for the fundamental mode [Black et. al.,

1986 and references therein].

For a few modes, the second approximation leads to a peak-discontinuity near their cut-off frequency in the power efficiency diagram. Such behavior is more evident at low V-numbers. However, at high V-numbers, the large number of modes tends to smooth out the whole distribution of power efficiency. As a consequence a sharp increase in the power efficiency near cut-off becomes less perceptible. Instead, by using Equations (III-35a), (III-36a) and (III-37a) we avoid this discontinuity in the power efficiency curve. Tables (III-2) and (III-3) summarizes the results of this Section.

In conclusion, the power efficiency of a bulk distribution of sources can be expressed in the following functional form

$$P_{\text{eff}} = P_{\text{eff}}(a, r_{\text{out}}=b, n_{\text{core}}, n_{\text{clad}}, k). \qquad \text{(III-45)}$$

We will show that the number of parameters required for the power efficiency of a thin film distribution will be reduced.

III-8 Power Efficiency of a Thin Film Distribution of Sources

An optical fiber with a thin film distribution of fluorescent sources is illustrated in Figure (I-3b). It consists of a thin layer of sources concentrated at a specific distance from the center of the fiber in the cladding region. It can be represented by, but is not restricted to, a bare fiber core coated with a thin film.

TABLE III-2

	MODES	$\int_{V_{sources}} \lvert e_{\nu,\mu}\rvert^2 \, dV$	ASSUMPTIONS
Exact Solution	TE TM Hybrid	Equation (III-39) Equation (III-40) Equation (III-41)	A and B
Weakly guiding	TE, TM and Hybrid	Equation (III-42)	A thru C

Summary equations for the integral of the square of the electric field over the volume of a bulk distribution of sources. In this case, R_{in}=1.0, r_{in}=a and r_{out} and $R_{out}\rightarrow\infty$. Also the source material is the cladding itself, i.e., $n_{source}\cong n_{clad}$.

Assumptions:

A. Infinite cladding radius in the field solutions ($b\rightarrow\infty$).

B. Infinite outer radius of the source distribution ($r_{out}\rightarrow\infty$).

C. Weakly guiding approximation ($n_{core}\cong n_{clad}$).

TABLE III-3

	MODES	P_{core}/P_{rad}	ASSUMPTIONS
Exact Solution	TE	Equation (III-43a)	A and B
	TM	Equation (III-43b)	
	Hybrid	Equation (III-43c)	
Weakly guiding	TE, TM and Hybrid	Equation (III-43d)	A thru C

Summary equations for the power efficiency of a bulk distribution of sources. The corresponding Equations are obtained by substituting Equations (III-39) thru (III-42) and Equations (III-35b), (III-36b), (III-37b) and (III-38b) into Equation (III-34). In this case the source material is the cladding itself, i.e., $n_{source} \equiv n_{clad}$. Equation (III-43d) is similar to Equation (8) of Marcuse [1988].

Assumptions:

A. Infinite cladding radius in the field solutions ($b \to \infty$).

B. Infinite outer radius of the source distribution ($r_{out} \to \infty$) in Equations (III-39) thru (III-42).

C. Weakly guiding approximation ($n_{core} \approx n_{clad}$).

In this case, the air itself acts as an infinite radius cladding.

The power efficiency of a thin film can be obtained by writing r_{out} in terms of r_{in} where r_{out}-r_{in}=δ is the layer thickness of the film. For a thin film, the thickness δ has to be much lesser than $a / W_{\nu,\mu}$. Substituting R_{out}=R_{in}+δ/a into Equations (III-35a), (III-36a), (III-37a) and (III-38a) we can find their corresponding thin-film expressions. These equations are a function of the determinant of $\mathbf{K}_l(AR_{out})$ which can be found by expanding it in terms of powers of δ. The first order approximation for the above determinant is given by

$$|\mathbf{K}_l\ (A\ R_{out})| = |\mathbf{K}_l\ (A\ R_{in})| + A\delta/a\ \frac{d\,|\mathbf{K}_l\ (A\ R_{in})|}{d\,(AR_{in})} + \ \ldots. \qquad \text{(III-46)}$$

Again, using the first order approximation in δ for R_{out} and substituting Equation (III-46) into Equations (III-35a), (III-36a), (III-37a) and (III-38a) for the thin film case, we get the results below

i) $TE_{0,\mu}$ modes

$$\int_{V_{sources}} |e_{0,\mu}|^2\, dV \cong \frac{\delta\,\pi L a R_{in}}{K_1^{\,2}(W_{0,\mu})}\left(R_{in} W_{0,\mu}\, \frac{d\,|\mathbf{K}_1(W_{0,\mu}\ R_{in}|}{d\,(W_{0,\mu}R_{in})} + 2\,|\mathbf{K}_1\,(W_{0,\mu}\ R_{in})|\right) \qquad \text{(III-47a)}$$

ii) $TM_{0,\mu}$ modes

$$\int_{V_{sources}} |e_{0,\mu}|^2 \, dV \equiv \frac{n_{core}^4}{n_{clad}^4} \frac{\delta \pi L a \, R_{in}}{K_1^2(W_{0,\mu})} \left(R_{in} W_{0,\mu} \frac{d\,|K_1(W_{0,\mu} R_{in})|}{d(W_{0,\mu} R_{in})} + \right.$$
$$\left. + 2\,|K_1(W_{0,\mu} R_{in})| + \frac{W_{0,\mu}^2 R_{in}}{a^2 \beta_{0,\mu}^2} \left(R_{in} W_{0,\mu} \frac{d\,|K_0(W_{0,\mu} R_{in})|}{d(W_{0,\mu} R_{in})} + 2\,|K_0(W_{0,\mu} R_{in})| \right) \right) \tag{III-47b}$$

iii) $EH_{\nu,\mu}$ and $HE_{\nu,\mu}$ modes ($\nu > 0$)

$$\int_{V_{source}} |e_{\nu,\mu}|^2 \, dV = \frac{\delta \pi U_{\nu,\mu}^2 \, L R_{in}}{2 K_\nu^2(W_{\nu,\mu})} \times$$
$$\left(\frac{2aa_1^2}{W_{\nu,\mu}^2} \left(R_{in} W_{\nu,\mu} \frac{d\,|K_{\nu-1}(W_{\nu,\mu} R_{in})|}{d(W_{\nu,\mu} R_{in})} + 2\,|K_{\nu-1}(W_{\nu,\mu} R_{in})| \right) + \right.$$
$$+ \frac{2aa_2^2}{W_{\nu,\mu}^2} \left(R_{in} W_{\nu,\mu} \frac{d\,|K_{\nu+1}(W_{\nu,\mu} R_{in})|}{d(W_{\nu,\mu} R_{in})} + 2\,|K_{\nu+1}(W_{\nu,\mu} R_{in})| \right) +$$
$$\left. + \frac{1}{a\beta_{\nu,\mu}^2} \left(R_{in} W_{\nu,\mu} \frac{d\,|K_\nu(W_{\nu,\mu} R_{in})|}{d(W_{\nu,\mu} R_{in})} + 2\,|K_\nu(W_{\nu,\mu} R_{in})| \right) \right) \tag{III-47c}$$

iv) weakly guiding

$$\int_{V_{source}} |e_{\lambda,\mu}|^2 \, dV = \frac{\delta \pi \, a L R_{in}}{K_\lambda^2(\widetilde{W}_{\lambda,\mu})} \left(R_{in} \widetilde{W}_{\lambda,\mu} \frac{d\,|K_\lambda(\widetilde{W}_{\lambda,\mu} R_{in})|}{d(\widetilde{W}_{\lambda,\mu} R_{in})} + 2\,|K_\lambda(\widetilde{W}_{\lambda,\mu} R_{in})| \right) \tag{III-47d}$$

which are also a first order approximation in δ.

Neglecting the second higher order terms in δ of Equation (III-33) we get

$$P_{rad} \equiv \frac{\delta \omega \mu_o a R_{in}}{2} nkSL \tag{III-48}$$

Notice that Equations (III-47) and (III-48) are all linear in δ. Consequently, the result of P_{eff} is independent of this parameter. If we substitute these expressions into Equation (III-34), we get the power efficiency of a thin film located anywhere in the cladding. However, of particular interest, is the optical fiber which has a thin film located in the core/cladding boundary, i.e., R_{in}=1.0. It is easier to make such fiber and it is also the one that has the highest power efficiency. Equations (III-47) and (III-48) can be easily reduced to this case.

Using Equations (III-48) and (III-25) and substituting R_{in}=1.0 in it, we get the power efficiency of a thin film distribution at the core/cladding interface

$$\frac{P_{core}}{P_{rad}} = \frac{\sqrt{\varepsilon_o/\mu_o}}{8a\ L\ n_{clad}\ k^2} \lim_{\delta \to 0} \left(\frac{1}{\delta} \sum_{\nu,\mu} \frac{1}{P_{\nu,\mu}} \int_{V_{source}} |e_{\nu,\mu}|^2\ dV \right) \qquad \text{(III-49)}$$

Although not published, Equation (III-49) was obtained previously by Marcuse.

The expresssion

$$W_{\nu,\mu} \frac{d\,|K_l\,(W_{\nu,\mu})|}{d\ W_{\nu,\mu}} + 2\,|K_l\,(W_{\nu,\mu})|$$

can be simplified if we expand it and use the recurrence relationship to eliminate the highest and lowest order terms of the Bessel function. The arithmethic is very involved. The final result is

$$W_{\nu,\mu}\frac{d\,|\mathbf{K}_l\,(W_{\nu,\mu})|}{d\,W_{\nu,\mu}} + 2\,|\mathbf{K}_l\,(W_{\nu,\mu})| = 2\,K_l^{\,2}(W_{\nu,\mu}). \qquad \text{(III-50)}$$

Substituting Equation (III-50) into Equations (III-47) we get

i) $TE_{0,\mu}$ modes

$$\int_{V_{source}} |e_{0,\mu}|^2\,dV = 2\pi aL\delta \qquad \text{(III-51a)}$$

ii) $TM_{0,\mu}$ modes

$$\int_{V_{sources}} |e_{0,\mu}|^2\,dV \cong \frac{n_{core}^4\;2\delta\pi La}{n_{clad}^4 K_1^{\,2}(W_{0,\mu})}\left(K_1^{\,2}(W_{0,\mu}) + \frac{W_{0,\mu}^2}{a^2\beta_{0,\mu}^2}\,K_0^{\,2}(W_{0,\mu}) \right) \qquad \text{(III-51b)}$$

iii) $EH_{\nu,\mu}$ and $HE_{\nu,\mu}$ modes ($\nu > 0$)

$$\int_{V_{source}} |e_{\nu,\mu}|^2\,dV = \frac{\delta\pi U_{\nu,\mu}^2\,L}{K_\nu^2(W_{\nu,\mu})}\times$$

$$\left(\frac{2aa_1^{\,2}}{W_{\nu,\mu}^{\,2}}K_{\nu-1}^{\,2}(W_{\nu,\mu}) + \frac{2aa_2^{\,2}}{W_{\nu,\mu}^{\,2}}K_{\nu+1}^{\,2}(W_{\nu,\mu}) + \frac{1}{2}K_\nu^{\,2}(W_{\nu,\mu}) \right) \qquad \text{(III-51c)}$$

iv) weakly guiding

$$\int_{V_{source}} |e_{\lambda,\mu}|^2 \, dV = 2\pi a L \delta \qquad \text{(III-51d)}$$

Remember that, for the thin-film, the δ in the equations above is very small. Finally, substituting Equations (III-51), (III-35c), (III-36b), (III-37b) and (III-38b) into Equation (III-49) and taking the limit, $\delta \to 0$, we get the power efficiency of a thin film distribution over the core/cladding boundary or

$$\left.\frac{P_{core}}{P_{rad}}\right|_{TE} = \frac{1}{2 n_{clad} k a^2 V^2} \sum_{\mu} \frac{U_{0,\mu}^2 K_1^2(W_{0,\mu})}{\beta_{0,\mu} K_0(W_{0,\mu}) K_2(W_{0,\mu})} \qquad \text{(III-52a)}$$

$$\left.\frac{P_{core}}{P_{rad}}\right|_{TM} = \frac{1}{2a^2 k^3} \frac{n_{core}^2}{n_{clad}^5} \sum_{\mu} \left| \frac{\beta_{0,\mu} \left(1 + \frac{W_{0,\mu}^2}{a^2 \beta_{0,\mu}^2} \frac{K_0^2(W_{0,\mu})}{K_1^2(W_{0,\mu})} \right)}{\left(\frac{|J_1(U_{0,\mu})|}{J_1^2(U_{0,\mu})} - \frac{n_{core}^2}{n_{clad}^2} \frac{|K_1(W_{0,\mu})|}{K_1^2(W_{0,\mu})} \right)} \right| \qquad \text{(III-52b)}$$

$$\left.\frac{P_{core}}{P_{rad}}\right|_{\substack{EH \\ HE}} = \frac{1}{n_{clad} n_{co}^2 k^3 a^3} \times$$

$$\sum_{\nu,\mu} \frac{U_{\nu,\mu}^2 a\beta_{\nu,\mu} \left| \frac{2a_1^2 K_{\nu-1}^2(W_{\nu,\mu})}{W_{\nu,\mu}^2} + \frac{2a_2^2 K_{\nu+1}^2(W_{\nu,\mu})}{W_{\nu,\mu}^2} + \frac{K_\nu^2(W_{\nu,\mu})}{a^2\beta_{\nu,\mu}^2} \right|}{K_\nu^2(W_{\nu,\mu}) \left| \frac{a_1 a_3 |J_{\nu-1}| + a_2 a_4 |J_{\nu+1}|}{J_\nu^2(U_{\nu,\mu})} - \frac{U_{\nu,\mu}^2}{W_{\nu,\mu}^2} \frac{a_1 a_5 |K_{\nu-1}| + a_2 a_6 |K_{\nu+1}|}{K_\nu^2(W_{\nu,\mu})} \right|} \qquad \text{(III-52c)}$$

$$\left.\frac{P_{\text{core}}}{P_{\text{rad}}}\right|_{\substack{\text{weakly} \\ \text{guiding}}} = \frac{1}{a^2 n_{\text{clad}}^2 k^2 V^2} \sum_{\nu,\mu} \frac{(2-\delta_{0,\lambda})\tilde{U}_{\lambda,\mu}^2 K_\lambda^2(\tilde{W}_{\lambda,\mu})}{K_{\lambda-1}(\tilde{W}_{\lambda,\mu}) K_{\lambda+1}(\tilde{W}_{\lambda,\mu})} \qquad \text{(III-52d)}$$

For simplicity, we have dropped the arguments of K_l and J_l. The total power efficiency is given by Equation (III-44).

Equations (III-52a) thru (III-52c) are the result of this work whereas the weakly guiding case, Equation (III-52d), is similar to that derived by Marcuse [1988].

As it was summarized in Tables (III-4) thru (III-6) all Equations obtained involve at least one approximation -the infinite cladding radius approximation of the field solution. However, for the special case in which the cladding of our thin-film fiber is the outside air, n_{clad}=1.0, Equations (III-52a) thru (III-52c) involve no approximation at all. That is because the outside medium, air, essentially extends to infinity. The power efficiency P_{eff} of a thin film coated fiber is a function of

$$P_{eff} = P_{eff}(a, r_{in}, n_{core}, n_{clad}, k). \qquad \text{(III-53)}$$

For a bare core fiber coated in the core/air interface $r_{in}=a$ and $n_{clad}=1.0$ and the number of variables is reduced by two. Notice that in both the case of a thin film and a bulk distribution of sources the power efficiency is a function of many variables. This complex functionality makes it difficult to analyze the behavior of P_{eff}. It is also difficult to sketch general predictions for a high injection efficiency by a fluorescent cladding optical fiber. In the next chapter, some results of model calculations based upon the above expressions allowed us to formulate a few rules for designing an optical fiber sensor.

TABLE III-4

	MODES	$\int_{V_{sources}} \lvert e_{\nu,\mu}\rvert^2 \, dV$	ASSUMPTIONS
Exact Solution	TE	Equation (III-47a)	A
	TM	Equation (III-47b)	
	Hybrid	Equation (III-47c)	
Weakly guiding	TE, TM and Hybrid	Equation (III-47d)	A and B

Summary equations for the integral of the square of the electric field of a thin film source at an arbitrary position in the cladding. Inner and outer radial limits of the distribution are given by r_{in} and $r_{out} = r_{in} + \delta$ ($\delta \to 0$). R_{in} and R_{out} are the normalized inner and outer radius and are given by r_{in}/a and r_{out}/a respectively.

Assumptions:
A. Infinite cladding radius in the field solutions ($b \to \infty$).
B. Weakly guiding approximation ($n_{core} \approx n_{clad}$).

TABLE III-5

	MODES	$\int_{V_{sources}} \lvert e_{\nu,\mu} \rvert^2 \, dV$	ASSUMPTIONS
Exact Solution	TE	Equation (III-51a)	
	TM	Equation (III-51b)	A
	Hybrid	Equation (III-51c)	
Weakly guiding	TE, TM and Hybrid	Equation (III-51d)	A and B

Summary equations for the integral of the square of the electric field of a thin film source at the core/cladding boundary. Inner and outer radial limits of the distribution are given by $r_{in}=a$ and $r_{out}= a+\delta$ ($\delta \rightarrow 0$). R_{in} and R_{out} are the normalized inner and outer radius and are given by 1.0 and $1.0+\delta/a$ respectively.

Assumptions:
A. Infinite cladding radius in the field solutions ($b \rightarrow \infty$).
B. Weakly guiding approximation ($n_{core} \approx n_{clad}$).

TABLE III-6

	MODES	P_{core}/P_{rad}	ASSUMPTIONS
Exact Solution	TE	Equation (III-52a)	A
	TM	Equation (III-52b)	
	Hybrid	Equation (III-52c)	
Weakly guiding	TE, TM and Hybrid	Equation (III-52d)	A and B

Summary equations for the power efficiency of a thin film distribution of sources. The corresponding Equations are obtained by substituting Equations (III-51), (III-35c), (III-36b), (III-37b) and (III-38b) into Equation (III-49). Equation (III-52d) is similar to Equation (8) of Marcuse [1988].

Assumptions:
A. Infinite cladding radius in the field solutions ($b \rightarrow \infty$).
B. Weakly guiding approximation ($n_{core} \approx n_{clad}$).

IV. POWER EFFICIENCY OF A DISTRIBUTION OF SOURCES

IV-1 Introduction

In this chapter we have used the results of the power efficiency of the previous chapter to determine its behavior as a function of different parameters and their combinations for specific conditions.

As it can be seem from Equations (III-43a) thru (III-43c) and Equations (III-52a) thru (III-52c) the functional behavior of the power efficiency is too involved to be determined by direct analysis. Added to this, there is also the need to determine the eigenvalues of our problem from a complicated transcendental equation. A problem of this magnitude requires the use of computational techniques. For this reason, we have written a program in FORTRAN to compute the P_{eff} against many of the possible variables. In certain cases, the parametric values used to determine the power efficiency are not realistic. This approach was used in order to determine the general behavior of the power efficiency. However, some of the parametric values are within the realm of the real world.

We have used Equations (III-43a) thru (III-43c) for the bulk and Equations (III-35) thru (III-37) for both bulk and thin film distributions. As discussed

before, if we use Equations (III-35) thru (III-37) into Equations (III-34) we get a more exact and general result. I.e., by using an appropriate R_{out} and R_{in} we can determine the P_{eff} for any distribution of sources with cylindrical symmetry. For the bulk distribution, the difference between the two approaches lies in the upper radial limit used in the integral of the square of the electric field of the bulk distribution. The first one used an infinite value for the upper radial limit or

$$\int_{V_{sources}} |e_{\nu,\mu}|^2 \, dV = \iiint_{r=r_{in}}^{\infty} |e_{\nu,\mu}|^2 \, r \, dr \, d\varphi \, dz$$

and the second one used the actual value of the outer radius of this distribution or

$$\int_{V_{sources}} |e_{\nu,\mu}|^2 \, dV = \iiint_{r=r_{in}}^{r_{out}} |e_{\nu,\mu}|^2 \, r \, dr \, d\varphi \, dz$$

These calculations were performed differently in a heuristic approach.

The eigenvalues $U_{\nu,\mu}$ and $W_{\nu,\mu}$ are found by using four different transcendental equations for TM, TE, HE and EH modes. They have limits that are either well-known or can be calculated [Snyder et. al., 1983]. Using these limits, we can square the eigenvalues. The ZBRENT subroutine of Numerical Recipes [Press et. al., 1986] was used to find them. This subroutine employes the Secant method in conjunction with the Bisection method.

As it was noticed before, the power efficiency of both bulk and thin film distributions are very complicated. It is a function of up to five parameters which involve different combinations of a, r_{in}, r_{out}, n_{core} n_{clad} and λ. In order to predict its behavior, we have used two different approaches: in the first one we have analyzed the behavior of the P_{eff} for a variable V-number and in the second one for a constant V-number.

In the first approach, the V-number

$$V = a k \sqrt{n_{core}^2 - n_{clad}^2} = \sqrt{U^2 + W^2}$$

can be varied by changing one of its parameters separately namely, a, λ, n_{core} and n_{clad}. The results were plotted either against the V-number or against the actual variable. All of them have revealed a jagged appearance more or less perceptible depending on whether we are treating the thin-film or the bulk distribution (Figures (IV-1) thru (IV-4) and Figures (IV-6) thru (IV-11)). Marcuse [1988] was the first one to discuss this sharp increase. In his paper he has plotted the power efficiency of a weakly guiding fiber against the V-number for a fixed core/cladding radius and wavelength. He has also pointed out that this sharp increase occurs near the cut-off values of the modes. Near cut-off, the evanescent field is stronger and there is a higher probability of power injection. The weakly guiding formulas obtained is simple enough to allow him to vary the V-number freely, with no regard to the other parameters. Although, in the real world, his graphs are equivalent

to a plot of the power efficiency against the index/indices of refraction, he has not treated neither this case nor the remaining ones, i.e., variable wavelength and core radius. All these cases are treated in this work and the results are displayed in this chapter.

In the second approach the behavior of the P_{eff} was analyzed for a constant V-number. The V-number was kept constant by changing *only* two of its parameters. It was used two techniques:

1) to vary the core and cladding radius a and b and the wavelength λ at a constant ratios a/λ and b/a and constant indices of refraction n_{core} and n_{clad} (notice that although we are varying three parameters only two are a V-number parameter). It is interesting to notice that for this specific case, the power efficiency remained constant for variable wavelength and core radius. This result suggests that both a/λ and b/a are two independent variables. Notice that the expressions of the thin-film do not involve the cladding radius b. Consequently, a similar conclusion which does not involve b and combinations of it also applies. This result essentially decreases the dimension of the problem by one variable. This makes its analysis simpler and

2) to vary the indices of refraction of the core and cladding, n_{core} and n_{clad} respectively, at the same time. Remember that there are specific values for the indices of refraction n_{core} and n_{clad} that allow a constant V-value. The final result was plotted against the difference n_{core}-n_{clad} and revealed an almost linear increase in a log-log scale.

The constant V approach can be justified by the fact that for a constant V-number the power efficiency curve is smoother (there are no sharp peaks). This makes it easier to fit a polynomial equation to the graphs and analyze its behavior. Notice that since the eigenvalues of a weakly guiding fiber are independent of the fiber parameters, the P_{eff} of this fiber at constant V-number is directly proportional to the coefficient of the terms inside the summation sign (Equations (III-43d) and (III-52d)). However, this simplification *does not* occur in the expressions of P_{eff} derived in this work (Equations (III-43a) thru (III-43c) and Equations (III-52a) thru (III-52c)). This is because the eigenvalue equation of the exact solution is more complicated and dependent on more parameters.

IV-2 Power Efficiency at Constant a/λ

By varying a and λ in such a way to make the ratio a/λ constant and fixing the indices of refraction, n_{core} and n_{clad} and the normalized radius, R_{out} and R_{in} (b/a and 1.0 respectively for the bulk distribution), it can be concluded that the P_{eff} remains unchanged. In order to see that, first we should recall the values of $U_{\nu,\mu}$, $W_{\nu,\mu}$ and V or

$$U_{\nu,\mu} = a\sqrt{k^2 n_{core}^2 - \beta_{\nu,\mu}^2}\,, \tag{II-13c}$$

$$W_{\nu,\mu} = a\sqrt{\beta_{\nu,\mu}^2 - k^2 n_{clad}^2} \quad \text{and} \tag{II-13d}$$

$$V = ak\sqrt{n_{core}^2 - n_{clad}^2} = \sqrt{U^2 + W^2}\,. \qquad \text{(II-13e)}$$

Notice that $\beta_{\nu,\mu}$ can be rewritten as

$$\beta_{\nu,\mu} = kn_{efc} \qquad \text{(IV-1)}$$

where n_{efc} is the effective index of refraction which obeys the inequality

$$n_{clad} \leq n_{efc} \leq n_{core}\,.$$

Since $k = 2\pi/\lambda$, it can be easily seen that $U_{\nu,\mu}$, $W_{\nu,\mu}$ and V are the same for the prescribed conditions

$$\frac{a}{\lambda} = \frac{a_1}{\lambda_1} = \ldots = \frac{a_n}{\lambda_n} \qquad \text{(IV-2a)}$$

and

$$n_{core}, n_{clad}, R_{in} \text{ and } R_{out} \text{ constant.} \qquad \text{(IV-2b)}$$

Finally, substituting Equation (IV-1) into Equations (III-43) and (III-52) under Conditions (IV-2), writing b as a proportion in a and having in mind the previous result for $U_{\nu,\mu}$, $W_{\nu,\mu}$ and V, we find that the P_{eff} is the same for different values of a and λ. The same conclusion also applies whenever we use Equations (III-35a), (III-36a) and (III-37a) in Equations (III-34) of the power

efficiency using the relations or $r_{out} = aR_{out}$ and $r_{in} = aR_{in}$. In consequence the functional dependence of the power efficiency of both bulk and thin-film distribution are reduced to

$$P_{eff} = P_{eff}(ka, b/a, n_{core}, n_{clad}).$$

$$P_{eff} = P_{eff}(ka, R_{in}, n_{core}, n_{clad}).$$

respectively. For the special case of a thin film distributed in the core/cladding boundary, R_{in}=1.0, the previous functionality dependence is reduced to

$$P_{eff} = P_{eff}(ka, n_{core}, n_{clad}).$$

IV-3 Power Efficiency of a Weakly Guiding Fiber

The results for the weakly guiding case are presented in Figures (IV-1) thru (IV-4). They were derived using the same values as those in Marcuse [1988], namely, λ=1.3 μm, a= 10.0μm and b/a= 5.0. In order to vary V, we used a fixed index of refraction for the core and varied the index of refraction of the cladding, n_{clad}. The difference $ep = n_{core} - n_{clad}$ had to be small enough to simulate a weakly guiding fiber (ep<0.1). For Figures (IV-1a), (IV-3) and (IV-4a) ep varied roughly from 10^{-3} at V= 0.05 to 10^{-2} at V= 10. For Figure (IV-2) it varied from 10^{-7} to 10^{-2}. For higher V-numbers ep would increase even more invalidating the weak guidance condition. For this reason, we have avoided going further into a higher V-number region. For sake of

comparision, we have reproduced with permission Figures 2 and 3 of Marcuse [1988] (Figures (IV-1b) and (IV-4b), respectively). The figures are for the bulk distribution, Figures (IV-1) thru (IV-3), and thin film, Figures (IV-4).

i) Bulk Distribution

We have plotted three graphs for the bulk distribution. Figures (IV-1a) and (IV-2) follow from Equations (III-43a) thru (III-43c). Figure (IV-3) was obtained using the actual radial outer limit b of the source distribution (Equations III-35 thru III-37). We start by discussing Figures (IV-1) and (IV-2).

The labels of Figures (IV-1a) and (IV-2) correspond to the V-values at which the modes start to propagate. For instance, in a weakly-guiding fiber the modes$TE_{0,1}$, $TM_{0,1}$ and $HE_{2,1}$ have a cut-off at $V=2.405$. This is the corresponding V-value for the first sharp peak in Figures (IV-1) and (IV-2). All plotted peaks occur at cut-off of the labeled modes [Marcuse, 1988]. Between 0 and 2.405 only the fundamental mode, $HE_{1,1}$, propagates, consequently only this mode contributes to the power efficiency in this region. The plateau observed between V=0 and 0.5 occurs because between these values

$$U_{\lambda=0,1} \cong V \,. \tag{IV-3}$$

The height of each plateau can be found by substituting Equation (IV-3) into (III-43d) or

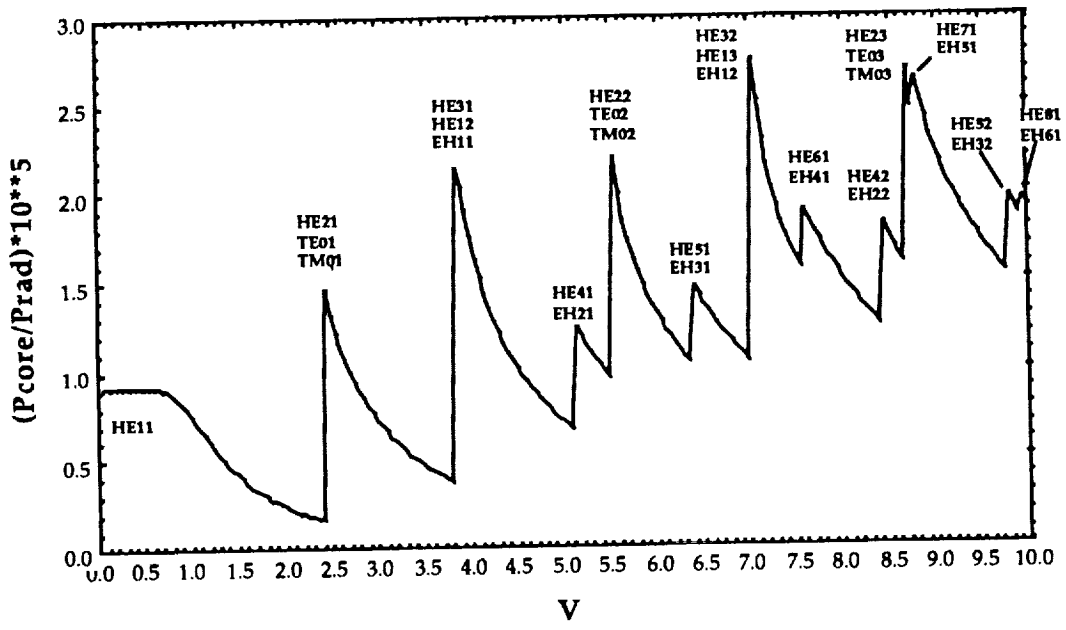

Figure IV-1a. Power Efficiency of a bulk distribution of fluorescent sources versus the V-number (weakly guiding case). The wavelength, the index of refraction of the core and the core and cladding radius are held fixed at λ=1.3μm, n_{core}=1.4, a=10μm and b=50.0μm respectively. The Index of refraction of the cladding varied from 1.399 at V=0.05 to 1.385 at V=10.0.

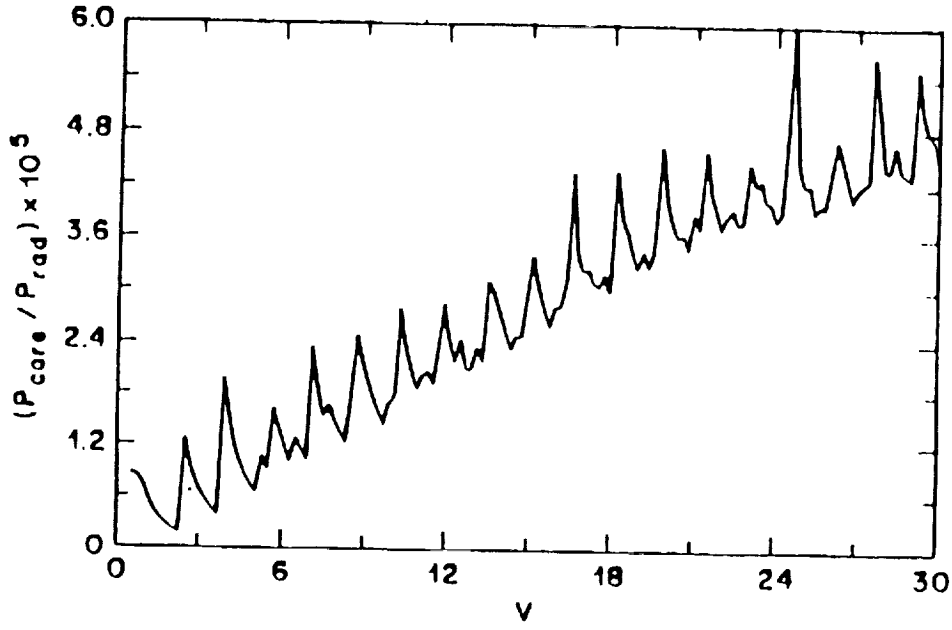

Figure IV-1b. Power Efficiency of a bulk distribution of fluorescent sources versus the V-number using the weakly guiding approximation. The wavelength and the core and cladding radii are held fixed at λ=1.3μm, a=10.0μm and b=50.0μm respectively. (From D. Marcuse, "Launching Light into Fiber Cores from Sources Located in the Cladding", *IEEE Journal of Lightwave Technology*, Vol. 6, No. 8, Aug. 1988, pp. 1273, reproduced with permission; © 1988 IEEE).

$$\left.\frac{P_{core}}{P_{rad}}\right|_{\substack{0<V<0.5 \\ \lambda=0,\,\mu=1}} = \frac{1}{\left(b^2 - a^2\right) n_{clad}^2 k^2} \left(1 - \frac{K_0^2\left(W_{\lambda=0,1}\right)}{K_1^2\left(W_{\lambda=0,1}\right)}\right) \cong \frac{1}{\left(b^2 - a^2\right) n_{clad}^2 k^2}. \quad \text{(IV-4)}$$

where

$$W_{\lambda=0,1} \equiv 0,$$

$$\lim_{z \to 0} K_0(z) \equiv - \ln z + \ln 2 - 0.577$$

and

$$\lim_{z \to 0} K_m(z) \equiv \frac{(m-1)!}{2}\left(\frac{2}{z}\right)^m.$$

For n_{clad}=1.4 Equation (IV-4) becomes 9.1×10^{-6}.

Notice that there is a cut-off degeneracy among many modes in a weakly guiding fiber. For instance, the modes $HE_{2,\mu}$, $TE_{0,\mu}$ and $TM_{0,\mu}$ have the same cut-off frequency. However, for an arbitrary fiber, part of this degeneracy is removed.

The results in Figure (IV-1a) are essentially the same as those of, Figure (IV-1b) [Marcuse, 1988]. However, the results of this work are slightly higher. We attribute this difference, possibly, to three factors:

1) we may have used a higher density of points than Marcuse did. By doing so we calculated more points near cut-off. As discussed by the previous author, this would give us a higher value for the power efficiency near the cut-off region (the closer to cut-off the higher the power efficiency),

2) Marcuse's results assumed the weakly guiding approximation $n_{core} \approx n_{clad} \approx n$ over the whole interval of V-values. For this reason, his result is independent of the two indices of refraction and, in order to obtain his figure, all he had to do was to vary the V-value only. In our case, in order to vary V we had to vary either n_{core} or n_{clad} or both. This results in bigger differences *ep* for bigger V-values. This difference, makes the final result of the power efficiency bigger than using the weakly guiding approximation and

3) the index of refraction used in Marcuse [1988] might have been slightly higher than the one used in this work. This conclusion can be justified by analysing Equation (III-43d). Within the weak guidance approximation $U_{\nu,\mu}$ and $W_{\nu,\mu}$ depend only on V. So, for a fixed V-number, the sum in Equation (III-43-d) is always equal no matter what are the values of the other parameters of the weakly guiding fiber [Marcuse, 1988]. Consequently, at a specific V-number, the power efficiency of a weakly guiding fiber would be directly proportional to the square of the wavelength and inversely proportional to the square of the index of refraction and the difference of the square of the cladding and core radius. Stated in another way

$$\left.\frac{P_{core}}{P_{rad}}\right|_{\substack{weakly\\guiding}} \propto \frac{1}{(b^2 - a^2)\, n_{clad}^2\, k^2} \,. \qquad \text{(IV-5)}$$

Equation (IV-5) does not apply when $b \equiv a$.

Figure (IV-2) was obtained for n_{core}=2.6. The plot was made between V= 0 to V= 10 so we could compare it more easily with Figure (IV-1a). It can easily be seen that the power efficiency of the first fiber is 3.45 times greater than the power efficiency of the second. This result is in agreement with Equation (IV-5) which gives us the ratio

$$(n_1/n_2)^2 = (2.6/1.4)^2 = 3.45 \,.$$

Figure (IV-3) was plotted so we could analyze the effect of the infinite outer radius approximation introduced in the integral of the square of the electric field. We can see from there that the peaks corresponding to the $HE_{1,n}$ modes are slightly lower. Also notice that the plateau observed in the previous figures does not appear here suggesting that this feature is an artifact introduced by the previous approximation. A closer analysis of the numerical data indicates that, for some reason, this difference is restricted only to the cut-off region of the $HE_{1,n}$ modes. In conclusion, the infinite outer radius approximation influences only the region near cut-off for the $HE_{1,n}$ modes and does not introduce serious errors in the results of this work.

C-2

ii) Thin Film Distribution

The result for the thin film distribution is presented in Figure (IV-4a). In this graph, we have used a index of refraction n_{clad}=1.46. The thin film is assumed to be located in the core/cladding interface. Compared with the bulk case, it is much smoother. The reason for this smoothness was discussed by Marcuse [1988] and is related to the evanescent wave that is emitted from the sources located further from the core/cladding interface. In other words, in a bulk distribution we have several layers of fluorescent material which are at increasing distances from the core boundary. The layers contribute more power near cut-off which produces the sharp increase in power in these regions. Therefore, in a bulk distribution, the power efficiency near cut-off is the sum of the contributions of many infinitesimal layers. This yields the discontinuity observed. However, for the thin film, we have only one layer. Consequently the integrated contribution near cut-off is not as dramatic. However we still have small peaks that occur nearby cut-off.

It is clear from the figures that a thin film distribution in the core/cladding boundary is more efficient than a bulk one. However the *total* power radiated by the thin film is lower because there are fewer sources. In addition to that, the nearer the sources are to the core/cladding interface the more evanescent injection we get because the evanescent wave intensity decays exponentially from the sources. In this way, the closer the sources to the core/cladding interface, the higher the probability of exciting bound modes. This also results in a higher efficiency. Our graph reproduces very well

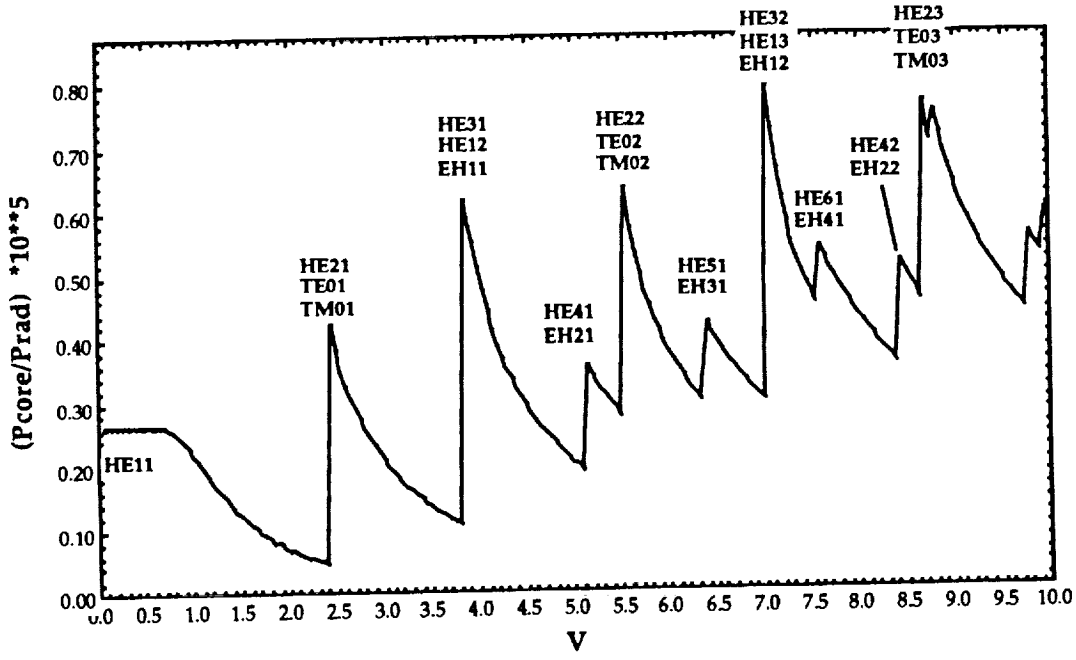

Figure IV-2. Power Efficiency of a bulk distribution of fluorescent sources versus the V-number (weakly guiding case). The wavelength, the index of refraction of the core and the core and cladding radius are held fixed at λ=1.3μm, n_{core}=2.6, a=10μm and b=50.0μm respectively. The Index of refraction of the cladding varied from 2.5999 at V = 0.05 to 2.592 at V = 10.0.

Marcuse's results, Figure (IV-4b), at low V-number [Marcuse, 1988]. However, at high V-number, it starts to diverge toward higher values for reasons discussed previously.

In summary, we have used the exact field solution of the step index profile fiber to calculate the power injection efficiency of a bulk distribution (Figures (IV-1a), (IV-2) and (IV-3)) and thin film distribution (Figure (IV-4a)). Figures (IV-1a) and (IV-2) were obtained using Equations (III-43a) thru (III-43c). However, Figure (IV-3) was obtained substituting Equations (III-35a), (III-36a) and (III-37a) in the general equation of the power efficiency (Equation (III-34)). We stress the fact that although Figures (IV-1a) and (IV-3) are very similar, they were obtained using two different upper radial limits, $r_{out}\rightarrow\infty$ and $r_{out}=b$ respectively, in the integral of the square of the electric field. The reason for the previous approximation resides in the simplification introduced in the final equations without introducing serious errors. Figure (IV-4a) was obtained using Equations (III-52a) thru (III-52c). All Figures agree very well with the weakly guiding results obtained previously by Marcuse [1988] (see Figures (IV-1b) and (IV-4b)). He has obtained his bulk distribution results (Equation (III-43d)), using the infinite outer radius limit, $r_{out}\rightarrow\infty$, in the volume integral of the square of the electric field (Equation III-42). Table (IV-1) summarizes the approximations involved in this Section.

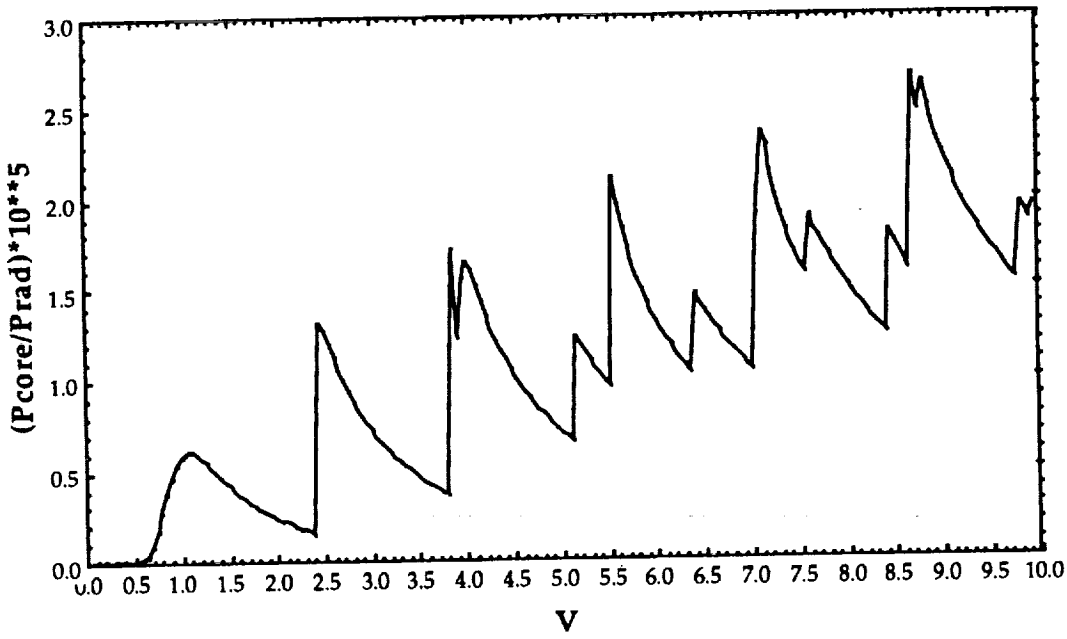

Figure IV-3. Power Efficiency of a bulk distribution of fluorescent sources versus the V-number (weakly guiding case). The wavelength, the index of refraction of the core and the core and cladding radius are held fixed at λ=1.3μm, n_{core}=1.4, a=10μm and b=50.0μm respectively. The Index of refraction of the cladding varied from 1.399 at V= 0.05 to 1.385 at V= 10.0. This graph was obtained using a finite value, b, for the outer radius of the distribution in the equation for the power efficiency.

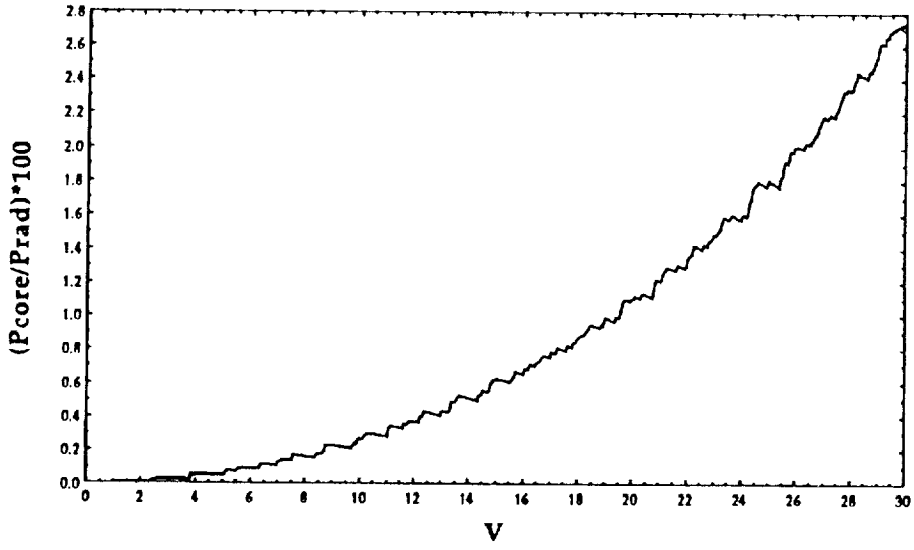

Figure IV-4a. Power efficiency of a thin film distribution of sources in the core/cladding boundary versus the V-number (weakly guiding case). The wavelength, the index of refraction of the core and the core radius are held fixed at λ=1.3μm, n_{core}=1.46, and a=10μm respectively. The index of refraction of the cladding varied from 1.4599 at V= 0.05 to 1.322 at V= 29.95.

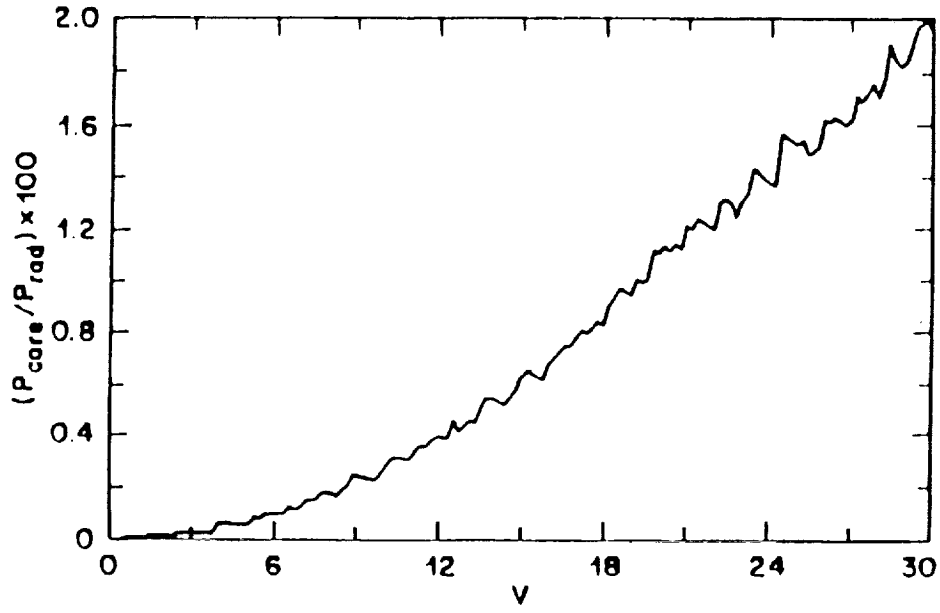

Figure IV-4b. Power Efficiency of a thin film distribution of fluorescent sources versus the V-number using the weakly guiding approximation. The wavelength and the core and cladding radii are held fixed at λ=1.3μm, a=10.0μm and b=50.0μm respectively. (From D. Marcuse, "Launching Light into Fiber Cores from Sources Located in the Cladding", *IEEE Journal of Lightwave Technology*, Vol. 6, No. 8, Aug. 1988, pp. 1273, reproduced with permission; © 1988 IEEE).

IV-4 Thin Film at an Arbitrary Distance

In order to determine the best position of the thin film within the cladding, we have plotted the logarithm of P_{eff} against the normalized position of the film $R_{in} = r_{in}/a$ (Figure (IV-5)) for $a=5.0\mu m$, $\lambda=0.4\mu m$, $n_{core}=1.6$ and $n_{clad}=1.4$. We can see that the P_{eff} decays exponentially with the distance from the boundary. Such behavior is expected since the total power associated with the evanescent field also decays in an exponential fashion. In consequence the closer the cladding sources are to the core/cladding boundary the higher the power efficiency.

IV-5 Power Efficiency Versus Wavelength

We have computed the power efficiency for $TE_{0,\mu}$, $TM_{0,\mu}$, $EH_{\nu,\mu}$ and $HE_{1,\mu}$modes (μ =1, 2, ... and ν =1, 2, 3, ...) for a wide range of wavelength. The results are presented in Figures (IV-6) thru (IV-9). We have plotted the same data first as a function of the V-number and then as a function of the wavelength λ. Notice that the actual independent variable is the wavelength. All other parameters are held constant. Since the V-number is inversely proportional to λ, the left-hand side of each graph which have V-number as independent variable, corresponds to the highest wavelength, $\lambda=2.0\mu m$. Similarly, the right-hand side corresponds to the lowest wavelength and vice-versa. As before, we present results for a bulk distribution and thin film.

TABLE IV-1

Figure (IV-1b)	Figure (IV-1a)	Figure (IV-3)
A	A	A
B	C	C
D	D	E

Comparative table on the assumptions used in three different results for the bulk distribution.

Assumptions:

A. Infinite cladding radius in the fields solutions ($b \to \infty$).

B. Weakly guiding approximation ($n_{core} \approx n_{clad}$).

C. Arbitrary indices of refraction ($n_{core} > n_{clad}$).

D. Infinite outer radius of the source distribution in the integral of the square of the electric field ($r_{out} \to \infty$).

E. *Finite* outer radius of the source distribution in the integral of the square of the electric field ($r_{out} = b$).

i) Bulk Distribution

We have plotted four graphs for the bulk distribution, Figures (IV-6) and (IV-7). In all of them, we have used $r_{in}=a=5.0\mu m$ and $r_{out}=b=25.0\mu m$ for the inner and outer radius of the distribution respectively. However, we have used $n_{core}=1.6$ and $n_{clad}=1.55$ in Figures (IV-6) we used and $n_{core}=3.0$ and $n_{clad}=1.1$ in Figures (IV-7). We have found that

1) for a given wavelength λ, the bigger the difference between n_{core} and n_{clad} the higher the power efficiency (we will show later that the same holds true for the V-number). It seems that a similar result (that the gain coefficient increases with the difference between the indices of refraction) was obtained for the $TE_{0,\mu}$ modes by Watanabe et. al. (see Figure 5 [Watanabe et. al., 1973]). This result can be easily explained for the $TM_{0,\mu}$ modes in terms of the amplitude of the electric field. The electric field of $TM_{0,\mu}$ modes in the cladding region is directly proportional to the square of the ratio n_{core}/n_{clad} [Snyder et. al., 1983]. Since the expansion coefficients are directly proportional to the amplitude of the electric field so will be the power injected into the core (see Equation (III-17)). No attempt was made to see whether there is a similarrelationship between the amplitude of the electric field of the hybrid modes and the ratio n_{core}/n_{clad}.

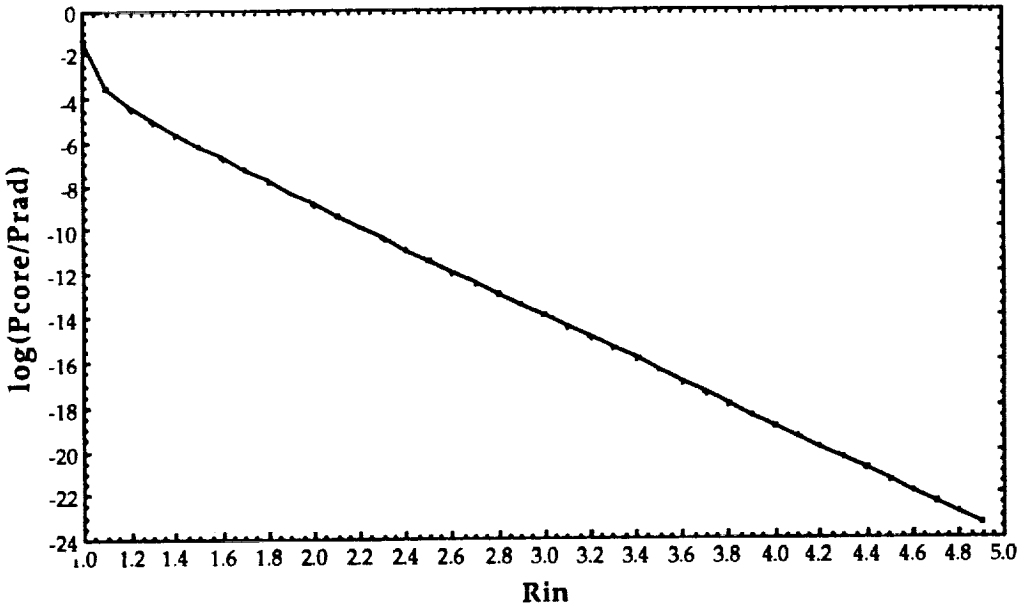

Figure IV-5. Logarithm of the power efficiency of a thin-film distribution of sources versus the thin film normalized distance, $R_{in}=r_{in}/a$. The wavelength, the core radius and the index of refraction of the core are held fixed at $\lambda=0.4\mu m$, $a=5.0\mu m$, $n_{core}=1.6$ and $n_{clad}=1.4$. The power efficiency is higher when the thin film is at the core/cladding boundary.

2) There is a reinforcement in the power efficiency among the $TE_{0,\mu}$ $TM_{0,\mu}$ and $HE_{2,\mu}$ modes of the weakly guiding fiber ($n_{core} \approx n_{clad}$) and a reinforcement between $HE_{1,\mu}$ and $HE_{2,\mu}$ modes of the strongly guiding fiber ($n_{core} >>> n_{clad}$). Reinforcement occurs because the corresponding modes have the same cut-off frequency in each guidance limit (see the cut-off equation of the hybrid modes in Table 12-4(b) of Snyder et. al.). In other words the corresponding modes have a degenerate cut-off frequency which can be removed whenever we use arbitrary indices of refraction, $n_{core} > n_{clad}$. Since they have the same cut-off frequency the power efficiency is necessarily reinforced,

3) In general the longer the wavelength the higher the power efficiency. Apparently, this result reflects the characteristics of the behavior of a wave. In other words the longer the wavelength with respect to the dimensions of the fiber the more tunneling one should expect from the cladding. This also implies that the lower the V-number the higher the power efficiency, a result which is contrary to the previous belief that a higher V-number would yield a higher power efficiency [Marcuse, 1988; Lieberman et. al., 1990]. Although, the curve of the power efficiency in Figures (IV-1) thru (IV-3) does increase with the V-number, it must be stated that in those cases, V was obtained by changing the *difference* between the indices of refraction while here we have changed the V-number by changing the wavelength. In conclusion, the behavior of the power efficiency against the V-number is dependent on how V is being changed or, in other words, the power

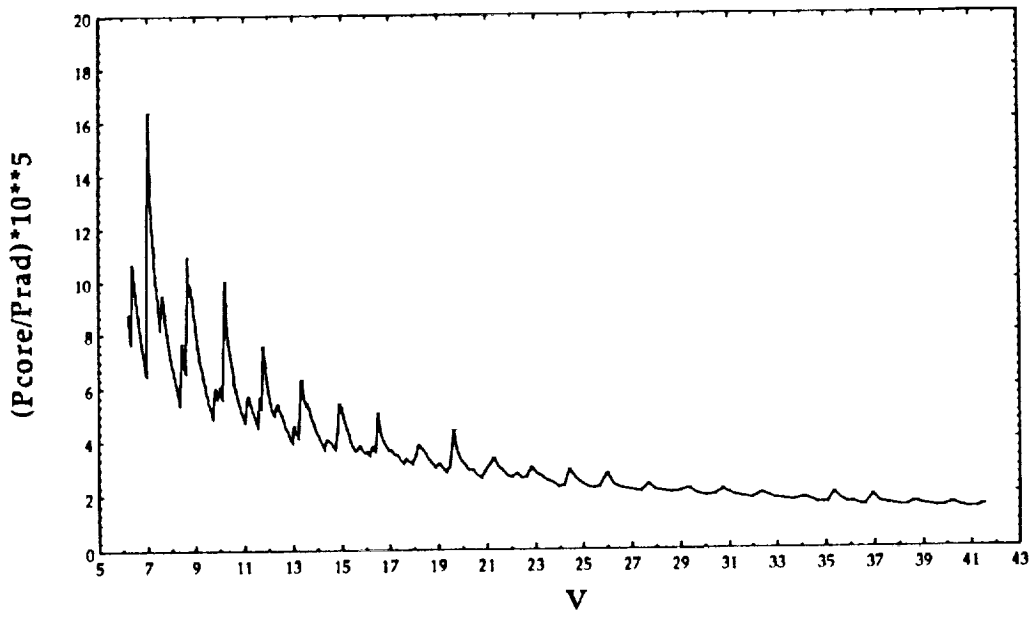

Figure IV-6a. Power efficiency of a bulk distribution of sources versus the V-number. This graph was obtained by varying the wavelength, λ, from 0.3μm to 2.0μm. The core radius, the cladding radius and the indices of refraction of the core and cladding are held fixed at a=5.0μm, b=25.0μm, n_{core}=1.6 and n_{clad}=1.55.

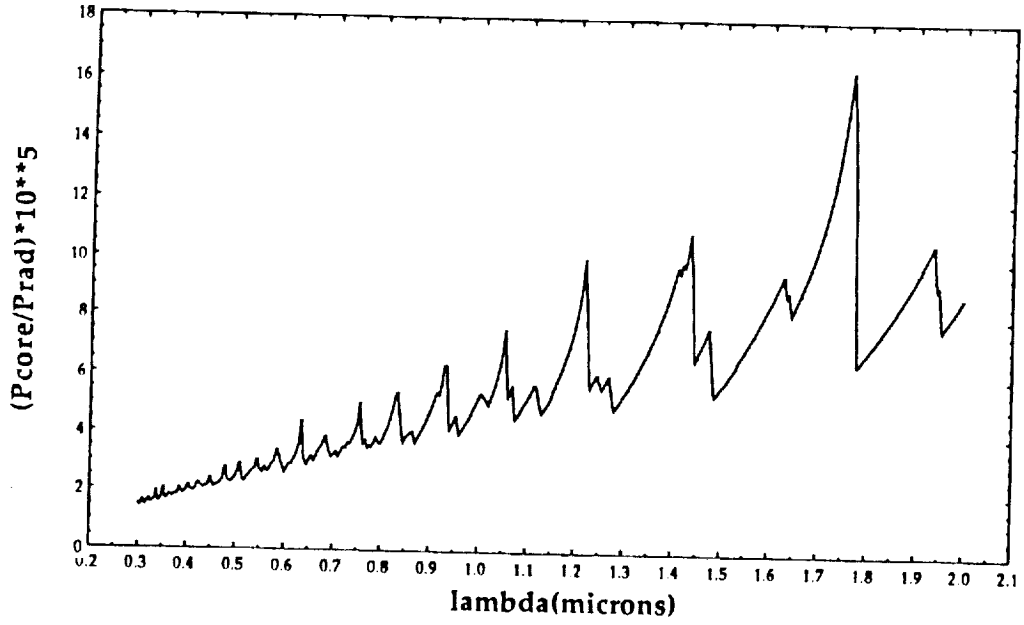

Figure IV-6b. Same as Figure IV-6a, using the wavelength, λ, instead of the V-number. The core radius, the cladding radius and the indices of refraction of the core and cladding are held fixed at a=5.0μm, b=25.0μm, n_{core}=1.6 and n_{clad}=1.55.

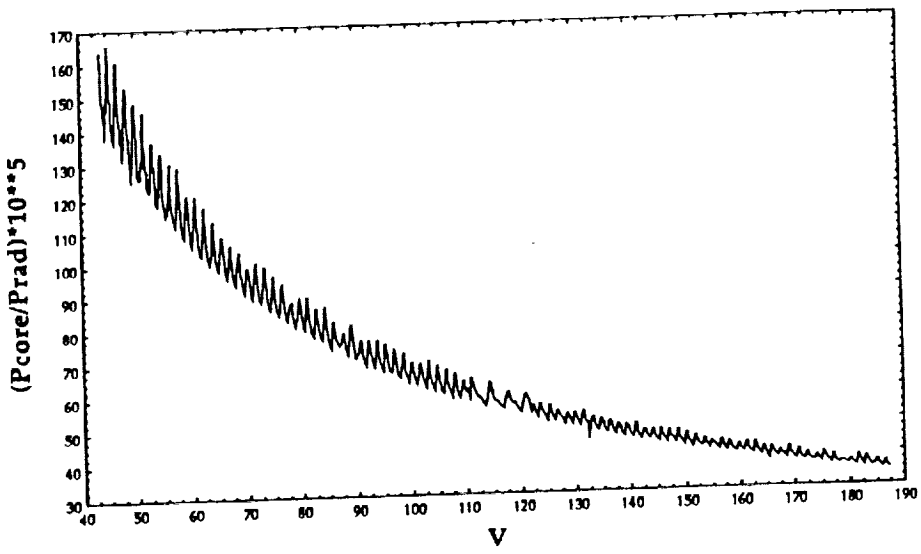

Figure IV-7a. Power efficiency of a bulk distribution of sources versus the V-number. This graph was obtained by varying the wavelength, λ, from 0.45μm to 2.0μm. The core radius, the cladding radius and the indices of refraction of the core and cladding are held fixed at a=5.0μm, b=25.0μm, n_{core}=3.0 and n_{clad}=1.1.

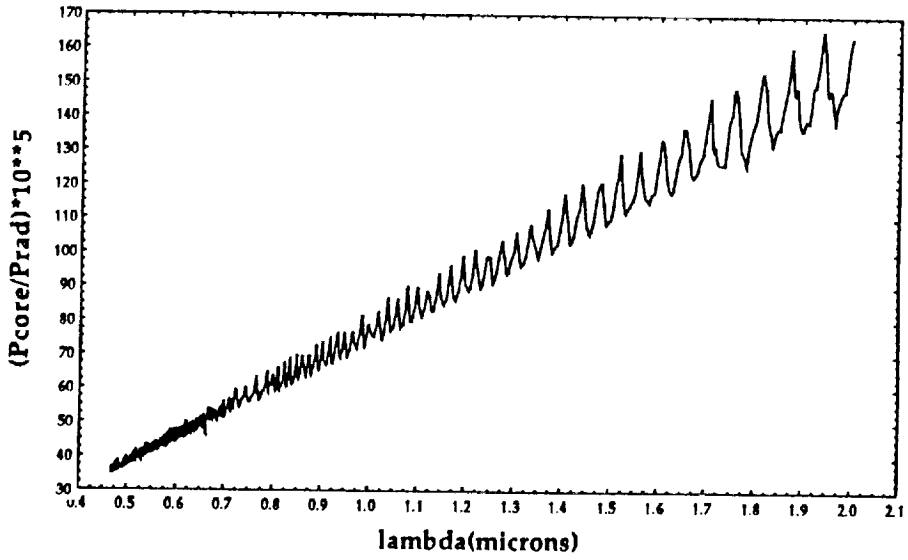

Figure IV-7b. Same as Figure IV-7a, using the wavelength, λ, instead of the V-number. The core radius, the cladding radius and the indices of refraction of the core and cladding are held fixed at a=5.0μm, b=25.0μm, n_{core}=3.0 and n_{clad}=1.1.

efficiency does not *always* increase with the V-number. Later results of this work have been consistent with the conclusion that the power efficiency does increase with the difference in indices of refraction, n_{core}-n_{clad} a conclusion which can explain Figures (IV-1) thru (IV-3).

4) In the range of small V-number the power efficiency tends to increase slightly (Figure (IV-6a)). Such behavior can also be observed in Figure (IV-6b) in the high wavelength region. Maybe, at small V-numbers, the rate of increase in the number of modes tends to catch up with the decrease in the wavelength. The final result is an increase of the power efficiency at low V-number and a gradual decrease for higher V-numbers. We did not observe the same behavior in Figures (IV-7) most likely because we could not reach the low V-number region (the higher the differences in the indices of refraction the larger the V-number).

ii) Thin Film Distribution

Figures (IV-8) and (IV-9) reproduce the results of the thin film for a variable wavelength. The values used for the parameters of Figures (IV-8) were the same as those in Figures (IV-6). We have used the indices of refraction n_{core}=2.5 and n_{clad}=1.4 in Figures (IV-9). All other parameters unchanged with respect to the previous figures. Notice that the P_{eff} remains almost constant over the whole spectrum of values. Probably, the tunneling effect that occurs at a high wavelength is no longer important for the thin film

because of the location and/or reduced number of layers of sources in the cladding.

IV-6 Power Efficiency Versus Core Radius

Figures (IV-10) and (IV-11) display the behavior of the P_{eff} with the core radius for bulk and thin film distributions respectively. For both cases we have used the values n_{core}=1.5 and λ=0.6μm. For n_{clad} we used 1.4 and 1.0 for bulk and thin film respectively. Notice that for the bulk distribution we have obtained a general decrease in P_{eff}. The peaks observed are the ones corresponding to the cut-off frequencies of the modes. Again, P_{eff} decreases with the V-number which varies from 5.64 to 56.4. It should be remembered that there is a linear relationship between the core radius and the V-number.

For the thin film case, we have an increase in the power efficiency, somehow abrupt, at low V-number, and a slight decrease at high V-number. It is interesting to notice that, for some reason, the decrease of the P_{eff} with the fiber radius is more pronounced in the bulk case than in the thin film case. In both cases this decrease may be related to the fact that a big core radius inhibits the tunneling from the cladding.

IV-7 Power Efficiency Versus n_{core}-n_{clad} (V Constant)

Figures (IV-12) and (IV-13) illustrate how the power efficiency behaves with the difference n_{core}-n_{clad} and constant V for bulk and thin film distribution

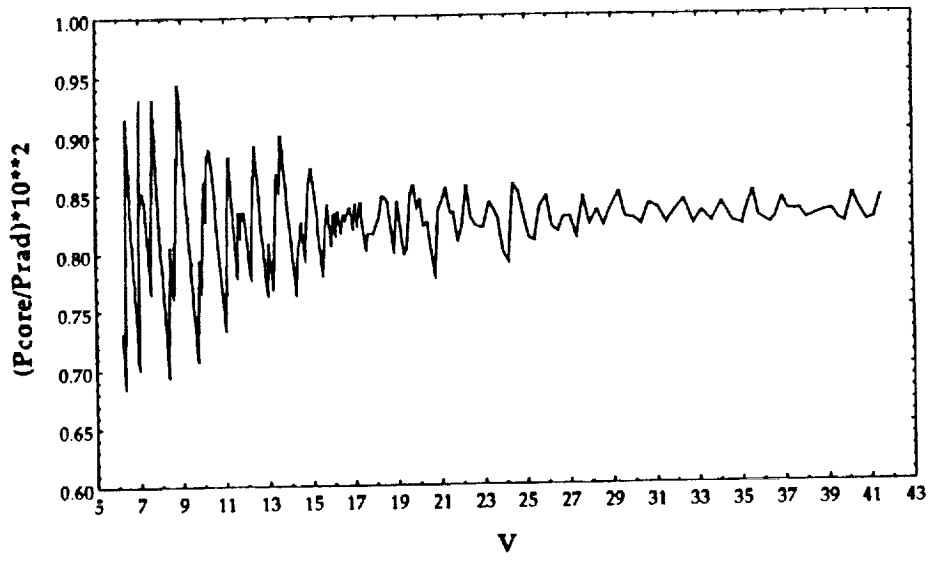

Figure IV-8a. Power efficiency of a thin-film distribution of sources versus the V-number. This graph was obtained by varying the wavelength, λ, from 0.3μm to 2.0μm. The core radius and the indices of refraction of the core and cladding are held fixed at a=5.0μm, n_{core}=1.6 and n_{clad}=1.55.

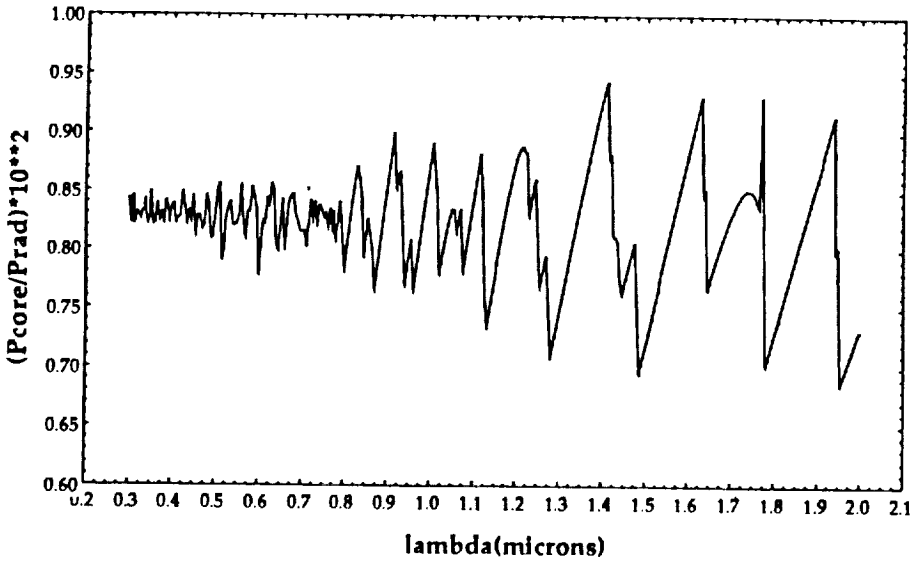

Figure IV-8b. Same as Figure IV-8a (thin-film) using the wavelength, λ, instead of the V-number. The core radius and the indices of refraction of the core and cladding are held fixed at a=5.0μm, n_{core}=1.6 and n_{clad}=1.55.

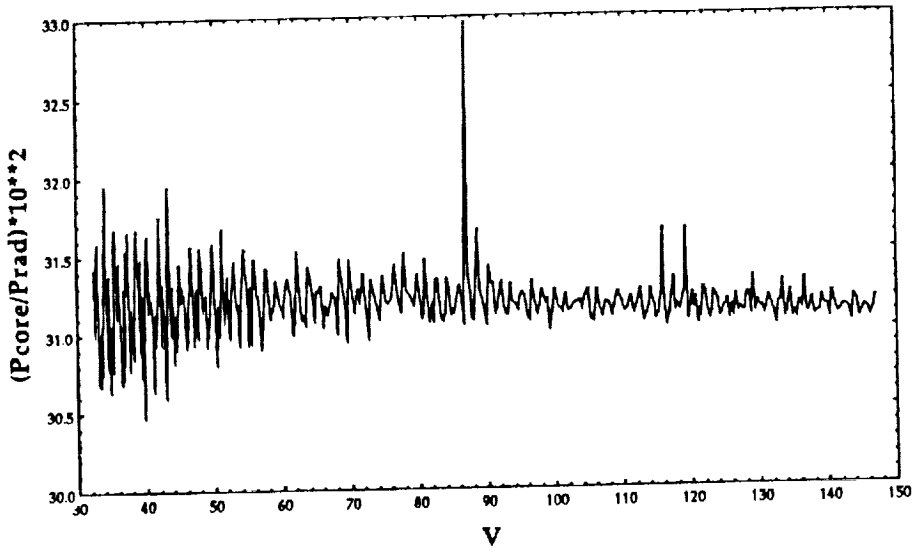

Figure IV-9a. Power efficiency of a thin-film distribution of sources versus the V-number. This graph was obtained by varying the wavelength, λ, from 0.3μm to 2.0μm. The core radius and the indices of refraction of the core and cladding are held fixed at a=5.0μm, n_{core}=2.5 and n_{clad}=1.4.

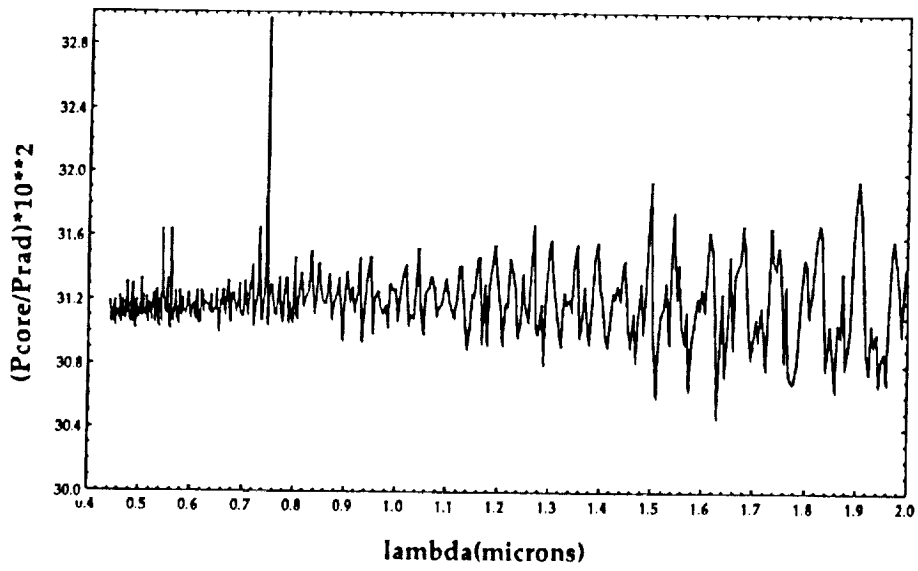

Figure IV-9b. Same as Figure IV-9a (thin-film) using the wavelength, λ, instead of the V-number. The core radius and the indices of refraction of the core and cladding are held fixed at a=5.0μm, n_{core}=2.5 and n_{clad}=1.4.

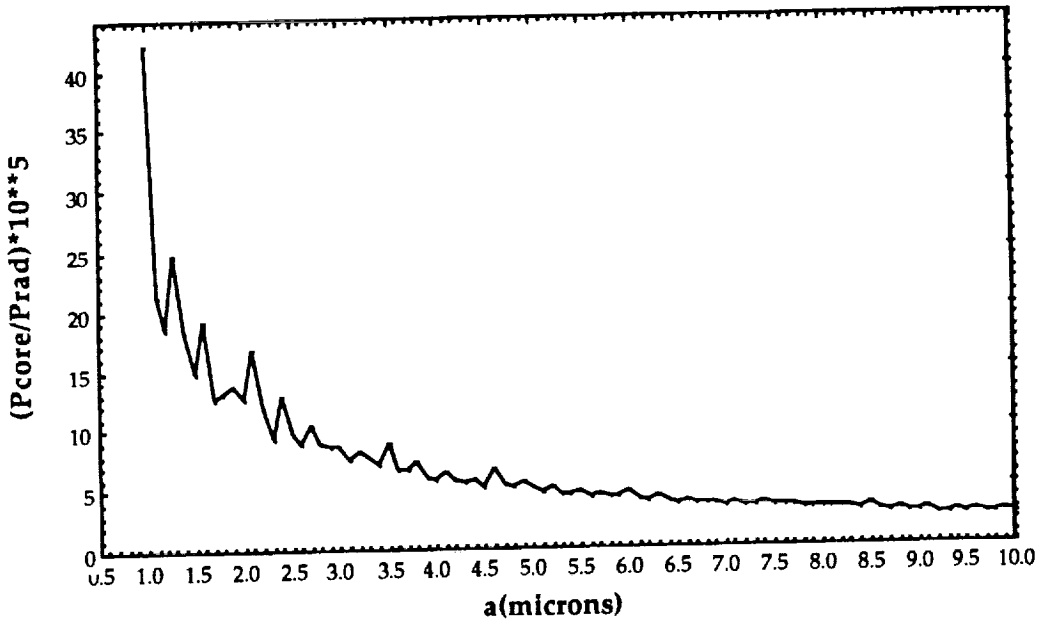

Figure IV-10. Power efficiency of a bulk distribution of sources versus the radius a. The cladding radius is given by $5.0a$. The V-number varied from 5.64 to 56.4. The wavelength, λ, and the indices of refraction of the core and cladding are held fixed at $\lambda=0.6\mu$m, $n_{core}=1.5$ and $n_{clad}=1.4$ respectively.

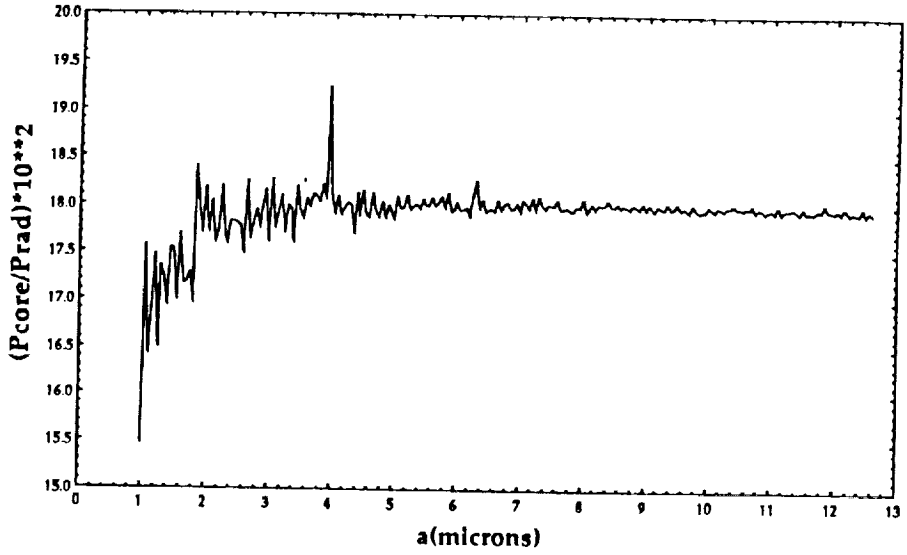

Figure IV-11. Power efficiency of a thin-film distribution of sources versus the radius a. The V-number varied from 11.7 to 186.74. The wavelength, λ, and the indices of refraction of the core and cladding are held fixed at λ=0.6μm, n_{core}=1.5 and n_{clad}=1.0 respectively.

respectively. The results were obtained for four different V-numbers and were plotted in a log-log scale. Using a linear equation we have found a correlation coefficient of one for the first three V-numbers. For the forth V-number, V=62.83, the correlation coefficient was 0.998 for a linear equation and 1.0 for a quadratic one. Apparently, the higher the V-number the more the graph deviates from a linear equation in a log-log scale. These show that the greater the difference between the indices of refraction, the higher the power efficiency. As discussed before, the apparent high value of the power efficiency at high V-number is due not to the increase in this value but to bigger differences between the indices of refraction. The upper portion of each curve is the highest power efficiency that can be reached at these particular values. That is because at those points, the index of refraction of the cladding is equal to one (the lowest possible index of refraction and the highest possible difference between the indices at V constant). As both indices of refraction increase, the difference between them and the power efficiency decrease. The indices of refraction obey the inequality $3.5>n_{core}>n_{clad}>1.0$. In this way, the lower extremes of each curve corresponds to n_{core}=3.5. It may be argued that this value of the index of refraction is not realistic. However, as a theoretical work, extreme cases like this one, are of interest because they help determining the general behavior of this system. Notice that the V-numbers used have a very big difference between each other. Have we had used values which were closer to each other we could have observed lines that obey the classical increase of the power efficiency at the cut-off value.

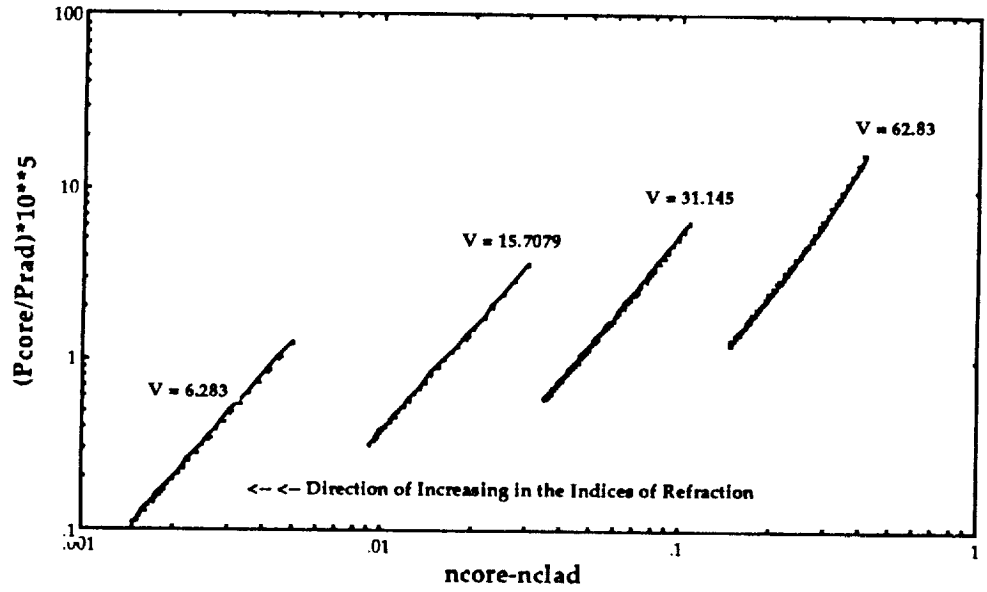

Figure IV-12. Power efficiency of a bulk distribution of sources versus the difference n_{core}-n_{clad}. The indices of refraction are restricted to the interval $3.5>n_{core}>n_{clad}>1.0$ under the condition of constant V-number. The smaller the difference, the greater the indices of refraction. The core radius, the cladding radius and the wavelength, λ, are held fixed at a=6.0μm, b=30.0μm and λ=0.6μm, respectively.

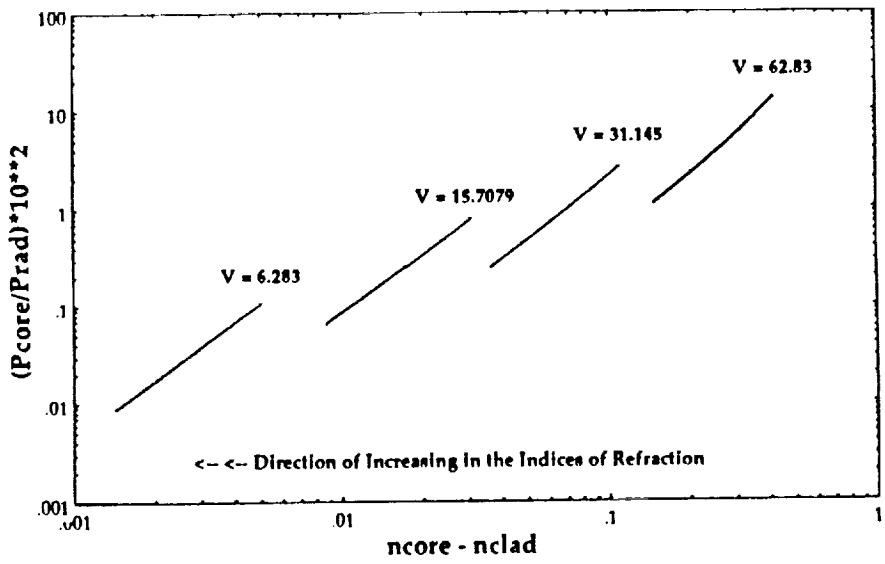

Figure IV-13. Power efficiency of a thin-film distribution of sources versus the difference n_{core}-n_{clad}. The indices of refraction are restricted to the interval $3.5>n_{core}>n_{clad}>1.0$ under the condition of constant V-number. The smaller the difference, the greater the indices of refraction. The core radius and the wavelength, λ, are held fixed at a=6.0μm and λ=0.6μm respectively.

IV-8 Bare Core Fiber with a Thin Film Coating

We conclude our data analysis with an additional graph that simulates a very useful fiber sensor: the bare fiber core coated with a thin film of fluorescent material. Such fiber can be modeled as a cylindrical rod whose cladding is the air itself (n_{clad}=1.0). The coating is assumed to be thin enough so the effect of its index of refraction can be ignored. In order to know what is the behavior of the power efficiency of this fiber for a variable n_{core} we have plotted Figure (IV-14). As it was already expected, the power efficiency increases with the n_{core} (the higher the difference n_{core}-n_{clad}, the higher the power efficiency). The increase in the power efficiency is almost linear but can not keep on growing indefinitely. Marcuse has found a power efficiency as high as 60% [Marcuse, 1988]. Our graph shows that it could go even higher, 85%. If we could use larger and larger core indices of refraction, we should expect higher efficiencies. However, we should point out that the results discussed refer only to the *forward propagating modes* of the fiber. Consequently, if we take into account both forward and backward propagating modes, the final result would exceed the 100% limit of the power efficiency! Later on, in a personal communication to Marcuse, we have suggested that the total power radiated, P_{rad}, may had been understimated by a factor of two. However, in a subsequent communication, Marcuse has stated that although the total power radiated may had been understimated, the correct expression for P_{rad} *may* include the sum of both forward and backward propagating bound modes yielding the following result for the power efficiency

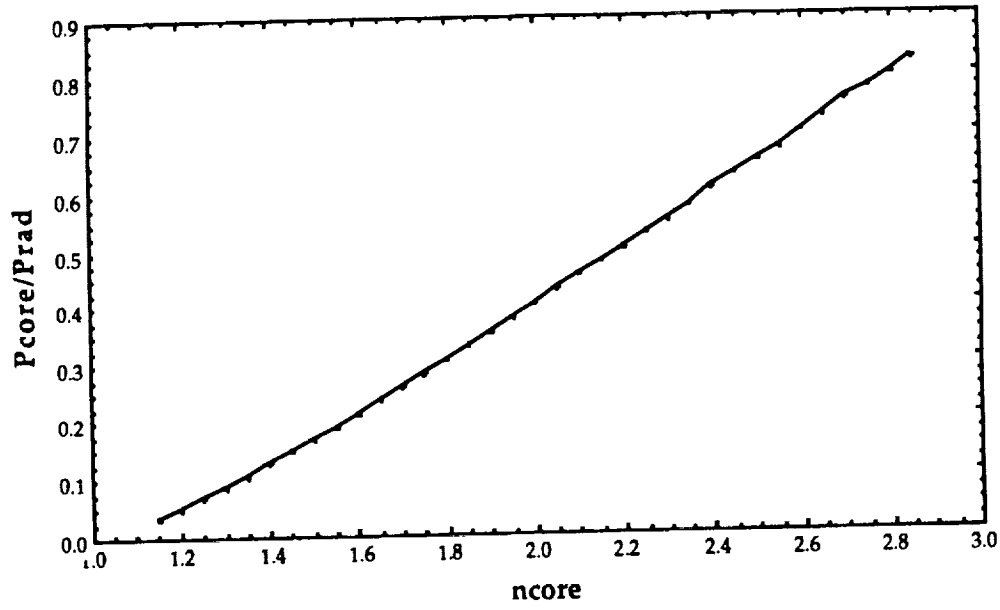

Figure IV-14. Power efficiency of a thin-film distribution of sources versus the index of refraction of the core n_{core} The core radius, the wavelength and the index of refraction of the cladding are held fixed at a=5.0μm, λ=0.6μm and n_{clad}=1.0 respectively. The V-number varied from 29.73 to 202.79.

$$P_{\text{eff}} = \frac{P_{\text{core}}}{P_{\text{rad}} + 2P_{\text{core}}} \tag{IV-6}$$

as opposed to

$$P_{\text{eff}} = \frac{P_{\text{core}}}{P_{\text{rad}}}. \tag{III-34a}$$

So, *if* Equation (IV-6) is correct, the problem of the P_{eff} greater than 100% has been solved, Equation (III-34a) would *still* be a good approximation whenever $P_{\text{rad}} >>> P_{\text{core}}$ or P_{eff} is small enough (lesser than 0.1) and most of the plots presented, particularly the ones of the bulk distribution, would be valid.

Marcuse has cautioned (in a private communication) that the expression for P_{rad} is still approximate. More specifically, back in the calculation of P_{rad}, Section (III-4), a plane wave was used to describe both electric and magnetic fields of the radiation modes [Marcuse, 1975]. Accordingly, the expression of the total power radiated, P'_{rad}, has to involve the actual fields of the radiation modes. Although these expressions were presented by Snyder et. al. [1983], Chapter 25, Snyder [1971] and Sammut [1982], they haven't been used yet in the corresponding integral. However, since at infinity the radiation fields are well described by a plane wave, it is our belief that the plane wave approximation is a good one.

V. CONCLUSIONS AND FURTHER WORK

Previous work on the light injection efficiency into the core of a fiber from sources in the cladding have made use of the fields of a weakly guiding fiber [Marcuse, 1988]. This approximation simplifies the analysis of the power efficiency by introducing universal values for the eigenvalues of different fibers with same V-number, but can not predict accurately the behavior of the injected light into a fiber with arbitrary differences in indices of refraction. Although Marcuse has analyzed the behavior of his weakly guiding fiber as a function of the V-number, he did not do so for the other parameters. We have extended Marcuse's work by using the exact field solution in the expressions of the power efficiency, P_{eff}, and analyzed its behavior as a function of the remaining parameters. Although more complicated and harder to interpret, our formulas allow us to analyze the power injection efficiency of fibers with arbitrary differences in the indices of refraction. The results obtained are relevant for the design of more efficient optical fiber distributed sensors and are summarized below.

We have confirmed the weakly guiding results of Marcuse [1988]. However, we found that the P_{eff} does not *always* increase with the V-number but with the difference in the indices of refraction, n_{core}-n_{clad}. This conclusion could not be easily reached by Marcuse because of his approximation.

For a fixed ratio a/λ, outer radius of the distribution and indices of refraction, the P_{eff} is independent of the core radius, a, and the wavelength, λ. This suggests that a/λ is an independent variable.

We have also found that, in general, the P_{eff} of the bulk distribution increases with the wavelength, λ. However, for the thin film, the P_{eff} remains almost constant. The first result implies a *decrease* of the power efficiency with the V-number which is contrary to the general belief that the power efficiency would increase with the V-number [Marcuse, 1988; Lieberman et. al., 1990].

The behavior of the P_{eff} with the fiber radius is also different for the bulk and thin film distributions. For the bulk case the power efficiency decreases for bigger values of the core radius. However, for the thin film it increases at small values of core radius and decreases slightly for bigger values. Again, we have obtained a decrease of the power efficiency with the V-number.

A final result states that the power efficiency increases with the difference between the indices of refraction n_{core}-n_{clad} for both bulk and thin film distributions. Consequently, in order to build a fiber sensor which has the best performance, we should use a source coating that emits light of high wavelength, use the smallest possible core for fibers with a bulk distribution and a slightly larger one for a thin film fiber. A fiber with a large refractive indices differential is optimum for both distributions. Nothing can be concluded for the dependence of the power efficiency with the cladding radius

b because of the infinite cladding approximation used at the very beginning.

It is hard to compare a thin film fiber coating with the bulk one. Although, the efficiency of the thin film is at least three orders of magnitude higher, what really matters is the total signal collected at the end of the fiber [Marcuse, 1988]. Experimental results by Glass et. al. [1987] on the signal response of both distributions have determined that the bulk distribution signal is higher. However we must have in mind that, for both distributions, most of the evanescent interaction occurs at the core/cladding boundary, for this reason, it is desirable to accumulate as many sources as possible in this region.

Due to the infinite cladding approximation, the fields used to compute the power efficiency are independent of the cladding radius, b. The later dependency in b in the expression of the power efficiency of the bulk distribution arises because of the finite distribution of the cladding sources, in other words, the parameter b that appears in these equations is related to r_{out} and not to the cladding radius itself! Additional work is required to determine a more accurate behavior of the P_{eff} with b.

The plane wave approximation used to calculate the total power radiated could be tested if we could integrate Equation (III-27) using the actual radiation modes of the fiber. Apparently, it can be done. However, if that is not the case, we still could compare both results (plane wave and the expression for the radiation modes) using the special case of a current source j polarized in the z-direction. Choosing this polarization could simplify the

integration of Equation (III-27).

Further experimental work should be undertaken to verify our model. This seems to be the most logical follow up to this work. Such an experiment was conducted earlier by Glass et. al. [1987], Love et. al. [1988] and Lieberman et. al. [1990]. The first two authors used a ray theory approach (geometric optics) to compare their experimental results. They were mainly interested in the total power injected into the fiber. However, Lieberman et. al. [1990], have determined the power efficiency of a fluorescent cladding fiber for a single experimental data point. They have found an agreement within an order of magnitude; a result that lends support to Marcuse's theory and the current work as well.

In summary, the richness of results provided by this rather simple fiber, the circular step index profile, suggests that more complicated fiber geometries and index profiles may have many other characteristics well worth exploring.

BIBLIOGRAPHY

Black, R.J. and Bourbonnais, R., "Core-Mode Cutoff for Finite-Cladding Lightguides", IEE Proceedings, Vol. 133, No. 6, Dec. 1986, pp. 377.

Block, M. J. and Hirschfeld, T. B., "Assay Apparatus and Method", U.S. Patent 4,558,014 (1984).

Block, M. J. and Hirschfeld, T. B., "Apparatus Including Optical Fiber for Fluorescence Immunoassay", U.S. Patent 4,582,809 (1986).

Blyler, L. L., Jr., Ferrara, J. A. and Macchesney, J. B., "A Plastic-Clad Chemical Sensors for Ammonia", Optical Fiber Sensors, 1988 Tech. Dig. Vol. 2, Washington, DC, Optical Society of America, 1988, pp. 369.

Blyler, L. L., Jr., Lieberman, R. A., Cohen, L. G., Ferrara, J. A. and Macchesney,J.B., "Optical Fiber Chemical Sensors Utilizing Dye-Doped Silicone Polymer Claddings", Polymer Engineering and Science, Vol. 29, No. 17, mid-Sep. 1989, pp. 1215.

Carniglia, C. K., Mandel, L. and Drexhage, K. H., "Absorption and Emission of Evanescent Photons", *J. Opt. Soc. Am.*, Vol. 62, No. 4, Ap. 1972, pp. 479.

Christensen, D., Andrade, J., Wang, J., Ives, J. and Yoshida, D., "Evanescent-Wave Coupling of Fluorescence into Guided Mode: FDTD Analysis", Chemical, Biochemical and Environmental Applications of Fibers, Proc. SPIE, Boston, 1989.

Cox, M.E., Dunn, B., "Detection of Oxygen by Fluorescence Quenching", *Appl. Opt.*, Vol. 24, No. 14, Jul. 1985, pp. 2114.

Culshaw, B., Optical Fibre Sensing and Signal Processing, Peter Peregrinus Ltd., London, UK, 1984.

Fröhlich, P., "Die Gültigkeitsgrenze des Geometrischen Gesetzes des Lichtbrechung", *Ann. Physik*, IV, Vol. 65, No. 15, 1921, pp. 577.

Ghatak, A.K. and Thyagarajan, K., Contemporary Optics, Plenum Press, New York, N.Y., 1978.

Glass, T.R., Lackie, S. and Hirschfeld, T., "Effect of Numerical Aperture on Signal Level in Cylindrical Waveguide Evanescent Fluorosensors", *Appl. Opt.*, Vol. 26, No. 11, Jun. 1987, pp. 2181.

Hardy, E. E., David, D. J., Kapany, N. S. and Unterleitner, F. C., "Coated Optical Guides for Spectro-photometry of Chemical Reactions", *Nature*, Vol. 357, pp. 666, 1975.

Hirschfeld, T. B. and Block, M. J., "Fluorescent Immunoassay Employing Optical Fiber in Capillary Tube", U.S. Patent 4,447,546 (1984).

Hirschfeld, T. B. and Block, M. J., "Fluorescent Immunoassay Using Optical Fibers and Antibodies Immobilized on Surfaces", FACCS Eleventh Annual Meeting, 16 Sept. 1984a.

Jackson, J.D., Classical Electrodynamics, John Wiley & Sons, New York, N.Y., Second Ed., 1975.

Kuhn, M.H., " The Influence of the Refractive Index Step Due to the Finite Cladding of Homogeneous Fibres on the Hybrid Properties of Modes", Archiv für Elektronik und Übertragungstechnik, Vol. 28, No. 10, Oct. 1974, pp. 393.

Lee, E.H., Benner, R.E., Fenn, J.B. and Chang, R.K., "Angular Distribution of Fluorescence from Liquids and Monodispersed Spheres by Evanescent Wave Excitation", *Appl. Opt.*, Vol. 18, No. 6, Mar. 1979, pp. 862.

Lieberman, R.A., Brown,K.E., "Intrinsic Fiber Optic Chemical Sensor Based on two-Stage Fluorescence Coupling", Chemical, Biochemical and Environmental Applications of Fibers, Proc. SPIE 990, 1988.

Lieberman, R.A., Blyler,L.L., Cohen, L.G., "Distributed Fiber Optic Sensor Based on Cladding Fluorescence", *IEEE J. of Lightwave Technol.*, Vol. 8,

No. 2, February 1990, pp. 212.

Love, W.F. and Button, L.J., "Optical Characteristics of Fiber Optic Evanescent Wave Sensor", Chemical, Biochemical and Environmental Applications of Fibers, Proc. SPIE 990, 1988.

Marcuse, D., Theory of Dielectric Optical Waveguides, Academic Press, New York, N.Y., 1974.

Marcuse, D., "Excitation of Parabolic-Index Fibers with Incoherent Sources", *Bell Syst. Tech. J.*, Vol. 54, No. 9, November, 1975, pp. 1507.

Marcuse, D., "Launching Light into Fiber Cores from Sources Located in the Cladding", *IEEE Journal of Lightwave Technology*, Vol. 6, No. 8, Aug. 1988, pp. 1273.

Midwinter, J. E., Optical Fibers for Transmission, John Wiley & Sons, New York, N.Y., 1979.

Press, W. H., Flannery, B.P., Teukolsky, S. A., Vetterling, W. T., Numerical Recipes, The Art of Scientific Computing, Cambridge University Press, Cambridge, MA, 1986.

Rogowski, R. S., Heyman, J. S. ,Holben, Jr., M. S., Egalon, C., Dehart, D. W., Doederlein, T. and Koury, J., "Fiber Optic Strain Measurements in

Filament-Wound Graphite-Epoxy Tubes Containing Embedded Fibers", Fiber Optic Smart Structures and Skin, Proc. SPIE 986, 1988, pp. 194 .

Sammut, R.A., "Orthogonality and Normalization of Radiation Modes in Dielectric Waveguides", *J. Op.Soc. Am.*, Vol. 72, 1982, pp. 1335.

Selenyi, M. P., "Sur L'Existence et L'Observation des Ondes Lumineuses Sphériques Inhomogenénes", *Compt. Rend.*, Vol. 157, 1913, pp. 1408.

Snitzer, E., "Cylindrical Dielectric Waveguide Modes", *J. Op. Soc. Am.*, Vol. 51, No. 5, May 1961, pp. 491.

Snyder, A.W., "Continuous Mode Spectrum of a Circular Dielectric Rod", *I.E.E.E. Trans. MTT*, Vol. 19, 1971, pp. 720.

Snyder, A. W. and Love, J. D., Optical Waveguide Theory, Chapman and Hall, New York, N.Y., 1983.

Tai, H., Tanaka, H. and Yoshino, T., "Fiber-Optic Evanescent-Wave Methane-Gas Sensor Using Optical Absorption for the 3.392-μm line of a He-Ne laser", *Opt. Let.*, Vol. 12, No. 6, Jun. 1987, pp. 437.

Watanabe, A., Hill, K. O. and Mintz, D., "Calculation of Evanescent-Wave Gain in the TE_{0m} and TM_{0m} Modes of an Optical Fibre", Report No. 1247, Communications Research Centre, Department of Communications,

Ottawa, Canada, Jul. 1973.

Wolfbeis, O. S., Weis, L. J., Liener, M. J. P. and Ziegler, W. E., "Fiber-Optic Fluorosensor for Oxygen and Carbon Dioxide", *Anal. Chem.*, Vol. 60, No. 19, 1988, pp. 2028.

Report Documentation Page

NASA National Aeronautics and Space Administration

1. Report No.	2. Government Accession No.	3. Recipient's Catalog No.
NASA CR-4333		

4. Title and Subtitle	5. Report Date
Injection Efficiency of Bound Modes	November 1990
	6. Performing Organization Code

7. Author(s)	8. Performing Organization Report No.
Claudio Oliviera Egalon	10. Work Unit No. 506-43-11-03

9. Performing Organization Name and Address	11. Contract or Grant No.
The College of William and Mary Department of Physics Williamsburg, VA 23185	NAS1-18347
	13. Type of Report and Period Covered
12. Sponsoring Agency Name and Address	Contractor Report
National Aeronautics and Space Administration Langley Research Center Hampton, VA 23665-5225	14. Sponsoring Agency Code

15. Supplementary Notes

Dissertation submitted to The College of William and Mary in partial fulfillment of the requirements for the degree of Doctor of Philosophy.

Langley Technical Monitor: Robert S. Rogowski

16. Abstract

Previous work on efficiency of light injection into the core of a fiber from a thin film and a bulk distribution of sources in the cladding have made use of the fields of a weakly guiding fiber. This approximation simplifies the analysis of the power efficiency by introducing universal values for the eigenvalues of different fibers with the same V-number, but cannot predict accurately the behavior of the injected light into a fiber with arbitrary differences in indices of refraction. We have used the exact field solution in the expressions of the power efficiency, P_{eff}, and analyzed its behavior as a function of the fiber parameters.

We have confirmed weakly guiding results obtained previously. However, P_{eff} does not always increase with the V-number but with the difference in the indices of refraction, $\eta_{core} - \eta_{clad}$.

For the bulk distribution we have found that P_{eff} increases with the wavelength, λ, and decreases with the fiber core radius, a, i.e., it decreases with the V-number. However, for the thin film, the P_{eff} remains almost constant with the wavelength, λ, and the fiber core radius, a.

17. Key Words (Suggested by Author(s))	18. Distribution Statement
Fiber Optic Sensor Power Injection Fluorescence Cladding	Unclassified - Unlimited Subject Category - 74

19. Security Classif. (of this report)	20. Security Classif. (of this page)	21. No. of pages	22. Price
Unclassified	Unclassified	144	A07

NASA FORM 1626 OCT 86

For sale by the National Technical Information Service, Springfield, Virginia 22161-2171

NASA-Langley, 1990